AD-A152 612 SHEAR WAVE ATTENUATION IN UNCONSOLIDATED LABORATORY SEDIMENTS(U) PLANNING SYSTEMS INC MCLEAN VA B A BRUNSON JUN 83 NORDA-TN-159 N00014-81-C-0275 1/3

UNCLASSIFIED F/G 8/8 NL

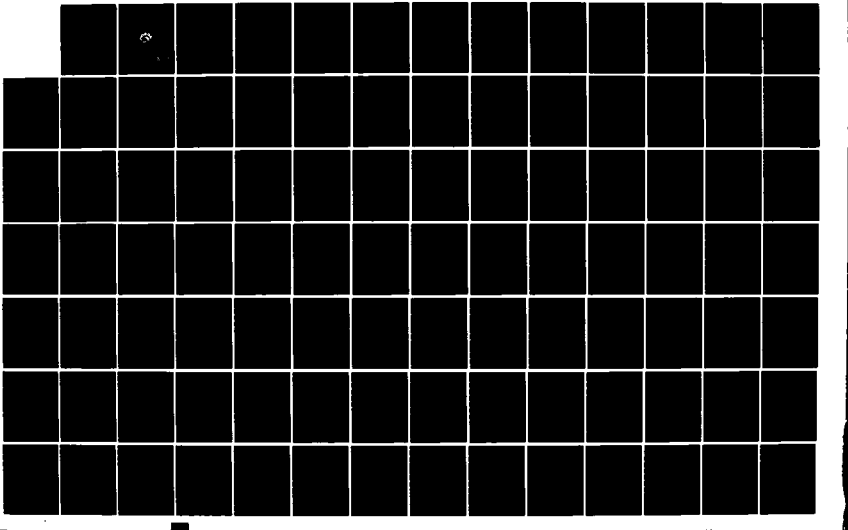

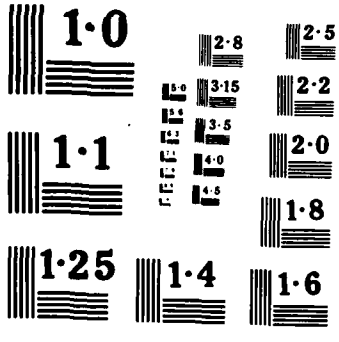
1·0
1·1
1·25
1·4
1·6
1·8
2·0
2·2
2·5
2·8
3·15
3·5
4·0
4·5

(2)

NORDA Technical Note 159

Naval Ocean Research
and Development Activity
NSTL, Mississippi 39529

Shear Wave Attenuation in Unconsolidated Laboratory Sediments

Burlie A. Brunson
Planning Systems Incorporated
McLean, Virginia 22102

June 1983

ABSTRACT

Shear wave attenuation measurements were made using ceramic bimorph transducers to excite transverse vibrations in a cylindrical column of unconsolidated sediment. Three different water-saturated sediments were used in an attempt to determine the effects of grain shape and sorting on the frequency dependence of attenuation. The mean grain size of the sediments was held constant while the grain shape and size distributions were varied. The sediment assemblages used in the attenuation measurements included a moderately-sorted angular quartz sand, a well-sorted angular quartz sand, and well-sorted spherical glass beads. The moderately-sorted sand showed the greatest attenuation over the measurement frequency range of 1 to 20 kHz. The well-sorted sand and the glass beads showed generally lower attenuation with the beads being the least lossy propagation medium. All three sediments showed evidence of viscous attenuation due to fluid-to-grain relative motion. This mechanism leads to a non-linear relationship between attenuation and frequency.

Sediment physical properties were measured for use as inputs to a theoretical attenuation model based on the Biot theory of propagation of waves in porous media. The model allowed attenuation versus frequency predictions to be made for each of the three sediment assemblages. The resultant comparisons between the measured and predicted attenuations demonstrated the importance of using measured model inputs obtained under controlled laboratory conditions when theoretical model capabilities are being evaluated. The model comparisons shed significant light on the ability of this particular model to predict shear wave attenuation in non-ideal sediments.

PREFACE

The author would like to thank all those who have given of their time to see this project through. Particular thanks go to Dr. Richard K. Johnson, my doctoral committee chairman at Oregon State University. Mr. James Matthews of NORDA was quite helpful during the laboratory measurements stage.

This project was supported by the Bottom Interaction Program, Naval Electronics Systems Command, Code 612, under Office of Naval Research Contract N00014-82-C-0275 Modification P0003. Grateful appreciation is expressed to LCDR Hollis, NAVELEX 612, and Mr. W.W. Worsley, NORDA, for their support.

This report has been submitted to the School of Oceanography, Oregon State University, and has been accepted in partial fulfillment of the requirements for the degree of Doctor of Philosophy.

TABLE OF CONTENTS

LIST OF FIGURES

LIST OF FIGURES (Cont.)

LIST OF FIGURES (Cont.)

LIST OF TABLES

SHEAR WAVE ATTENUATION IN UNCONSOLIDATED LABORATORY SEDIMENTS

I. INTRODUCTION

In recent years investigators in underwater acoustics have formulated propagation models which are capable of accurately predicting the properties of the acoustic field in regions where boundary effects are of secondary importance. These same models have been utilized, with limited success, in shallow water or bottom limited environments where interaction with the seafloor is a dominant factor. As acoustic modeling capabilities have become more sophisticated, including the formulation of range dependent models based on wave theory, the requirements for more accurate descriptions of the environment have increased. In ocean areas where acoustic bottom interaction is important, particular interest is focused on the accurate portrayal of the properties of the seafloor.

In a recent paper, Hamilton[1] has presented a comprehensive review of the state of geoacoustic modeling of the seafloor. He defines a geoacoustic model as, "a model of the real seafloor with emphasis on measured, extrapolated, and predicted values of those properties important in underwater acoustics and those aspects of geophysics involving sound transmission." Accordingly, information required for a complete geoacoustic model should include the following for each sediment layer:

1. Identification of sediment type of the seafloor and in the underlying layers

2. True thickness and shapes of layers and locations of significant reflectors

3. Compressional wave velocities of the seafloor surface; as a function of depth; and at the surface of the acoustic basement

4. Shear wave velocities at the seafloor surface; as a function of depth; and at the surface of the acoustic basement

5. Attenuation of compressional waves at the seafloor surface; as a function of depth; and at the surface of the acoustic basement

6. Attenuation of shear waves at the seafloor surface; as a function of depth; and at the surface of the acoustic basement

7. Density at the seafloor surface; as a function of depth; and at the surface of the acoustic basement

8. Elastic properties of the sediment (e.g., dynamic rigidity, Lame's constants).

Since the seafloor is made up of an almost infinite variety of sediment and rock assemblages, there is an equally diverse variety of geoacoustic models. To expect to measure the required physical and acoustical properties of the seafloor listed above, for each area where an acoustic prediction is required, is clearly impossible. Hamilton[1,2] and others[3,4] have tried to approach this problem by grouping the seafloor into three general

environments: the continental terrace (shelf and slope), the abyssal hill environment (pelagic), and the abyssal plain environment (turbidite). Each of these main environments usually has distinctive sediment types. The averaged results of sediment acoustic and related properties based on measurements and computations have been summarized for each of the environments.[1] These properties together with other geological and bathymetric information may be used by investigators to construct area models for regions of interest. Even so, certain of the required properties may be poorly characterized or virtually nonexistent. Chief among these are shear wave speed and attenuation.

Another approach to sediment modeling is that described by Stoll.[5] This approach relies on the utilization of a mathematical model[6-10] based upon the classical work of Biot [11-14] in acoustic propagation in porous media. The model takes into account the effects of certain key mechanisms that play principal roles in controlling the dynamic response of sediments, and predicts body wave damping and velocity in fluid saturated sediments. Two mechanisms for energy dissipation are included in the Biot-Stoll model; one accounts for losses due to the inelasticity of the sediment skeleton, and the other for viscous losses in the sediment as the interstitial fluid moves relative to the sediment skeleton during passage of an acoustic disturbance. The complex interaction of these mechanisms results in damping which is frequency dependent and which depends upon sediment physical properties such as porosity, grain size, and permeability, and the effective stress on the sediment.

data[23] were supplemented and analyzed further by Hardin and Black[46] resulting in empirical equations relating shear speed or shear modulus and overburden pressure which were recommended by Richart, et al.,[47] for use with both angular and round grained materials (sands and some clays, wet or dry). The resultant equations take the form:

$$G = A(T)F(e)\bar{\sigma}_0^n \qquad \text{(II-1)}$$

where G is the shear modulus, A is the function accounting for the time history of the sample including loading increment, F(e) accounts for the effects of void ratio e (porosity, $\emptyset$), and $\bar{\sigma}_0$ is the isotropic component of effective stress. For G and $\bar{\sigma}_0$ in units of pounds per square inch in clays, the equation is

$$G = \frac{1630(2.973-e)^2}{(1-e)} \bar{\sigma}_0^{0.5} \qquad \text{(II-2)}$$

and for angular-grained sands

$$G = \frac{1230(2.973-e)^2}{(1-e)} \bar{\sigma}_0^{0.5} \qquad \text{(II-3)}$$

Equation (II-2) holds for void ratios $0.5 \leq e \leq 1.5$ ($0.33 \leq \emptyset \leq 0.60$) and to pressures of 20 to 100 psi (138-690 kPa). Equation (II-3) applies to void ratios $0.38 \leq e \leq 1.26$ ($0.24 \leq \emptyset \leq 0.56$) and to pressures of 3.5 to 42 psi (24-290 kPa). These equations have been used extensively by several authors[8,20] seeking to include pressure effects or corrections in shear wave calculations.

More recently Pilbeam and Vaisnys[24] have found the shear wave speeds in dry glass beads to vary as the one-third power of confining pressure, but lubricated glass

mean effective pressure due to overburden of 0.5 to 1.4 kPa in saturated sediments and 0.9 to 2.2 kPa in dry sediments. Speeds in dry glass beads ranged from 76 to 122 m/sec at 0.9 kPa, while dry sands showed speeds between 73 and 220 m/sec under the same mean effective stress. Wet speeds were always lower than the dry speeds with the beads showing speeds from 53 to 82 m/sec at 0.6 kPa, and the sands showing speeds ranging from 47 to 105 m/sec at the same effective stress level.

Extensive measurements of elastic wave velocities in granular soils as a function of "effective confining pressure" (determined by Hamilton[36] to be 90 to 97 percent of normal overburden pressures) were reported by Hardin and Richart.[23] They reported shear and compressional wave speeds for both dry and saturated aggregates of Ottawa sand, crushed quartz sand, and crushed quartz silt. The normal overburden pressure was varied between 6.5 and 365 kPa. For shear waves at pressures exceeding approximately 90 kPa the velocity of shear waves in Ottawa sand was found to vary with approximately the one-fourth power of pressure with the exponent for dry sand being slightly lower (0.238) than that for the wet sand (0.252). Similar measurements at lower overburden pressures produced larger pressure exponents, varying from 0.293 in dry sediments to 0.420 in wet sediments. At low confining pressures, even a modest amount of moisture (1.4 percent) resulted in a decrease of as much as 7 percent in the shear wave speeds in the Ottawa sand. Wilson and Miller[45] showed a similar one-fourth power pressure dependence of shear wave speeds in wet medium-to-fine sands over a pressure range of 33.5 kPa to 479 kPa. The Hardin and Richart

and 300 m/sec for depths to 12 m below the sediment surface. In general, this variation of speed with depth was similar to that shown in the silt, clay, turbidite data with higher values of shear speeds reported at similar depths. Some degree of caution must be shown in assuming that these measurements are for sediments with high water content.

One may correctly infer that shear speeds in unconsolidated sediments are sensitive to overburden pressure or compaction. This observation has led to numerous studies of the effects of pressure on the elastic properties of unconsolidated sediments. Many of these studies have dealt with pressure effects on wave speed, and generally were performed under laboratory conditions. This has allowed a more carefully controlled set of observations, particularly with respect to the degree of saturation.

Iida[43] performed torsional vibration tests on columns of wet quartz sand and, for reported resonance frequencies and column heights, showed speeds between 60 and 70 m/sec at normal overburden pressures of 0.5 to 1.4 kPa due to specimen weight. The data show constant speeds of 70 m/sec above 0.7 kPa. Schmidt[44] showed a change in shear speed for dry sand samples from 76 to 120 m/sec for columns 3.2 to 11 cm in height. For a typical sand,[8] this is equivalent to overburden pressures between 0.3 and 1.1 kPa. Shirley and Hampton[26] reported shear speeds of 6 to 29 m/sec for a water saturated kaolinite clay allowed to settle under the influence of gravitational and interparticle forces for 120 hrs. Bell[27] reported shear speed measurements taken on dry and wet glass beads and natural sands at

were found in sediments with some sand fraction, particularly when they occurred deep in the sediment column. For depths of burial of 10 m or less, the range of speeds was much narrower; varying from 50 to 230 m/sec at the surface and a depth of 10 m, respectively. In general, this direct speed-to-depth correlation did not hold, being complicated by sediment type, among other factors. An important factor to be taken into consideration is the degree of saturation of the sediment whose speed is being measured. Some of the values cited above are for land sediments where the degree of saturation is unknown.

Field measurements for sands were listed separately in Hamilton's review. Most were from sediments found at or near the surface of the sediment column. Cunny and Fry[38] provided the most extensive set of in situ measurements of shear wave speed in sands. They reported values ranging from 53 to 140 m/sec in the upper meter of medium to fine sands, with no observable correlation with stated grain size. However, all of these observations were for depths above the water table; thus, their degree of saturation is unknown. Other authors[39,40,41] cite shear speed values ranging from 98 to 567 m/sec in sands at depths of less than one meter. The highest values are reported by Barnes, et al.,[41] for medium to fine sands observed during a survey of Monterey Bay, California. These values are substantially greater than any cited except for those reported at depths on the order of 20 m below the sediment surface.[42]
Other speeds reported range from 101 m/sec computed from Stoneley waves estimated to be 1.1 m below the sediment surface,[42] to 579 m/sec at depths of 27 m in loose sands.[41] Most values fall between 150 m/sec

field measurements of the velocity of shear waves in unlithified, water-saturated sediments. The cited field studies included data taken at various depths and pressures including data from the literature of land geophysics. The latter were included because of the lack of data for the full range of marine sediments. The data were divided between velocities in silts, clays, and turbidites; and velocities in sands.

Shear speeds reported by Zhadin (in Molotova and Vassilev[37]) from borehole measurements in saturated clays range from 120 m/sec at 10 m to 359 m/sec at 63 m. Warrick[30] reported shear speeds at 90 m/sec at 6 m in a tidal mud flat. Cunny and Fry[38] reported shear speeds ranging from 137 m/sec at 1 m in a silty clay to 239 m/sec in a shaley clay at a depth of 27 m. Kudo and Shima[29], using a surface source and a borehole receiver in saturated silts, reported shear speeds from 102 m/sec at 16 m depth to 270 m/sec at 42 m. Davies[39] measured Stoneley waves propagating along the seafloor and calculated speeds varying from 50 m/sec at the sediment surface to 190 m/sec at a depth of 16 m. Hamilton et al.[22], used Stoneley wave observations to calculate sediment shear wave speeds between 88 and 108 m/sec at a depth of 2 m in a clayey-silt seafloor.

The data cited by Hamilton[36] were from a number of widespread sites, for a number of sediment types, and at several different depths. They showed a spread of speeds from 50 m/sec in a deep sea surface sediment,[39] to 700 m/sec in a saturated clay, siltstone, and sandstone found 650 m down a borehole.[37] As expected, the lowest speeds were for shallow muds or clays while the highest speeds

Such statements are essential to sorting out the mechanisms responsible for the observed acoustical response of sediments.

There are, then, several techniques available to the investigator which will allow the accurate measurement of shear wave speed and attenuation under carefully controlled laboratory conditions. While some may argue that such laboratory measurements cannot duplicate the conditions found in nature, it is felt that their value in allowing a better understanding of the various mechanisms controlling the dynamic response of unconsolidated sediments overrides those objections. Their value is further enhanced when the acoustical measurements are accompanied by those sediment parameters listed at the beginning of this section.

Shear Wave Observations

Measurements of shear wave speed and attenuation in porous unconsolidated sediments are sparse. This is particularly true for fully saturated sediments at small confining pressures. When measurements are reported they seldom include descriptions of the environmental conditions prevailing at the time of observation. Especially important, and often lacking, are the stress and frequency ranges over which the measurements were taken. These are essential to valid intercomparisons of data sets.

Speeds

In a review of shear wave velocity measurements, Hamilton[36] presented a study of selected published

in the 200 Hz to 2500 Hz frequency range. Pilbeam and Vaisnys[24] report laboratory measurements of longitudinal and torsional velocity and energy damping in granular media using a bar resonance method over the frequency range of 1-20 kHz. Pulse methods using crystal transducers to measure shear and compressional waves in unconsolidated porous sediments are reported by Domenico.[25] In these experiments, only wave velocities were reported. Brunson and Johnson,[21] report shear wave attenuation measurements in unconsolidated saturated sand over a frequency range of 450 Hz to 7 kHz using transversely vibrating piezoceramic bender elements. These transducers are similar to those used by Shirley and Hampton[26] to measure shear wave speed and attenuation in clays in the 200-400 Hz frequency ranges. Bell[27] reports values for shear wave speeds and attenuation for seven laboratory sediments obtained using the same type of bender elements to generate transverse vibrations in the sediments. He reports shear wave attenuation and speed over a frequency range of 0.5 to 20 kHz. Direct field measurements of wave speeds using diver implanted probes[22] as well as transducers attached to sediment corers[28] have been reported, but the supporting sediment physical properties are generally not available. Other measurement techniques include generating polarized shear waves by imparting transverse motion to a wooden beam held in place by a truck;[29-32] mechanical vibration of a horizontal plate coupled to the ground;[33] explosions;[34, 30]; or seismic reflection and refraction techniques.[35] The common shortcoming of these field techniques is that little is known about the physical properties of the sediment through which the energy has propagated. Because of this, no definitive statements may be made about sediment physical and acoustical property relationships.

generally present in the natural environment. In addition, the physical properties of such a natural transmission medium are difficult to determine and impossible to control. Thus, it is difficult to extract reliable estimates for the material damping from the overall losses observed in field data. Parametric studies to extract the relationships between acoustical and physical properties are extremely difficult and often ambiguous or inconclusive.

On the other hand, there is the possibility of studying the characteristics of low-frequency shear or rotational wave motion in the laboratory under carefully controlled conditions or in the field over propagation paths short enough to allow assumptions of sediment homogeneity to be reasonably valid. This is possible because of the relatively short wavelengths of these types of waves. Hamilton, et al.[22], report compressional to shear wave speed ratios ranging from 9 in naturally occurring sands to 15 in clayey-silts. This translates to shear wavelengths shorter by an equivalent factor. Thus, we may reasonably expect to make laboratory measurements of shear waves at frequencies as low as a few hundred hertz in sands and even lower in softer sediments such as clays. Various investigators have demonstrated this capability. Numerous authors[10,23] have reported the use of torsional pendulum or resonant column methods to obtain longitudinal and shear wave speed and damping of sediment samples in the laboratory. Stoll[10] reports logarithmic decrements for a range of frequency from 20 Hz to 1 kHz for both dry and water saturated sediments. The measurements reported by Hardin and Richart[23] used the resonant column techniques to measure longitudinal and shear wave speeds and damping

II. OBSERVATIONAL CONSIDERATIONS

Background

A review of the literature indicates that several parameters have important effects on the dynamic response of unconsolidated sediments. Of these, some of the most important include: strain amplitude, vibration frequency, porosity, permeability, intergranular stress, grain shape, grain size distribution, grain material properties, and degree of saturation. In order to compare measurements of wave speed and attenuation, these parameters should be known. Of particular importance are stress, frequency, and porosity. If these are available with the measurements, intercomparisons are usually possible.

Observational Techniques

Available techniques for accurately measuring acoustic properties of unconsolidated sediments are often limited by the desire on the part of the investigator to be able to relate the observed acoustical response of the sample to the physical properties and stress conditions under which the measurements are performed. In general, a specimen with dimensions many times the wave-length of the propagating wave is necessary to determine attenuation accurately.[5] In the laboratory, this limits dilatational wave studies to frequencies of tens of kilohertz or more. If we wish to make dilatational attenuation measurements below these frequencies we must rely upon measurements taken in the field. These necessarily come with the complications of reflections or scattering which are due to the inhomogeneities

parameters and structure constant were determined empirically by seeking a "best fit" to the observed attenuation. Tests of various theoretical approaches to providing these parameters were conducted. It is felt that the results of this study will allow the Biot-Stoll model to become a more useful tool for the underwater acoustics community, by providing a basis for its range of applicability. The addition of a substantial set of measurements taken under carefully controlled and documented conditions should provide other researchers the means to further test and refine theoretical descriptions of the acoustical response of unconsolidated sediments.

been heretofore considered empirical; being estimated in conjunction with attenuation data.[6] The parameters in question are commonly known as the pore-size parameter, a, a parameter with the dimension of length that depends on both the size and shape of the pores; and the structure or coupling factor α, which accounts for the fact that not all of the fluid moves in the direction of the macroscopic pressure gradient because of the shape and orientation of the interstitial pore spaces.[9] The generally complex configuration of the pore spaces have made these parameters difficult to estimate a priori. However, research in related fields may shed some light on the nature of these two parameters. Various approaches to estimate them from sediment physical properties will be discussed in a later section of this paper.

In light of the foregoing discussions, the study reported here was initiated to determine the effect of grain shape and sorting on the frequency dependence of shear wave attenuation in unconsolidated water-saturated sediments. The results will add a substantial number of attenuation versus frequency values to the sparse set of shear wave data currently available. These data will also allow one to test the Biot-Stoll model's ability to predict the shear wave attenuation observed in simple and complex sediment assemblages. The required model inputs were carefully measured under the same stress conditions which prevailed during acoustic measurements. Having these measured input parameters eliminated the need to adjust sediment frame properties, thus allowing insight to be gained into the validity of the functions which account for the frequency effect on viscodynamic flow. Additionally, the pore-size

by the viscous model given a reasonable range of latitude in the specification of the sediment elastic frame moduli. Brunson and Johnson[21] showed good agreement between Biot-Stoll model calculations and the observed frequency dependence of shear waves in a saturated sand over a frequency range from 450 Hz to 7 kHz. Here, too, the sediment frame properties were adjusted within reasonable bounds to obtain good agreement.

In all of the cases cited, the data and model agree reasonably well if the sediment frame moduli are adjusted within reasonable bounds. However, for extrapolations or predictions of acoustical properties in areas where the available data are not amenable to this type of model "tuning," one would like to know that given accurate descriptions of the sediment physical properties, the Biot-Stoll model is capable of reproducing the observed acoustical properties of that sediment. This test would indicate the validity of the mathematical formulations of the dissipation processes included in the model. Especially troublesome are questions concerning the function which describes the effect of frequency on viscodynamic flow. This complex function, to be discussed in detail in a later section of this paper, was derived by Biot for an idealized capillary model, and predicts a non-linear relationship between attenuation and frequency with some wave speed dispersion apparent. Whether or not it is adequate in light of the tortuous and irregular flow paths present in real sediments should be demonstrated by carefully controlled experimental observations.

Another major difficulty in applying the Biot theory is the need to specify two input parameters which have

both empirical and dynamic relationships between the sediment constituents ar[illegible] properties.

A major obstacle to the more widespread use of the Biot-Stoll physical approach to sediment modeling is the lack of data to verify the model's validity when predictions are made for complex sediment assemblages over a significant frequency range.

Recently, comparisons have been made between predictions based on Biot theory and laboratory or field observations. Plona [15,16] appears to have verified the existence of dilatational waves of the "second kind" predicted by Biot theory, and seldom if ever observed in sediments because their amplitude is much smaller than the amplitude of the more common dilatational or compressional wave.[5] Stoll[10] has shown that viscous losses included in the Biot model are important in determining the overall attenuation observed in laboratory measurements of rotational wave speed and attenuation. Measurements were made using a torsional pendulum to measure attenuation and velocity over a range of frequency from 20 Hz to 1 kHz in both dry and water saturated silts and sands. Hovem and Ingram[17] have shown the model to be capable of correctly indicating the observed dispersion in compressional wave speed and attenuation in spherical glass beads over a range of frequency from 20 kHz to 300 kHz. The elastic parameters of the frame were adjusted to obtain agreement between the observed and calculated compressional speed at 100 kHz. They also show comparisons between compressional wave attenuation in sands reported by Nolle, et al.,[18] Hampton,[19] and Hamilton,[20] and calculated attenuation using the Biot theory. All observations appear to be well represented

The acoustic modeler requires the acoustical properties of the sediment, principally the density and body wave speeds and attenuations, as a function of location and depth in the seafloor. Often these properties are not available for a given location, or they have not been measured at the appropriate frequency for the problem at hand. The use of some "model," whether empirical or mathematical, is required to extrapolate the sediment properties from the location or frequency where information exists to the location or frequency where information is desired.

Either of the techniques described above may be used to do this. The important issue is which model can perform the required extrapolation in the most accurate manner given the available data. The empirical approach has been used quite effectively in acoustic modeling and numerous citations of Hamilton's empirical relationships may be found in the literature of underwater acoustic modeling. The mathematical or physical model has not received the same degree of acceptance.

While not a simple theory, the physical approach does allow one to predict the required acoustical properties of the sediments including their frequency and depth dependence.[8] The required model inputs are the physical properties of the sediment constituents and the effective stress conditions. Certain of these may be derived from others based upon empirical relationships between the various physical properties such as grain size, porosity, and permeability. Many of these properties are readily obtainable, for areas of interest, from sediment grab samples, cores, or drill holes. In this form the model becomes a hybrid, making use of

beads tended toward a one-fourth power pressure dependence. The measurements were reported for a range of pressures from 20 to 120 kPa, thus spanning the high and low pressure regimes reported by Hardin and Richart.[23] Shell Development Company shear wave speed data for dry and brine saturated sand have been reported by Hamilton.[36] The shear speed was found to vary as the one-fourth power of pressure for fine sands under pressures of 137 kPa to 2.3 MPa and for coarse sands from 686 kPa to 2.8 MPa confining pressure. Coarse sands under pressures from 137 to 686 kPa exhibited speeds which varied approximately as the three-tenths power of effective pressure. All of these measurements fall in the high pressure regime of Hardin and Richart. Domenico[25] obtained a one-fourth power variation of shear wave speed in dry and brine-saturated specimens of both Ottawa sand and glass beads over an effective confining pressure from 3 to 34 MPa.

Hamilton[36] recommends using a depth (pressure) exponent of one-fourth for prediction of shear wave velocities in sands. This recommendation is based upon both in situ and laboratory measurements. However, as we have seen from the data presented, there is considerable scatter in the pressure exponent with values varying from approximately 0.2 to 0.4 being reported in the literature.

Attenuation

Acoustic waves may dissipate energy as they propagate through unconsolidated porous materials as a result of a number of different mechanisms. The most important

of these are related to the two-phase nature of the transmission medium. The presence of solid grains surrounded by a fluid gives rise to the possibility of energy loss due to grain-to-grain friction as well as fluid-to-grain viscous interaction. The friction occurring at the grain contacts will dissipate energy whether or not there is fluid present in the sediment pore spaces. On the other hand, with fluid present in the pores, there is the possibility of viscous dissipation if there is any relative motion between the pore fluid and the skeletal frame. The resultant observed energy loss will reflect the combined effect of these two primary loss mechanisms plus any additional secondary effects that may contribute.

As discussed in the introduction, the complex interaction of these loss mechanisms results in damping which is dependent upon the sediment physical properties such as porosity, grain size, grain sorting, grain shape, and permeability; the degree of saturation; the amplitude of vibration; the effective intergranular stress; and the frequency of vibration. The data relating these conditions to acoustic wave damping are scarce, particularly for shear waves in unconsolidated sediments. For this reason we will consider their effects on both shear and compressional wave attenuation as reported in the literature of acoustics, geophysics, and engineering.

Morse[48] considered the effects of grain size, sorting, flow resistance, and frequency on compressional wave attenuation and speed. Using data reported by Ferrero and Sacerdote[49] and Nyborg, et al.,[50] Morse determined the attenuation to be dependent upon the grain size as reflected by the intergranular pore

size, with a frequency dependent effect apparently related to the pore size distribution resulting from a non-uniform particle size distribution. At high frequencies (high frequency being a relative term affected by the pore size radius, fluid density, and fluid viscosity)[11,12] the attenuation in large-grained well-sorted sands and lead balls was shown to vary as the square root of the product of the vibration frequency and the static fluid flow resistance. This static flow resistance included an empirical structure constant which accounted for the fact that not all fluid motion is in the direction of the macroscopic pressure gradient.

In a series of papers, Shumway[51-53] describes a set of compressional wave speed and attenuation studies performed using a resonant chamber to excite unconsolidated marine sediment samples. Frequencies between 20 and 37 kHz were used for the acoustic studies. He reported that absorption maxima were apparent when absorption versus median grain diameter or porosity was plotted. These maxima were observed for sediments of intermediate porosity (0.45-0.55) and grain size (.031-.250 mm; coarse silt-fine sands). The explanation offered was that the "acoustically effective" particle area was maximized in the intermediate porosity and grain size cases. This in turn lead to greater viscous losses at grain boundaries and in channels between grains as the fluid moved relative to the grains. Reported absorption values ranged from 0.15 dB/m in a medium clay at 28.4 kHz to about 6 dB/m for silts and fine sands at 30 to 37 kHz. Assuming the attenuation to be directly proportional to frequency raised to a power n, the data yielded a value of n equal to 1.799 with a standard deviation of 0.98. Hamilton[54] takes

exception to this frequency exponent, pointing out several indications of experimental errors which lead to variations in attenuation which are not supported by theory or experiments in similar materials.

McDonal, et al[55], measured acoustic attenuation in Pierre shale and concluded that absorption of shear and compressional waves were approximately linear with frequency over the range from 20-450 Hz. However, they also reported that the best power curve fit (in a least squares sense) to the compressional data yielded a frequency exponent equal to 1.4. In addition, the shear wave attenuation data showed a marked slope change above 100 Hz when plotted against vibration frequency. Busby and Richardson[56] reported compressional wave absorption at ultrasonic frequencies (0.5 to 3 MHz) for three grades of marine sands ranging from very fine to coarse (0.06 to 0.65 mm in diameter). The finest sands and a sediment composed of glass beads with a mean diameter of 0.12 mm showed attenuation proportional to frequency to the fourth power. This power law was not obeyed by larger grained sediment assemblages. It is probable, as Hamilton[54] has pointed out, that the observed frequency dependence is due to Rayleigh scattering since the acoustic wavelengths are approaching the size of the smallest grains.

Wyllie, Gardner, and Gregory[57] conducted an extensive set of measurements of elastic wave attenuation in consolidated porous media. Their purpose was to test the validity of the assumptions in the Biot[11-14] theory of wave propagation in porous media. They applied resonant bar measurement techniques at frequencies less than 20 kHz to dry and saturated sandstone

bars. They concluded that at low frequencies: the Biot theory appeared to be an appropriate description for losses due to the relative motion between the frame of the porous body and the fluid; the total dissipation in a porous body containing fluid is the sum of the dissipation due to frame inelasticity and that due to the relative motion of the frame and fluid; and the magnitudes of dissipation contributed by each mechanism is similar for porous rocks with permeabilities less than 5×10^{-9} cm^2. When permeabilities exceed that, the viscous mechanism is likely to dominate the frame anelasticity. At all frequencies, the effect of overburden pressure is to reduce the frame losses; its effect on viscous losses is smaller and results from pressure induced changes in porosity, permeability, and elastic properties of the rock.

Nolle, et al.,[18] reported the results of experimental studies of compressional wave propagation in water-filled quartz sand. The sand particles were grouped in size ranges representative of coarse, medium, fine, and very fine sands (0.1 to 0.7 mm diameter). For measurements over a frequency range of 400 kHz to 1.0 MHz, the attenuation was found to vary in a manner inversely proportional to the average particle radius and proportional to the square root of the acoustic frequency. As mentioned before, these data appear to be consistent with predictions obtained using the Biot theory as reported by Hovem and Ingram.[17]

Tests on Ottawa sand, glass beads, and quartz powder approximating a silt were run by Hall and Richart[58] to determine the effect of vibration amplitude, pore fluid, density, and grain size on compressional and torsional

damping. Vibration amplitude was the principal parameter studied. The logarithmic decrement, defined as the natural logarithm of the ratio of two successive amplitudes in an exponentially decaying sinusoidal wave, was found to vary as the 0.25 power of amplitude for dry Ottawa sand, with little variation indicated for the water saturated case. This indicates that the contribution to total damping due to water apparently increases at lower amplitudes. Additionally, the dissipation in both Ottawa sands and glass beads behaved like viscous damping. Tests in all three types of material showed the value of log decrement to decrease with decreasing grain size. The Ottawa sand showed less damping than glass beads of similar size and porosity at comparable confining pressures. This held true for compressional and torsional vibrations in both wet and dry specimens and was more pronounced in the dry cases.

Pressure and saturation effects on attenuation in consolidated and unconsolidated granular specimens were studied by Gardner, et al.[59] Comparisons were made between the torsional decrements of two sands with significantly different permeabilities. The two sands behaved quite differently as water was added to their pores. The high permeability sand showed a tenfold increase in log decrement as the saturation increased to 30 percent, becoming nearly constant beyond 60 percent saturation. In contrast, the low permeability sand showed little increase in log decrement until the degree of saturation reached approximately 40 percent; a rapid increase in dissipation as saturation increased to about 75 percent; and a reduced rate of increase in log decrement beyond. Since the comparisons were made

between samples under high confining pressures (about 5 MPa), the observations indicate that viscous losses are important in high permeability sediments at any degree of saturation, while grain to grain frictional losses predominate in low permeability sediments until a significant portion of the available pore space is filled with fluid. The nearly constant log decrement at low saturation in the low permeability sediments probably resulted from the inability of the grains to move relative to one another at the high confining pressures prevalent during the tests. These results were found to be consistent with what one would expect given the dissipation mechanisms included in Biot theory. Tests on dry sands indicated that log decrements were independent of both porosity and grain size and decreases only slightly with increasing pressure beyond approximately 750 kPa. The data indicated an overall dissipation decrease proportional to the one-sixth power of confining pressure. The log decrement versus overburden pressure plots did indicate that glass spheres are consistently more lossy than Ottawa sand, a conclusion agreeing with data previously cited.[58] Tests on dry limestone indicated a constant torsional log decrement and shear speed over the frequency range from 10 Hz to 20 kHz. These data coupled with log decrements measured at 3.6 Hz on the same material[60] led to the conclusion that decrements are constant for frequencies below 100 kHz for dry rocks. Wet sandstones showed a marked increase in log decrement with increasing water saturation at low overburden pressures, but tend toward the same decrement as the dry rock at high pressures (greater than 35 MPa).

Hardin[60] performed static and harmonic torsion tests on cylindrical specimens of dry sand to study the nature of viscous damping in such materials. For medium grain size (0.3 to 0.6 mm), angular sands at low confining pressures (21 to 92 kPa), and low frequencies (140 to 600 Hz), the decrements decreased as the 0.6 power of increasing pressure. Data taken at these low confining pressures are scarce and serve to assist in comparing other attenuation data taken at low overburden pressures by providing a means for extrapolating data to a common pressure.

In high frequency pulse measurements of compressional wave speed and attenuation in water-saturated sediments, Hampton[61] found attenuation to be proportional to frequency in a nonlinear manner. Sediments composed of pure kaolinite clay or kaolinite and sand up to 15 percent showed attenuation values ranging from 0.5 to 30 dB/m with a frequency exponent of 1.37 over the frequency range 4 to 600 kHz. Pure sand and kaolinite with greater than 30% sand showed attenuation from 4 to 100 dB/m with a frequency exponent of approximately 0.5 over the frequency range from 10 to 600 kHz. The sand data showed a sensitivity to mean grain size, with attenuation values being greater for smaller grained sands at a particular frequency. Some increase in the frequency exponent was indicated as the mean grain size decreased. These observations are in general consistent with predictions based upon Biot theory.

As will be discussed more thoroughly in a later section of this paper, the Biot[11,12] theory divides sediment response into "high" and "low" frequency regimes based upon pore fluid properties, sediment porosity, and

most importantly, sediment permeability. The "high" frequency regime is characterized by attenuation proportional to frequency raised to the 0.5 power. The "low" frequency regime is represented by a frequency exponent of two. There is no allowance made in the theory for a linear frequency dependence since the sediment frame is assumed to be elastic. Most clays fall in the "low" frequency regime by nature of their low permeability. Sand, on the other hand, is generally included in the "high" frequency category, certainly at frequencies in excess of 10 kHz. In actuality, the frequency exponent may be modified by a significant amount of grain-to-grain friction which is characterized by a first power frequency dependence.

In contrast to the results presented by Hampton, McLeroy and DeLoach[62] reported a linear frequency dependence of attenuation for five natural sediments ranging in size from a silty-clay to a beach sand over a frequency range from 15 kHz to 1.5 MHz. Values of the attenuation coefficient ranged from 0.2 dB/m at 15 kHz for silty-clay to 23 dB/m at 1.5 MHz for medium sand. They attribute the first power frequency dependence to the complex interaction of the viscous loss mechanisms at work over the entire "low" to "high" frequency conditions concurrently prevalent in a natural sediment with distributed particle and pore sizes. This conclusion is consistent with remarks by Shumway[53] about the frequency dependence of attenuation in natural sediments.

McCann and McCann[63] attempted to determine the range of particle sizes over which various candidate attenuation mechanisms would hold. They concluded that for

sediments of mean grain size less than 0.0156 mm (silt, clay) the attenuation is primarily due to viscous losses at the surface of the nonsurface active particles. For sediments of greater mean grain size one must consider both solid friction between the grains and viscous losses due to particle-fluid interaction. The results of acoustic attenuation measurements valid for a frequency range 5 to 50 kHz show the solid friction mechanism to dominate. This is particularly true when measurements are made for overburden pressures equivalent to a depth of burial of 2 m (approximately 12 kPa). The frequency exponent for the larger grained sediments varied from 1.0 for medium-silt to very-fine sands to 1.26 for fine sand.

Bore hole measurements of shear waves produced by a source located at the surface were reported by Kudo and Shima.[29] The waves were detected by borehole seismometers placed at various positions below the surface to depths of up to 43 m. The propagation medium consisted of semi-saturated water-laid sands, silts, and mudstones. They reported that the attenuation is approximately proportional to the first power of frequency from 10 to 90 Hz. The significance of these findings is clouded by the absence of sediment physical properties including degree of saturation, and the effects of overburden pressure on the attenuation coefficients.

Hardin and Drnevich[64] conducted shear modulus and damping experiments on clean sands and cohesive soils to determine the relative importance of several parameters which affect sediment acoustic response. The four most important parameters affecting damping in sediments were found to be strain amplitude, effective stress on the

sample, porosity, and the number of cycles of loading. The damping ratio, a measure of energy lost during one cycle of loading, was shown to increase with increasing strain amplitude; decrease at a rate proportional to the 0.5 power of effective mean stress; decrease with increasing porosity, especially at high mean effective stress levels (200 kPa); decrease as the log of the number of cycles of loading; and remain nearly constant over a frequency range of 0.1 to 38 Hz at a mean effective stress of 98 kPa.

Pilbeam and Vaisnys[24] reported measurements of acoustic velocities and energy losses in dry and lubricated spherical and angular granular aggregates. They found the specific attenuation factor 1/Q (equal to the log decrement divided by Pi), to be independent of vibration frequency for both torsional (shear) and extensional vibrations over a range from 1 to 20 kHz. Vibration amplitude had no effect on damping for vibration amplitudes not exceeding 10^{-4} cm. Lubrication generally increased relative energy losses. Dissipation was found to decrease as the 0.3 to 0.8 power of confining pressure below 0.1 MPa. Angular grains exhibited a lower torsional decrement than spherical glass beads of the same size under the same confining pressure.

Shirley and Hampton[26] reported the results of shear wave measurements on kaolinite clays using a transversely vibrating ceramic bender element. Data presented included shear wave attenuation as a function of shear wave speed for kaolinite clay during consolidation under the influence of gravity and interparticle attraction. For vibrations at 338 Hz, attenuation coefficients

varied from 180 dB/m at a shear wave speed of 6 m/sec to 100 dB/m at a speed of 16 m/sec.

Toksoz, Johnston, and Timur[65] presented the results of ultrasonic pulse laboratory measurements of attenuation in dry and saturated rocks. The measurements were made at ultrasonic frequencies (0.1 to 1.0 MHz) and differential pressures (confining pressure minus pore fluid pressure) from 100 kPa to 55 MPa. Results showed attenuation coefficients for both shear and compressional waves to increase linearly with frequency in both dry and brine saturated rocks. Attenuation in saturated rocks was shown to decrease with increasing differential pressure for saturated rocks. The rate of decrease was higher at low pressures, leveling off at high pressures.

Stoll[10] has reported the results of experimental studies of attenuation in sediments under torsional excitation. Dry and saturated samples of sediment ranging in grain size from silt to a coarse sand were excited over a frequency range of 34 to 391 Hz; under an axially applied stress ranging from 24 to 71 kPa; with peak-to-peak torsional amplitudes from 10^{-7} to 10^{-3} radians. For dry sand the logarithmic decrement increased with increasing amplitude, but tended toward a constant value as a function of frequency at low amplitudes. Wet sands showed increased log decrements for increases of both vibration amplitude and frequency. The change in log decrement as a function of sediment grain size (and hence permeability) was shown to be consistent with Biot theory as modified by Stoll[7] to include frame losses. The low permeability silts showed constant log decrements as frequency increased. This is equivalent to a linear or first power frequency dependence for

the attenuation coefficient. Highly permeable Ottawa sand samples, on the other hand, showed significantly increased log decrements with increasing frequency. The observed increase indicated an attenuation coefficient frequency exponent approaching two; an exponent consistent with a substantial viscous loss component due to grain-to-fluid relative motion. The medium-to-fine sands showed an intermediate degree of frequency dependence, indicating a mixture of frame and viscous losses.

Bell[27] has reported shear wave attenuation measurements in both dry and saturated glass beads and sands. Bender transducers similar to those used by Shirley and Hampton[26] were employed to excite transverse vibrations in the sediments at frequencies from 600 Hz to 20 kHz. He concluded that increases in grain angularity and overburden pressure led to significant increases in sediment rigidity and decreases in shear wave damping. Shear wave attenuation was linearly dependent on frequency for dry sediments. A linear variation of attenuation with frequency was approximately true for saturated sediments, but there was evidence of viscous damping in highly permeable samples.

Hovem and Ingram[17] have reported agreement between the Biot viscous theory and measurements of compressional wave attenuation in saturated glass beads at frequencies ranging from 20 to 300 kHz.

Shear wave attenuation as a function of frequency for a moderately-sorted, angular, medium grain, water-saturated-sand was reported by Brunson and Johnson.[21] Ceramic bender transducers were used to excite transverse

motion in the unconsolidated sediment over a frequency range from 450 Hz to 7 kHz. The attenuation values did not exhibit a simple first power frequency dependence. Comparisons with calculations using Biot theory as modified by Stoll showed consistency in both the amplitude and frequency dependence of attenuation.

Recently Winkler and Nur[66] have studied seismic wave attenuation in sandstones with particular attention focused on frictional sliding and fluid flow loss mechanisms. Sandstone bars were resonated at frequencies from 500 Hz to 9 kHz, and the effects of confining and pore pressure, degree of saturation, strain amplitude, and frequency were studied. Shear attenuation in saturated specimens decreased with increasing confining pressure, approaching a constant value above 30 MPa. Attenuation was nearly constant in dry sandstone at all pressures above 4 MPa. Log decrements for dry samples were nearly independent of frequency. Shear wave attenuation increased with degree of saturation, reaching a maximum at total saturation. Attenuation showed a distinct increase with frequency between 1 and 4 kHz for saturated samples, thus indicating the importance of fluid related loss mechanisms, especially at small differences between the confining pressure and the pore pressure. There was some indication of an attenuation peak at a particular frequency dependent upon the differential pressure on the specimen.

Summary of Current Understanding

In this review section we have considered some of the limitations on accurate determination of relation-

Suspension Models

One of the simplest suspension models is that formulated by Wood[74] for the speed of compressional waves in a composite medium consisting of an emulsion or suspension of solid particles in a continuous liquid phase. The theory assumes that the medium has no frame rigidity, i.e., that both the shear and frame bulk moduli are zero. The assumption is also made that, within an elementary volume, all constituents move together, so that the effective density is simply the volume-weighted average of the densities of the constituents:

$$\rho_e = n_f \rho_f + n_s \rho_s \qquad \text{(III-11)}$$

in like manner the effective bulk modulus is:

$$K_e = \left(\frac{n_f}{K_f} + \frac{n_s}{K_s} \right)^{-1} \qquad \text{(III-12)}$$

and the compressional wave speed in a two-component mixture of this type is:

$$V_p = \left[\frac{K_e}{\rho_e} \right]^{\frac{1}{2}} = \left[\left(n_f \rho_f + n_s \rho_s \right) \left(\frac{n_f}{K_f} + \frac{n_s}{K_s} \right) \right]^{-\frac{1}{2}} \qquad \text{(III-13)}$$

where

n_f, ρ_f, K_f are the volume, density, and bulk modulus of the fluid

n_s, ρ_s, K_s are the volume, density, and bulk modulus of the solid.

The fluid and solid volumes may be represented by the porosity, ϕ, since $n_f = \phi$ and $n_s = (1-\phi)$ in a two-component suspension. White[67] reviews several examples where

transverse (shear) wave disturbances. This characterization will be described in later chapters in conjunction with direct measurement of the physical and acoustic properties of laboratory sediments.

Scattering Models

At high frequencies where the wavelength of the acoustic disturbance approaches the size of the individual grains which comprise the sediment, acoustic scattering is the dominant loss mechanism. Busby and Richardson[56] observed absorption in sand at ultrasonic frequencies (0.5 to 3 MHz) to be proportional to the fourth power of frequency. Yamakawa[71] has shown the scattering of ultrasonic (f>1 MHz) compressional waves by spherical inclusions can be related to frequency to the fourth power and the cube of the inclusion radius. These same frequency and grain size relationships were used by Plona and Tsang[72] in a scattering theory representation of the attenuation in a granular porous material. In a study of attenuation mechanisms in dry and saturated rocks, Johnston, Toksoz, and Timur[73] have shown that scattering becomes an important and sometimes dominant attenuation mechanism for ultrasonic compressional waves propagating at frequencies in excess of one megahertz.

Since the work reported in this study is restricted to frequencies well below one megahertz, scattering will not be considered as an important mechanism influencing the acoustic properties of the sediments under investigation.

approach. They are generally supplied using empirical relationships.

Physical Sediment Models

Introduction

In porous, permeable sediments, three mechanisms are generally thought to account for most of the observed response of the sediment to acoustic waves; especially their attenuation. The three main mechanisms are scattering, frictional losses due to grain-to-grain contacts, and viscous losses due to the relative motion between the pore fluid and the grains or sediment frame. The observed properties generally result from the combination of all three mechanisms. However, under certain conditions for certain sediment types, one or two of the mechanisms may dominate. In order to assess the relative importance of these mechanisms, one would like to be able to relate the acoustic response of the sediment to the microstructure of the sediments in terms of the physical properties of the sediment constituent parts. This assessment may be carried out with the aid of one or more "physical sediment" models which are in reality mathematical models which account for the transfer and loss of acoustic energy as it propagates through the sediment assemblage.

In this section, we will examine various approaches to physically modeling sediment acoustic response. A discussion of the Biot theory as modified by Stoll will be presented. This will form the foundation for the application of this particular model's characterization of the response of porous, permeable, assemblages to

The equations which express the wave speeds in terms of the viscoelastic moduli take the form:

$$V_p^2 = \frac{(\lambda+2\mu)}{\rho} \frac{(1+r^2)^2}{(1-r^2)} \qquad \text{(III-7)}$$

$$V_s^2 = \frac{\mu}{\rho} \frac{(1+r^2)^2}{(1-r^2)} \qquad \text{(III-8)}$$

In Equations (III-7) and (III-8), the term $\frac{(1+r^2)^2}{(1-r^2)}$ accounts for velocity dispersion due to the anelastic nature of the material. If the damping is represented by $r<<1$, then the dispersion may be dropped, leaving us with the more familiar Hookean equations:

$$V_p^2 = \frac{(\lambda+2\mu)}{\rho} \qquad \text{(III-9)}$$

$$V_s^2 = \frac{\mu}{\rho} \quad . \qquad \text{(III-10)}$$

The implications of $r<<1$ are that the wave velocities, the specific attenuation factor, and the logarithmic decrement are independent of frequency if we assume the attenuation coefficient to be proportional to the first power of frequency.

These equations do not allow one to predict either attenuation or wave speed. Hamilton's approach is to use measured density and compressional wave speed together with an empirically derived sediment bulk modulus. These three constants allow computation of Lame's constants, the Poisson's ratio, and the shear wave velocity. No estimates of attenuation are generated using this

Equation (III-1) may be used to describe the behavior of either compressional or shear waves by inserting appropriate subscripts (p or s).

When energy damping is small (i.e., $\lambda' \ll \lambda$ and $\mu' \ll \mu$), then $r = aV/2\pi f \ll 1$ and the term $a^2V^2/4\pi f$ in the denominator of Equation (III-1) is negligible. The result is that Equation (III-1) reduces to the more familiar

$$\frac{1}{Q} = \frac{aV}{\pi f} \qquad \text{(III-2)}$$

$$\frac{1}{Q} = \frac{2aV}{\omega} = \frac{\Delta}{\pi} = \tan\theta \qquad \text{(III-3)}$$

Additionally,

$$\frac{1}{Q_p} = \tan\theta_p = \frac{\lambda'+2\mu'}{\lambda+2\mu} = \frac{\Delta_p}{\pi} \qquad \text{(III-4)}$$

$$\frac{1}{Q_s} = \tan\theta_s = \frac{\mu'}{\mu} = \frac{\Delta_s}{\pi} \qquad \text{(III-5)}$$

$$\alpha = 8.686a \qquad \text{(III-6)}$$

where:

Δ is the logarithmic decrement (natural log of the ratio of the amplitudes of two successive cycles of an exponentially decaying sinusoidal wave),

θ is the loss angle, and

α is the attenuation coefficient in decibels per unit length (e.g., dB/cm).

In the model, Lamé elastic moduli λ and μ are replaced by complex moduli, $\mu^*=\mu+i\mu'$ and $\lambda^*=\lambda+i\lambda'$, in which μ, λ, and the density, ρ, govern wave velocity and the imaginary moduli, $i\mu'$ and $i\lambda'$, govern energy damping. To illustrate the stress-strain relationships in this model we consider a sinusoidal wave for which, in a linear viscoelastic material, the strain will be out of phase with the stress. The stress can be vectorially decomposed into two components: one in phase with the strain and one 90° out of phase. For a shear wave, the complex modulus, $\mu^*=\mu+i\mu'$, represents this stress/ strain ratio. The phase angle, θ, which represents the anelastic energy damping is, in this case, $\tan\theta=\mu'/\mu$.

The basic derivation of this model may be found in Ferry[70] and White.[67] The resulting equations are presented by Hamilton[1] (for both shear and compressional waves with appropriate changes in notation) as:

$$\frac{1}{Q} = \frac{aV}{\pi f - a^2V^2/4\pi f} \qquad \text{(III-1)}$$

where

$\frac{1}{Q}$ is the specific attenuation factor, or specific dissipation function,

a is the attenuation coefficient,

V is the wave velocity, and

f is the frequency ($\omega=2\pi f$; circular frequency).

involved. When the dynamic behavior of a viscoelastic material is required for only a restricted region of frequencies, then the elasticity and viscosity obtained by modeling the observed behavior using a simple Voigt element may be useful in describing the properties of the material under the prescribed conditions. Both White[67] and Hamilton[69] cite examples which agree with the conclusions expressed by Kolsky.[68] If the purpose of a sediment "model" is to allow one to extrapolate acoustical properties of the sediment from a frequency where such properties are known to a frequency where information is required but unavailable, then the restrictions imposed on models such as the Kelvin-Voigt model render them of limited usefulness.

The Hamilton Viscoelastic Model

Hamilton[1,69] has presented a linear viscoelastic model selected to allow the geoacoustic modeler to understand the interrelationships between the elastic and viscoelastic moduli which describe the dynamic response of the sediment. In general, it is assumed that most marine sediments may be represented by a macroscopically isotropic two-phase system composed of sediment grains and water. The compressional and shear waves passing through the system are small sinusoidal stresses with wavelengths much larger than grain sizes. The mechanics of attenuation are not specified and provision is made for velocity dispersion and nonlinear dependence of attenuation on frequency. Those factors involving velocity dispersion and nonlinear attenuation are clearly identified and if negligible may be dropped from consideration.

Viscoelastic Models

The Kelvin-Voigt Model

The homogeneous viscoelastic model most generally recognized in connection with rocks and sediments is the Kelvin-Voigt solid model. This is often represented mechanically by a spring with a viscous dashpot in parallel. The arrangement leads to viscoelastic relationships in which the stress, instead of being directly proportional to the strain as is the case in Hookean elasticity, is proportional to the time rate of change of strain as well. Mathematically this is equivalent to replacing both Lame's constants, λ and μ, with the operators $\lambda + \lambda'(\partial/\partial t)$ and $\mu + \mu'(\partial/\partial t)$. The result is generally rather complicated equations where the compressibility, $K=(\lambda + 2\mu/3)$, and the shear rigidity μ, are used together with associated viscous constants $K'=(\lambda'+2\mu'/3)$ known as the dilatational viscosity, and μ', the shear viscosity. Solutions to such equations have been discussed by several authors, including White,[67], Kolsky,[68] and Hamilton.[69] Upon solving the equations describing a Kelvin-Voigt system one finds that for low frequencies the wave speed is constant while the attenuation varies as the frequency squared. At higher frequencies both speed and attenuation increase as the square root of frequency.[67] Kolsky[68] states that very few solids behave in a manner like that resulting from the Kelvin-Voigt model and that only a model encompassing a spectrum of relaxation times (e.g., by adding additional Voigt elements) can adequately define the dynamic behavior of actual materials. Such models are seldom used because the mathematics become extremely

III. THEORETICAL CONSIDERATIONS

Background

In the previous chapters we have cited the results of several studies designed to identify and quantify the relative importance of various physical mechanisms which affect the propagation of acoustic energy through sediment assemblages. In the present chapter we will attempt to fit these observations into the framework of mathematical theory.

The candidate theories can be divided into two broad categories depending upon the extent to which the porous medium is considered to be homogeneous. One approach considers the medium as a continuum with viscoelastic properties characteristic of the bulk material without regard to the constituents of the material. The acoustic response of the material is then described by complex moduli and relaxation functions which give results consistent with the observed behavior of real materials. The second approach assumes that wave propagation in the composite porous material depends upon the individual properties of the constituents and on the structural characteristics of the skeleton. Using the latter approach, one may relate the observed acoustic properties of the sediment to observable macroscopic physical properties of the sediment. These may include the densities and moduli (real or complex) of the fluid, solid, dry skeleton, and the composite saturated porous medium.

We have now discussed several observations of the acoustic behavior of sediments. In the next chapter we will discuss several theoretical approaches which have been proposed to describe the mechanisms which interact to bring about the observed behavior.

Permeability has been shown to significantly affect the magnitude and frequency dependence of shear wave attenuation.[10, 48,57,59] The viscous loss mechanisms included in the Biot theory are affected by the degree of mobility of the fluid. Wyllie, et al.,[57] have concluded that for permeabilities greater than 5×10^{-9} cm^2 the viscous losses in a fluid-saturated specimen dominate the frame losses.

Whether losses are attributable to grain-to-grain friction, or fluid-to-grain viscous losses, shear wave attenuation increases with increasing frequency. The frequency of vibration becomes more important for highly permeable, saturated sediments. When conditions are such that viscous losses dominate, the frequency dependence of attenuation can become non-linear.

The importance of grain shape, size, and sorting is included in effects attributable to porosity and permeability. Grain shape, size, and sorting are important factors in determining the porosity and permeability of a particular sediment. These properties in turn determine the degree to which viscous or grain-to-grain friction loss mechanisms are manifest. A key element in this paper is to determine whether a model such as the one proposed by Stoll[5-10] based on Biot theory[11-14] is capable of predicting shear wave attenuation for a sediment composed of angular, non-uniform grains.

The degree of saturation is important since it determines the amount of available pore space occupied by fluid which is in turn capable of moving relative to the sediment grains. The degree of mobility is a function of the permeability of the sediment assemblage.

Parameters thought to be very important to shear wave damping or attenuation include strain amplitude, effective stress, porosity, permeability, vibration frequency, and the degree of saturation.

The effects of strain amplitude on attenuation have been reported by several authors[10,24,58,64,66] with attenuation increasing as strain amplitude increases beyond 10^{-6} for both sand and cohesive soils.

Stress is also shown to be very important in determining the magnitude of shear wave attenuation.[24,27,57,59,60,63,64,65,66] The effect of increasing effective intergranular stress is to reduce the frame or grain-to-grain frictional losses, with the effect on viscous losses being smaller and resulting from pressure induced changes in porosity, permeability, and sediment properties. The attenuation decreases in proportion to the mean effective pressure raised to some power. The exponent of pressure is reported to range from 0.17 to 0.8 with the rate of decrease in attenuation higher at low pressures, leveling off at high pressures.

The effect of void ratio on shear attenuation is difficult to isolate due to its relationship to grain size, shape, sorting, and permeability. Shumway[51-53] reports an increase in absorption with increasing porosity (0.45-0.55). This maximum or "plateau" of absorption is shown to exist between 0.35 and 0.47 for attenuation measurements taken in both cohesive and cohesionless sediments under "low" pressures (49 kPa), but attenuation decreases with increasing porosity between 0.34 and 0.67 for samples under "high" pressure (200 kPa).[64] Gardner, et al.,[59] report no porosity dependence for attenuation in dry sands.

The fact that the effective stress on a sample impacts the shear speed is evident from several of the studies cited earlier in this paper. The magnitude of that impact on speed has been shown to be approximately proportional to the 0.25 power of overburden pressure. These relationships have been discussed in terms of the shear modulus and appear as empirical Equations (II-1), (II-2), and (II-3) of this report. There is considerable scatter in the data, however, and exponents of pressure ranging from about 0.2 to 0.4 have been reported in the literature.

The degree of saturation has been shown to impact the shear speed in cohesive soils with little effect on clean sands.[64] The shear modulus for a silty-clay was shown to decrease by a factor in excess of two when the degree of saturation increased from 70 to 100 percent.

The impact of porosity (or void ratio) on the shear modulus has been reviewed in several references [46,64] and may be characterized by the function

$$G \propto (e) = \frac{(2.973-e)^2}{1+e} \qquad \text{(II-4)}$$

where e is the void ratio and may be related to the porosity ϕ by $e=\phi/(1-\phi)$. From equation (II-4) we may see that the shear modulus decreases with increasing void ratio or porosity. This function has been incorporated into empirical equations [Equations (II-2) and (II-3)] which allow investigators to characterize the effect of stress on shear modulus.

The other parameters identified above are considered to be less important in their impact on shear speed.

ships between acoustic and physical properties of unconsolidated sediments. Nonetheless, certain laboratory and field techniques have allowed investigations of the effect of several important parameters on the dynamic response of such sediments. Of greatest interest to us are the results of recent shear and compressional wave speed and attenuation studies. These have been thoroughly reviewed. While the emphasis of this paper is on shear waves, some compressional wave studies were discussed because of the scarcity of shear wave data. This is particularly true for shear wave attenuation in unconsolidated sediments.

The parameters which are most important to acoustic propagation through sediments have been identified as strain amplitude, vibration frequency, porosity, permeability, effective intergranular stress, grain shape, size, and material properties, and the degree of saturation. In this section, we will attempt to summarize the effects of the most important of these parameters on wave speed and attenuation.

Shear wave speed (or modulus) appears to be most affected by the dynamic strain amplitude, the effective intergranular stress, the degree of saturation, and the porosity (or void ratio).

Stoll[5] showed that for cyclic shear strain amplitudes less than 10^{-5} the shear wave velocity in clean dry sands approaches asymptotic values that are essentially independent of amplitude. This observation was confirmed by Hardin and Drnevich[64] who cited similar results from several sources, including data from measurements on cohesive soils in addition to sands.

the Wood equations [Equations (III-11)-(III-13)] have been used to fit observations. Nafe and Drake[75] and Sutton, et al.,[76] found the equations to provide good estimates of the observed speeds in high-porosity ocean sediments. Shumway[77] used the Wood equations to fit experimental data on the temperature dependence of sound speed in several water-saturated sediments; but for fine-grained sand, especially, the rigidity of the sediment skeleton should not be discounted. Wyllie, et al.,[57] and Shirley and Bell,[78] reported that speeds in fluid-saturated aggregates of grains were generally higher than speeds calculated from the Wood equation. White[67] concludes that while the Wood equation [Equation (III-13)] adequately accounts for observed compressional speeds in emulsions and suspensions, the simplicity of the model does not allow its application to fluid-saturated media in which the concentration of grains is sufficient to produce significant grain-to-grain contact resulting in a skeletal frame with appreciable rigidity.

Hovem[79] has reviewed and modified a theoretical model based on scattering theory for sound propagation in a suspension that was first formulated by Urick[80] and later by Urick and Ament.[81] The model accounts for attenuation due to monopole and dipole scattering of plane waves from spherical particles which are randomly distributed in a fluid. In the low frequency limit the scattering model yields the same speeds as the Wood equation. Hovem[79] showed the scattering suspension model to overestimate attenuation and speed as particle concentration and frequency increased. The attenuation discrepancy was said to be due to the model's basic assumption that attenuation increases linearly with

concentration. Since an increase in particle concentration will cause the flow around a single particle to be influenced by those particles in close proximity to it, the net effect is a reduction in viscous attenuation as the flow resistance is significantly increased. This is in contrast to the Urick-Ament model assumption that the flow around a single particle is completely unaffected by the presence of other particles.[79] Corrections were made to the model, and in a later paper, Hovem[82] shows better agreement between his modified suspension model and attenuation data reported by Hampton[19] and Urick.[80]

Even though the above suspension models have met with some success in being able to reproduce speed and attenuation observations for a limited class of sediment and sediment-like assemblages, they still have in common the assumption that the medium has no frame rigidity, i.e., that both the shear modulus and the frame bulk modulus are zero. The only loss mechanism is the viscous loss due to grain-fluid interaction.

White[67] once again provides a summary of the theoretical treatments which have been used to introduce some skeletal effects to the description of a fluid-filled porous medium. Gassman[83] is generally cited when reference is made to expressions which include skeletal effects in describing the interactions between the two constituents of a saturated porous medium. He formulated a "closed system" model in which no movement of pore fluid is allowed in or out of a unit volume, thus there is no significant relative motion between the fluid and the skeletal frame. The effective density, ρ_e, is the sum of the mass of fluid and solids in a

unit volume, and the effective bulk modulus, K_e, is a composite of the bulk moduli of the solid, fluid, and frame given as:

$$K_e = K_s \frac{K_c+K_q}{K_s+K_q} \qquad K_q = \frac{K_f(K_s-K_c)}{\phi(K_s-K_f)} \qquad \text{(III-14)}$$

where

K_e = "effective" bulk modulus of sediment
K_s = bulk modulus of solid grains
K_f = bulk modulus of pore fluid
K_c = bulk modulus of dry frame or skeleton
ϕ = porosity of sediment

Gassman's expressions for the shear and compressional speeds of such a sediment, assuming an isotropic saturated medium are:

$$V_p = \left(\frac{K_e+4\mu_e/3}{\rho_e}\right)^{\frac{1}{2}} \qquad \text{(III-15)}$$

$$V_s = \left(\frac{\mu_e}{\rho_e}\right)^{\frac{1}{2}} \qquad \text{(III-16)}$$

where

$\rho_e = \phi\rho_f+(1-\phi)\rho_s$, and
$\mu_e = \mu_c$, the frame shear modulus.

Using Gassman's equations one may calculate the speeds of acoustic waves in saturated sediments if the moduli of the individual sediment components are known. The bulk moduli of the fluid and grains are readily

obtainable, but the moduli of the frame are somewhat more difficult to come by. White[67] suggests that they may be obtained by static distortion of the unsaturated medium. Other methods include measurements of shear and compressional wave speeds assuming that Hookean elastic relations hold; and the use of empirical relationships such as those proposed by Hamilton[84] between the frame bulk modulus and porosity.

To introduce frame attenuation into models such as Gassman's we resort to the assumption that there are significant frictional losses at the grain contacts. White[67] has reviewed the work done, both theoretical and experimental, in various packings of spherical particles. He concludes that one must consider the static or "sticking" friction as well as the dynamic or "sliding" friction at grain contacts in order to reconcile theoretical predictions with experimental observations. In actuality, although one may achieve some qualitative understanding of frictional losses at grain contacts, including estimates of frequency dependence, quantitative results are hampered by a lack of knowledge of several parameters. These include static and dynamic friction coefficients, normal and tangential stresses at grain contacts, and the nature of the contacts themselves. Therefore, we are forced to determine the magnitude of frame losses due to friction and other mechanisms by experimental observation of losses in unsaturated porous media.

The Biot-Stoll Physical Sediment Model

Another approach to sediment modeling has been pursued by Stoll and described in a series of papers[5-10] spanning

nearly a decade. Stoll builds upon a general theory of acoustic propagation in porous media developed by Biot[11-14] based on earlier work by Zwikker and Kosten[85] and Morse.[48] This theory allows for relative motion to occur between the fluid which fills the pores of a saturated sediment and the skeletal frame of the sediment. The result of such relative motion is a viscous loss which is highly dependent upon the ability of the fluid to move through the sediment, an ability which is related to certain physical properties of the sediment such as permeability. This model predicts a slight dispersion in the wave propagation speeds and a non-linear relationship between attenuation and frequency. When no relative motion between fluid and frame exists, Biot's equations reduce to those of Gassman,[83] as reported by Geertsma and Smit.[86]

The theory developed by Biot[11-14] is a comprehensive description of the acoustic response of linear, porous materials containing compressible fluid.

Biot's theory predicts that in the absence of boundaries, three kinds of body waves may exist in a fluid saturated porous medium. One of the compressional waves, which is called the "first kind," and a shear wave are akin to those body waves found in ordinary elastic media. The "second kind" of compressional wave is highly attenuated in a manner similar to a diffusion process. These compressional waves of the "second kind" may be important in acoustical problems involving very compressible fluids like air or perhaps in very gassy sediments where the effective compressibility of the pore fluid has been greatly reduced due to the presence of dissolved or free gas. For most geophysical applications,

especially in unconsolidated sediments, compressional waves of the "second kind" are not important, and are not considered in this study.

When relative motion between the sediment frame and the pore fluid is allowed, the predicted values of speed and attenuation depend upon frequency. At low frequencies, the flow in the pores is laminar, the speed is essentially constant, and the attenuation varies as the square of the frequency. At high frequencies, the flow pattern is complex, the speed is again approximately constant, although higher than at low frequencies, and the attenuation varies as the square root of the frequency. At intermediate frequencies, a transition zone exists. The details of the frequency dependence in the transition zone depend upon the compressibility and viscosity of the fluid and the moduli and permeability of the sediment frame. Hovem[82] has also shown a dependence on the grain size distribution in very porous, near-suspensions. The frequency dependence of compressional wave speeds is more pronounced than shear wave speeds for the same sediment. The solution on which the frequency dependence of fluid flow resistance is based is valid for frequencies where the wavelength is large compared to the intergranular pore size. For sands, this puts the upper limit on frequencies at about 10^6 Hz, which is high enough to cover the frequency range of interest in most geophysical applications.

The initial Biot formulation[11,12] assumes a perfectly elastic sediment frame. To accommodate the observed loss presumed to be primarily due to frictional forces at the grain-to-grain contacts between particles,

Stoll[7-10] has regarded the bulk and shear moduli of the sediment assemblages as slightly nonlinear or complex constants with small imaginary parts. The bulk moduli of the individual grains and the fluid remain as elastic constants. This leads to a physically realistic model of a saturated sediment capable of accounting for both frictional and viscous losses in sediments of differing properties across a broad frequency range.

A mathematical formulation of the Biot sediment model incorporating the modification and notation presented by Stoll[8] follows below.

Assuming that the response of the framework of sediment particles in a fluid environment can be described by a set of constitutive relationships of the form (using tensor notation for brevity in presentation).

$$\tau_{ij} = 2\mu^* e_{ij} + \delta_{ij} \cdot [(H-2\mu^*)e - C\zeta] \qquad \text{(III-17)}$$

$$P = M \cdot \zeta - C \cdot e \qquad \text{(III-18)}$$

where τ_{ij} and e_{ij} are the stress and strain components, respectively, of an element of volume attached to the sediment frame; P is the pore fluid pressure; H, C, M and μ^* are linear or "slightly non-linear" operators that characterize the elastic and inelastic response of the frame; and δ_{ij} is the Kronecker delta. The volumetric strain of an element attached to the frame is represented by e, the divergence of the frame displacement, and ζ, the volume of fluid which has flowed out of the element:

$$\zeta = \phi \, \mathrm{div}(\vec{u}-\vec{U}) \ , \qquad \text{(III-19)}$$

where ϕ is the porosity, $\tilde{u}$ is frame displacement, and $\tilde{U}$ is fluid displacement.

Combining these constitutive relationships with the equation describing the motion of the fluid relative to the frame and the stress-equation of motion for the volume attached to the frame, Stoll derived the equations of motion governing the propagation of compressional and shear waves in the sediment. For the compressional motion of the frame,

$$\nabla^2(He-C\zeta) = \frac{\partial^2}{\partial t^2}(\rho e-\rho_f\zeta) \qquad \text{(III-20)}$$

For the motion of fluid relative to the frame,

$$\nabla^2(Ce-M\zeta) = \frac{\partial^2}{\partial t^2}(\rho_f e-m\zeta) - \frac{\eta}{k}\frac{\partial \zeta}{\partial t} \qquad \text{(III-21)}$$

Similarly for shear waves the motion of the frame is described by,

$$\mu^*\nabla^2\tilde{w} = \frac{\partial^2}{\partial t^2}(\rho\tilde{w}-\rho_f\tilde{\theta}) \qquad \text{(III-22)}$$

and for shear motion of fluid relative to the frame,

$$\frac{\eta}{k}\frac{\partial\tilde{\theta}}{\partial t} = \frac{\partial^2}{\partial t^2}(\rho_f w-m\tilde{\theta}) \qquad \text{(III-23)}$$

where $\tilde{w}$ is the curl of the frame displacement vector $\tilde{u}$; $\tilde{\theta}$ is a function of the porosity $\emptyset$ and the displacement vector of the frame $\tilde{u}$ and the fluid $\tilde{U}$; ρ is the total mass density; ρ_f is the fluid mass density, and m is a tortuosity factor which will be discussed later.

Solutions for e and ζ are assumed to be of the form

$$e = A_i e^{i(\omega t - \ell x)} \qquad \text{(III-24)}$$

and

$$\zeta = A_2 e^{i(\omega t - \ell x)} \qquad \text{(III-25)}$$

while $\tilde{w}$ and $\tilde{\theta}$ take the form

$$\tilde{w} = A_3 e^{i(\omega t - \ell x)} \qquad \text{(III-26)}$$

and

$$\tilde{\theta} = A_4 e^{i(\omega t - \ell x)} \qquad \text{(III-27)}$$

where ℓ is the wave number and ω is the circular frequency. Substituting Equations (III-24) and (III-25) into Equations (III-20) and (III-21) results in two equations in A_1 and A_2. If solutions exist for A_1 and A_2, it must hold that the determinant of the coefficients for A_1 and A_2 equals zero.

Stoll presents the determinant relation:

$$\begin{vmatrix} H\ell^2 - \rho\omega^2 & \rho_f\omega^2 - C\ell^2 \\ C\ell^2 - \rho_f\omega^2 & m\omega^2 - M\ell^2 - i\frac{\omega F\eta}{k} \end{vmatrix} = 0 \; . \qquad \text{(III-28)}$$

A solution for the complex wave number ℓ will yield the phase velocity (from the real part) and the absorption (from the imaginary part) for the two kinds of compressional waves.

A similar substitution of Equations (III-26) and (III-27) into Equations (III-22) and (III-23) leads to a determinant for the coefficients of A_3 and A_4 equal to:

$$\begin{vmatrix} \rho\omega^2 - \mu^* \ell^2 & \rho_f \omega^2 \\ \rho_f \omega^2 & m\omega^2 - \frac{i\omega F\eta}{k} \end{vmatrix} = 0 \quad . \qquad \text{(III-29)}$$

The solution for the complex wave number ℓ in this case yields the phase velocity (from the real part) and absorption (from the imaginary part) for the shear wave.

If the determinant in Equation (III-28) is reduced, we obtain the following fourth order complex equation

$$a_1 \ell^4 + a_2 \ell^2 + a_3 = 0 \qquad \text{(III-30)}$$

Similarly, the reduction of the determinant in Equation (III-29) yields the second order complex equation

$$b_1 \ell^2 + b_2 = 0 \qquad \text{(III-31)}$$

The constants a_1, a_2, a_3, b_1, and b_2 are complex and defined as follows:

$$a_1 = C^2 - HM \quad , \qquad \text{(III-32)}$$

$$a_2 = (Hm + \rho M - 2C\rho_f)\omega^2 - i\frac{\omega F\eta}{k} H \quad , \qquad \text{(III-33)}$$

$$a_3 = (\rho_f^2 - \rho m)\omega^4 + i\frac{\omega^3 F\eta}{k} \rho \quad , \qquad \text{(III-34)}$$

$$b_1 = -\mu^* m\omega^2 + i\frac{\omega\mu^* F\eta}{k} \qquad \text{(III-35)}$$

$$b_2 = (\rho m - \rho_f{}^2)\omega^4 - i\frac{\omega^3 F\eta}{k}\rho \ , \qquad \text{(III-36)}$$

We see from Equations (III-34) and (III-36) that

$$b_2 = -a_3 \ . \qquad \text{(III-37)}$$

In Equations (III-32), (III-33), (III-34), (III-35), and (III-36), ρ is the saturated sediment density; ρ_f is the density of the pore fluid; k is the sediment permeability; η is the fluid viscosity; ω is the circular frequency, $2\pi f$. The complex constants C, H, and M are functions of fluid, frame, and grain bulk moduli (K_f, K_C, and K_S, respectively), frame shear modulus μ^*, porosity $\emptyset$. They have been made complex to account for the frame inelasticity. This has been done by assuming the frame bulk modulus, $K_C^* = K_C + iK_C'$, and frame shear modulus, $\mu^* = \mu + i\mu'$, to be complex with small imaginary parts. These constants are defined by Stoll[8] as follows:

$$C = \frac{K_S(K_S - K_C^*)}{D - K_C^*} \qquad \text{(III-38)}$$

$$H = \frac{(K_S - K_C^*)^2}{D - K_C^*} + K_C^* + \frac{4\mu^*}{3} \qquad \text{(III-39)}$$

$$M = \frac{K_s^2}{D - K_c^*} \qquad \text{(III-40)}$$

where

$$D = K_s \left[1 + \phi \left(\frac{K_s}{K_f} - 1 \right) \right] . \qquad \text{(III-41)}$$

The term $\frac{F\eta}{k}$ has replaced $\frac{\eta}{k}$ and is used to account for frequency dependent viscous effects by applying the complex correction, F, to the fluid viscosity, η. This factor was derived by Biot[14] by considering the actual microvelocity field that exists within the pore channels and considering the ratio of the friction force exerted by the fluid on the frame to the average relative velocity for oscillatory motion to be $\phi^2 F \eta / k$. The correction factor is a function of κ, where

$$F = F(\kappa) = \frac{1}{4} \frac{kT(\kappa)}{1 - \frac{2T(\kappa)}{i\kappa}} \qquad \text{(III-42)}$$

$$\kappa = a(\omega \rho_f / \eta)^{0.5} \qquad \text{(III-43)}$$

and

$$T(\kappa) = \frac{\text{ber}'(\kappa) + i\, \text{bei}'(\kappa)}{\text{ber}(\kappa) + i\, \text{bei}(\kappa)} \qquad \text{(III-44)}$$

The functions ber(κ) and bei(κ) are real and imaginary parts of the Kelvin function. The functions ber'(κ) and bei'(κ) are the derivatives of the Kelvin functions.

To account for the unknown nature of the pore size and shape, the parameters a [in Equation (III-43)] and m [in Equations (III-33)-(III-36)] are introduced. The parameter a has the dimension of length and depends upon both the size and shape of the pores and can be related to grain size, permeability, and porosity. The parameter m is defined as:

$$m = \alpha\rho_f/\emptyset \qquad \alpha \geq 1 \tag{III-45}$$

This parameter, always greater than $\rho_f/\emptyset$, has been substituted for $\rho_f/\emptyset$ in Equations (III-21) and (III-23) to account for the fact that not all of the pore fluid moves in the direction of the macroscopic pressure gradient because of the tortuous, multi-directional nature of the pores. As a result, less fluid flows in or out of an element for a given acceleration than if all the pores were uniform and parallel to the gradient. This appears as an increase in the fluid inertia. Stoll[7] states that for uniform pores with axes parallel to the pressure gradient, α would equal one, while for a random system of uniform pores with all possible orientations the theoretical value of α is three. In practice, α is treated as an empirical parameter. The essential difference between a and m is in their usage; m has an inertial effect on the fluid flow, reducing this flow for the more random pore orientation; a affects the viscous resistance to fluid flow and results in an increased attenuation for high frequencies.

To evaluate the solutions of the compressional wave and shear wave determinants, Equations (III-28) and (III-29), one must specify values for thirteen physical parameters. The parameters are listed in Table III-1.

The solutions result in predictions of the phase speeds and absorption for the two types of compressional waves and the shear wave which propagates through a fluid saturated porous medium. Accommodations have been made to allow for frame inelasticity, thus predictions may be made for unconsolidated sediments. The predictions may be made at frequencies of interest as long as the basic assumption that the acoustic wavelength remains large compared to the intergranular pore size is valid. This allows predictions for frequencies up to approximately 10^6 Hz for sands with higher frequencies for smaller grained sediments typical of deep sea silts and clays.

For a given application, if both shear and compressional wave speeds and attenuations are desired, values for the thirteen parameters in Table III-1 must be provided; yet, direct measurement of all thirteen are rarely, if ever, available. Those parameters not directly measured can be assigned values in two ways. The unavailable parameters can be derived using their physical (i.e., theoretical) relationships to some or all of the measured parameters. The unavailable parameters can also be obtained empirically, either from the measured parameters or from other information available for the sediments being studied. Porosity and grain size distribution are two of the most useful properties from which many of the needed parameters may be derived.

water. This left a totally saturated column of densely packed sediment of measurable height across which shear waves could be propagated. Repeating this filling procedure results ir a path length change but retains the same packing and saturation conditions from step-to-step. The goal of this procedure was to maintain a constant porosity and total saturation throughout each acoustic measurement cycle. This was achieved and documented as part of the data recorded for each measurement.

Having attained control of the sediment properties through the choice of the sediment container and filling procedure, there remained the need to reproduce the coupling and stress conditions. Other investigators have documented the importance of maintaining a known or at least consistent stress condition. Stoll[5] has mentioned effective stress as one of the most important factors to be considered in making or interpreting acoustic measurements in sediments. This is particularly true at very low intergranular stress levels such as those due to overburden pressure corresponding to a small depth below the seafloor. Since the measurements reported in this study were taken in a vertical column which might lead to important vertical gradients of intergranular stress, a constant load of 2 kg was added to the projector which rested on the surface of the sediment column. This load served to stabilize the effective normal stress in the sediment column, overpowering, by comparison, the vertical gradients due to the sediment column itself. An additional attraction was the stabilization of the projector-to-sediment coupling, rendering it much less sensitive to the small

transducers-to-sediment coupling, sediment saturation, sediment packing, and effective stress. The ability to monitor and control these measurement conditions played an important role in the technique adopted.

The control and monitoring of the degree of sediment saturation and sediment packing was achieved through the use of a long cylindrical tube as a container for the propagation medium.

Given the cross-sectional area of the tube and the total length of the propagation path formed by the propagation medium, one can easily calculate the total volume of saturated sediment. If the weight of the solid grains in the sediment is known, then, given the density of the material comprising the grains, one may calculate the volume of the solid in the saturated sediment. This allows one to calculate the volume of the interstitial pores, and thus the porosity. If one measures the net volume of water introduced into the sediment, then the percent of the available pore space filled by water may be calculated, resulting in a determination of the degree of saturation.

The reproducibility of sediment packing and hence porosity for each series of measurements for a given sediment was achieved by mounting the cylinder vertically and vibrating the sediment sample in the tube to its densest state. The filling procedure to achieve a change in propagation path length consisted of adding a known volume of water to the vertical cylinder, adding a known volume of sediment to the water, vibrating the cylinder with a vibrator until no further sample compaction was observed, and then withdrawing the excess

reference medium of the same dimensions (i.e., path length) and compare the arrival times and amplitudes of the acoustic signals which have traversed the two transmission media. In the absence of interference one then has an absolute estimate of the speed and attenuation of compressional waves in the sample of interest for the environmental conditions prevailing during the measurement. Distilled water is a readily available standard for compressional wave measurements in porous saturated transmission media.

Unfortunately, this approach is not available to the shear wave experimentalist. There are no calibrated shear wave transducers. While one may calculate the transverse deflection of a piezoceramic bender element given a voltage potential impressed across the faces of the element, this is of little use during actual measurements. The mounting has an unknown effect on the response of the element. In addition, there is an unknown coupling factor with which to relate the amplitude of the motion of the granular propagation medium to the motion of the shear wave transducer face in either the projector or receiver mode. To further complicate the measurements there do not presently exist any standard propagation media with properties similar to an unconsolidated sediment.

The lack of calibrated transducers or standard propagation media required the development of a measurement technique which would allow the measurement of the transverse vibration amplitude of the propagation media as a function of changing transducer separation. In order to make such a measurement meaningful, each measurement had to be done under the same conditions of

Transducers

The design of the transducers was driven by a desire to attain the frequency range required, produce consistent signals with a minimum of electrical or compressional wave interference, and efficiently couple the transverse vibrations of the transducer into a granular medium. Investigations by the author,[21] together with work reported by researchers at the Applied Research Laboratories, University of Texas, Austin,[26-28] led to a transducer design capable of producing the transverse vibrations required in the experiment. Detailed discussion of the transducer design and their integration into a measurement system will be presented in a later section of this chapter

Measurement Technique

The measurement of shear waves in porous granular media present some challenges which are not normally faced in compressional wave measurements. For compressional waves, calibrated acoustic transmitters and receivers are readily available. With these one may readily determine the attenuation and speed of propagation of compressional waves knowing only the driving and receiving voltage levels and the propagation path lengths. Such measurements have been performed on innumerable propagation media at various temperatures, pressures, and frequencies. Given a propagation medium for which sound speed and attenuation as functions of temperature, pressure, and frequency have been determined, one may use this medium as a reference standard. In order to determine the speed and attenuation for a sample of interest one has only to replace the sample with a

The practical limitations on the frequency range selected included the length of the sample which could be accommodated in the laboratory, together with the ability to produce shear waves at the desired frequency. Previous work had shown that low frequency shear waves (< 500 Hz) could be produced, but the precision of the attenuation measurements was poor.[21] The low attenuation at such low frequencies (< 5 dB/m) together with the long wavelengths (> 20 cm) resulted in significant interference effects. These made attenuation values at such low frequencies, obtained over pathlengths shorter than one meter, of limited usefulness; particularly when attempting to verify a theoretical model. For these reasons, the measurements in this study were limited to frequencies equal to or greater than 1 kHz. At the other end of the spectrum, the upper frequency limit was determined by the ability to produce transverse (shear) vibrations of sufficient amplitude to be detectable across reasonable sediment path lengths. With earlier measurements[21] indicating attenuation coefficients exceeding 100 dB/m at 7 kHz, the expected upper limit could be no more than a few times that frequency. The choice of 20 kHz allowed measurements to span more than a decade of frequency with sufficient signal to noise ratio to allow high quality determination of the attenuation coefficient at all frequencies sampled.

Thus, the frequency range used in this investigation, 1 to 20 kHz, resulted from the consideration of both theoretical and practical factors.

type appropriate to the desired experiments. With speeds variously reported as 100 m/sec,[27,28] a 1 kHz shear wavelength would be 0.1 m. Attenuation of waves such as these can be measured. An additional property of shear waves, their relatively high attenuation, allows accurate determination of that attenuation over moderate propagation path lengths.

Frequency Range

The Biot theory predicts a change in the frequency dependence of attenuation as the nature of the fluid flow in the interstitial pores changes from Poiseuille flow, where the viscous resistance to fluid flow given by the ratio of fluid viscosity to sediment permeability, η/k, is approximately constant, to a potential flow with the effects of viscosity felt only in a thin boundary layer which is a function of frequency and the properties of the fluid. According to Biot[11] the assumption of Poiseuille flow breaks down when the quarter wavelength of this boundary layer is of the order of the diameter of the interstitial pores, d. Biot suggests that this breakdown of Poiseuille flow occurs at a frequency of about

$$f_t = \frac{\pi\eta}{4d^2\rho_f} \qquad \text{(IV-1)}$$

For water at 15°C, this gives a value of $f_t=10^2$ Hz for $d=10^{-2}$ cm, and $f_t=10^4$ Hz for $d=10^{-3}$ cm.[6,11] Using these values as guidelines, measurements were planned to span a frequency range from about 1 kHz to greater than 10 kHz.

of interest include porosity, grain density, permeability, grain size distribution, and certain frame properties which can be derived from acoustic measurements of speed and attenuation in the dry sediment.

As a result of the above considerations, an angular sand was selected for the moderately-sorted sediment, a subset with the same mean grain size was prepared by sieving the angular sand, and an assemblage of spherical glass beads with diameters equal to the mean grain size of the sand was obtained from industrial sources. The properties of these three sediments will be presented in Chapter VI.

Wave Type

As we have discussed in Chapter I, in order to control the experimental conditions one would like to work in the laboratory. Since we also wish to use a propagation path many times the wavelength in order to accurately determine the attenuation,[5] we are restricted to wave types with relatively slow wave speeds in order to make measurements at frequencies of interest to acousticians and geophysicists which span the low-to-high frequency range of the Biot-Stoll theory.[11,12] This effectively eliminates the normal compressional wave. With speeds on the order of 1500 to 2000 m/sec in unconsolidated laboratory sediments,[16,27] the compressional wavelengths are 1.5 to 2 m at 1 kHz, a frequency of some interest. This restricts us to the "second" compressional wave and the shear wave. Recent work[16] has indicated that the "second" compressional wave is not observable in unconsolidated water-saturated sediments. This leaves us with shear waves as the wave

theoretical considerations, lead to the identification of dominant loss mechanisms at work in the sediment. Since the two most widely accepted mechanisms are viscous loss due to the relative motion between the fluid and sediment frame, and the frictional losses due to grain-to-grain contact, the medium should be relatively permeable and unconsolidated. These properties will allow the two mechanisms to interplay, with one or the other dominating when appropriate. Since we are primarily interested in these two mechanisms, the presence of chemical or electrical bonding should be avoided, which, together with the permeability requirement, effectively eliminates clays. We are left with sediments in the sand category. Since natural sands are generally angular to some degree, one assemblage of interest is an angular sand. This sand should be available as a moderately-sorted sand for which the grain size may be determined. Another sediment derived from this assemblage should have the same mean grain size, but with a much smaller distribution about that mean diameter. For sands, this can be achieved by sieving. This will allow one to test the effect of grain size distribution on the frequency dependence of attenuation. A third assemblage, representing the artificial sediments upon which most theories are based, should be a collection of spherical quartz beads, well-sorted to the same mean grain size as the sieved angular sand. This latter assemblage will provide a direct test of the theory under most favorable conditions and will also allow one to test the effect of angularity on acoustic wave propagation.

Once the media are selected, the physical properties of each sediment should be determined. Properties

The ability to predict attenuation given only the physical properties of a sediment has substantial utility in the fields of acoustics and geophysics. An experiment was designed to test the ability of the Biot-Stoll model to reproduce shear wave observations under carefuly controlled laboratory conditions where the required model input parameters (i.e., the physical properties and stress conditions of the sediment) could be determined for a collection of laboratory sediments. Particular emphasis in the choice of sediments was placed upon grain shape (i.e., angular vs. spherical) and size distribution (i.e., well-sorted vs. moderately-sorted). Previously cited investigations[24,48,53,62,82] have indicated that these factors may affect the applicability of the Biot-Stoll model. In this chapter we will describe those factors considered in designing the acoustic measurement experiment and the resultant acoustic measurement system and procedures.

Experiment Design Considerations

In order to make measurements suitable for establishing the frequency dependence of attenuation from which one may infer the relative importance of the mechanisms included in the various theoretical descriptions presented in Chapter III, one must consider several related factors. These factors may be grouped into the major categories listed.

Propagation Medium

First, we must consider the propagation medium. The desire is to determine the frequency dependence of acoustic attenuation. This may, in conjunction with

IV. LABORATORY ACOUSTIC EXPERIMENTS

Background

In a recent paper,[21] the author presented the results of a laboratory experiment designed to measure the attenuation of shear waves excited in a porous, permeable, angular sand. Of particular interest was the frequency dependence of attenuation. At the time there were little data available on shear wave attenuation, and what there were did not span a very broad frequency range. The results from that work indicated that, contrary to the routinely accepted assumption that attenuation is proportional to the first power of frequency (i.e., linear) for all types of sediments and rocks,[1,2] one could observe a definite departure from linearity for certain permeable sediments. This behavior was also shown to be consistent with a theoretical model presented by Stoll[6-10] based on the classical work of Biot[11-14] in acoustic propagation in porous media. However, the model-to-data agreement was less than convincing in that only a few of the required model inputs were actually measured under the same conditions as the acoustic data. Thus, while the mechanisms included in the theoretical model were capable of reproducing the observed shear wave attenuation, the number of degrees of freedom available to the modeler would not allow one to conclude that the model would have been capable of predicting the observed behavior had all the required inputs been measured for the sediment under investigation.

The most general theory capable of describing the acoustic response of a realistic two-component medium where one component is a fluid, is that proposed by Biot.[11-14] This theory allows for acoustic velocity dispersion and attenuation due to relative fluid-solid motion which is manifest as either linear or non-linear in frequency depending on the properties of the sediment.[10,17,21,87] An additional result of the theory is that it predicts a compressional wave of the "second kind" for fluid-filled porous permeable solids. The confirmation of the existence of this wave has occurred recently,[15,16] and lends great credibility to the mechanisms proposed in the theory. The successful incorporation of frame losses into this theory by Stoll[5-10] has resulted in a theoretical model capable of reproducing, with reasonable accuracy, observations made in a number of sediment assemblages across a wide frequency range. The work cited testifies to the utility of this model when one attempts to understand the mechanisms dominating a particular set of measurements. However, the question remains as to the utility of the model when certain of its basic assumptions are violated, namely the macroscopic homogeneity of the propagation medium brought about by non-uniform grain size and shape. The pursuit of some insight into the answer to this question is an objective of the experiments and model comparisons described in the remainder of this paper.

may be used to define the dynamic behavior of actual sediments over some range of frequency for certain physical conditions. In order to be very useful, however, a model should be able to reasonably define the dynamic behavior of actual sediments over frequency ranges of interest to the acoustician or geophysicist for physical conditions which may be encountered in the laboratory or the field. In short, the model must be valid for wet or dry samples; with high or low porosity; with or without rigidity; for a broad frequency range. Few of the models presented can meet this test.

Of the viscoelastic models, the Hamilton-Ferry approach can handle most of the above conditions if the supporting measurements are available which will allow the derivation of the elastic moduli. However, there is evidence that at high frequencies in highly permeable sediments (i.e., sands) the Hamilton assumption of linear frequency dependence for attenuation does not hold.[21,87]

The physical sediment models, since they are related to the physical properties of the sediments under study, have been shown to hold as long as the assumptions with respect to those physical properties are valid. Even the simplest suspension model (Equation III-13) has been used to fit data from high porosity sediments.[75,76] However, several investigators have shown this approach to be incapable of representing the acoustic properties of sediments when the rigidity of the sediment is appreciable.[57,67,77,79] The addition of attenuation effects to suspension models has led to some success in model-to-data comparisons,[79-81] but the applicability once again breaks down when sediment rigidity becomes important.

One of the drawbacks to a model such as this is that although some reasonable estimates of the model inputs may be obtained, often there is a great deal of uncertainty as to the precise value for a given input parameter. Given the uncertainties and imprecision in the model inputs, and the resultant imprecision in the model outputs, it is sometimes difficult to assess whether the mechanisms in the model are appropriate to a particular sediment assemblage. Since the Biot-Stoll model does not directly allow for variability in grain size or shape, there is cause to question its applicability to natural sediments. One way to test this is to measure both the model inputs and model outputs under carefully controlled conditions which allow both to be precisely determined (e.g., in the laboratory). The resultant comparisons between model predictions and acoustic measurements may show the degree of applicability to complex sediments. This is particularly true if the measurements span a range of sediment complexity; i.e, sediment grain size and shape. The experiments described in the following chapters were designed to test the Biot-Stoll model, at least the shear wave portion, and its ability to reproduce observed acoustical behavior of progressively complex sediment assemblages, given careful control on the model inputs. In addition to the experimental results, a more detailed discussion of the Biot-Stoll model with particular emphasis on the prediction of shear wave properties will be presented in Chapter VIII.

Theory vs. Observations

As stated during the discussion of each of the theoretical approaches presented, a particular approach

Symbol	Physical Property	SI Units
ρ_s	Density of sediment grains	$kg \cdot m^{-3}$
K_s	Bulk modulus of sediment grains	$N \cdot m^{-2}$
ρ_f	Density of pore fluid	$kg \cdot m^{-3}$
K_f	Bulk modulus of pore fluid	$N \cdot m^{-2}$
η	Viscosity of pore fluid	$kg \cdot m^{-1}\ s^{-1}$
$\emptyset$	Porosity	--
k	Permeability	m^2
a	Pore size parameter	m
α	Structure factor	--
μ	Shear modulus of frame (real part)	$N \cdot m^{-2}$
μ'	Shear modulus of frame (imaginary part)	$N \cdot m^{-2}$
K_c	Bulk modulus of frame (real part)	$N \cdot m^{-2}$
K_c'	Bulk modulus of frame (imaginary part)	$N \cdot m^{-2}$

TABLE III-1. BIOT/STOLL PHYSICAL PARAMETERS

stresses introduced by the investigator during the course of taking the propagation data.

Frequency Control

Since one of the objectives of this work is to measure the frequency dependence of shear wave attenuation, one must be careful to establish that the frequency of the signal coming out of the receiver is the same as that being put in to drive the projector. Several factors have been identified which relate to this. If the projector is being driven by an amplified sine wave of known frequency, as is the case in this work, the frequency of the vibrations being produced by the transducer element will be somewhere between that of the input wave and the resonant frequency of the projector, unless the projector is driven to a steady state oscillation at the frequency of the input sine wave. This may be achieved by a driving pulse many cycles long. This procedure was adopted for this study, and a multi-cycle pulse was used to drive the projector at the discrete frequency of interest. To ensure that the received signal is at the desired frequency, a bandpass filter was used to reject extraneous noise away from the frequency of interest. The frequency of the received signal was checked using an oscilloscope as a continuous monitor, and a spectrum analyzer during the initial determination of the pulse length needed to achieve steady state oscillation.

Since the properties of the propagation path were reproduced and monitored for each projector-to-receiver separation using the techniques described above, one had but to change the driving frequency and bandpass

filter setting to get a measure of the amplitude of the transverse vibrations being propagated across a particular sediment path at a discrete frequency of interest. Since measurements for a particular path length were taken at all desired frequencies for a given tube filling, the effects of sediment path property inconsistencies on the determination of the frequency dependence of attenuation were minimal. Given this and the care taken to ensure propagation of the desired frequencies, it is felt that the frequency dependencies established by these measurements are accurate.

Interference Effects

As noted above, it was necessary to use multi-cycle pulses to ensure steady state oscillation of the projector at a particular frequency. To be able to achieve such long pulses in a tank would have necessitated tank dimensions which were large relative to the direct path separation between the transducers. This would have been required to avoid the interference of energy reflected from the bottom and sides of the tank which could arrive at nearly the same time as the direct path, becoming more noticeable at the greater separations. Such "multipath" arrivals could interfere with and distort the direct path arrival, thus rendering the determination of amplitude of the direct path virtually impossible. One answer to this multipath interference is to use short pulses a few cycles long. As discussed above, this results in a distortion of the propagation frequency dependent upon the pulse length, the driving frequency, and the resonant frequency of the transducers. Bell[27] used a small rectangular tank for measurements of shear waves in unconsolidated porous media and

reports noise interference and distortion as a result of his having to use short pulses. Of course, one could increase the size of the container, but the result would be a loss of control over the reproducibility and monitoring of the sediment properties, a problem whose consequences would severely impair the validity of the measurements.

In this work, we chose to use a long cylindrical tube. The hope was that such an arrangement would result in plane wave propagation along the tube axis once away from the near field of the projector. In general, this was the case. Beyond a separation of approximately one acoustic wavelength, the amplitude of transverse vibrations diminished at a rate directly proportional to the separation, that rate varying, of course, with frequency. Our ability to fit the amplitude versus separation data with a straight line attests to the degree to which the plane wave assumption was valid. The lower frequencies showed the poorest fits with the straight line, but even they had acceptable fits. A potential complicating factor at low frequency was the possibility of reflections from the receiver end of the tube which may have resulted in standing wave-like interference patterns. The waveforms displayed on the oscilloscope showed little evidence of the scalloping which would result from such interference, even at the lower frequencies. The plane wave assumption appeared to be better at higher frequencies where the great attenuation precluded reflective interference. However, the possibility existed that standing waves might be set up across the diameter of the tube at certain frequencies such that the diameter was equal to even multiples of the acoustic wavelength.

These frequencies can be calculated if the wave speed is known. Observation of the data at the critical frequencies showed no evidence of anomalous loss which might be attributable to such interference.

Summary

As a result of the experiment design considerations presented above, a shear wave measurement system and a set of measurement procedures have been established. One may measure the attenuation of shear waves in water-saturated, porous, unconsolidated sediments at frequencies spanning a range from 1 kHz to 20 kHz under controlled conditions. As will be shown in Chapter VII, the measurements are repeatable, and although there remain some inaccuracies and interferences, these may be incorporated into statistical confidence intervals about the attenuation estimates obtained. The care taken in separating effects on attenuation due to sediment property variability and frequency make the results useful as estimates of the actual frequency dependence of shear wave attenuation in the subject sediment assemblages. Such estimates together with measurements of the properties of the sediments under the measurement conditions are valuable in our investigations of the applicability of physical sediment models and the mechanisms which they simulate.

In the next section we will present a detailed discussion of the measurement system and techniques resulting from these experiment design considerations.

Sediment Acoustic Properties Measurements

The stated purpose of this study is the determination of the frequency dependence of shear wave attenuation in unconsolidated laboratory sediments. In order to accomplish this it was necessary to design and fabricate transducers capable of producing and receiving transverse vibrations in such sediments. These in turn were incorporated into a measurement system which allowed the generation, detection, and display of such vibrations. Finally, a set of measurement procedures which resulted in the determination of shear wave attenuation under controlled and reproducible conditions were established. These equipment and measurement procedures will be discussed in the following subsections.

Shear Wave Transducers

As stated in the previous section, the objective of the shear wave transducer design efforts was to construct a transducer capable of producing and receiving transverse vibrations in an unconsolidated laboratory sediment. This was to be accomplished across a frequency band from 1 kHz to 20 kHz. Previous work indicated that some attention would have to be paid to matching the motion of the transducer face to the motion of the sediment grains in order to obtain the repeatable, efficient, transducer-to-sediment coupling required for shear wave attenuation measurements.
Because of the need to work across short path lengths, the elimination of electrical feedover from projector-to-receiver as well as other types of electrical interference had to be addressed. These design considerations

were all achieved in the shear wave transducers used in this research which are adaptations of a transducer design proposed by Shirley[88] employing piezoceramic bimorph bender elements mounted as cantilevers to excite transverse particle motion in the granular propagation medium.

Referring now to Figures IV-1 and IV-2, a single piezoceramic bimorph bender element approximately 1-3 cm long (a) is mounted as a cantilever on a heavy slug of brass (b) using epoxy cement. Signal leads (c) are connected to each face of the bender element using a small amount of low-temperature solder. These leads allow the impression of a voltage across the polarized faces of the bender element, causing it to flex in the plane normal to its axis. This produces a transverse particle motion in a medium in contact with the end of the element. The brass slug is mounted in a cylinder of acrylic (d). One or more layers of cork gasket material (e) surrounds the slug to isolate it from the acrylic tube, thus avoiding the transmission of undesirable compressional wave energy into the surrounding medium. The mounted element is held in place in the inner acrylic cylinder by the tight fit formed between the gasket-wrapped slug and the cylinder wall. The signal leads are passed between the bender and the power cable (n) through channels (f) cut in the gasket material.

Electrical isolation is achieved by wrapping the inner acrylic cylinder with a ground shield (g) made of copper foil tape which is attached to the ground lead (h) of the shielded, twisted-pair power cable. This shielding prevents projector-to-receiver electrical

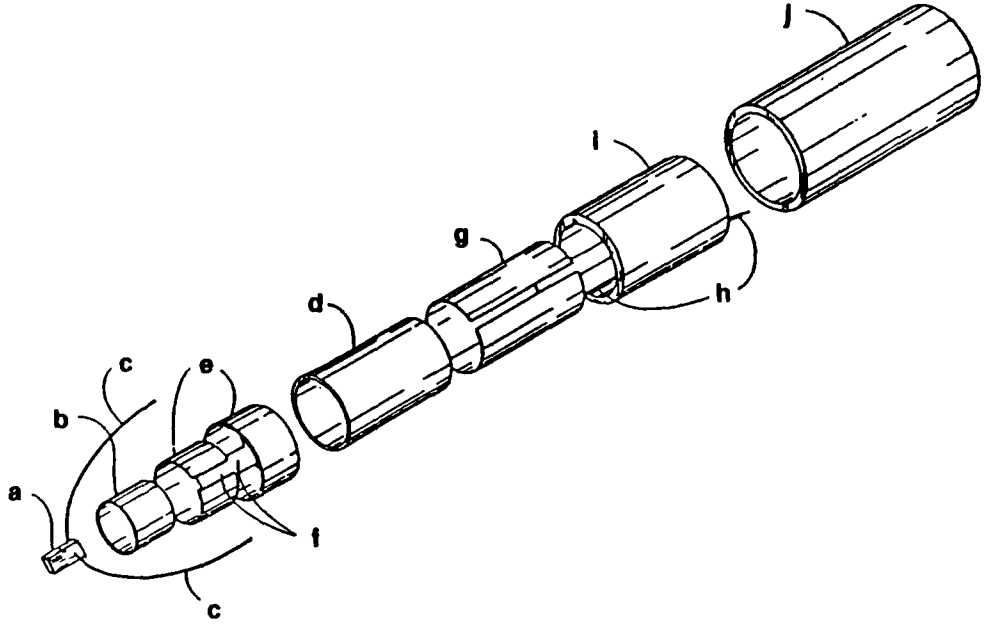

FIGURE IV-1. SHEAR WAVE TRANSDUCER (EXPLODED)

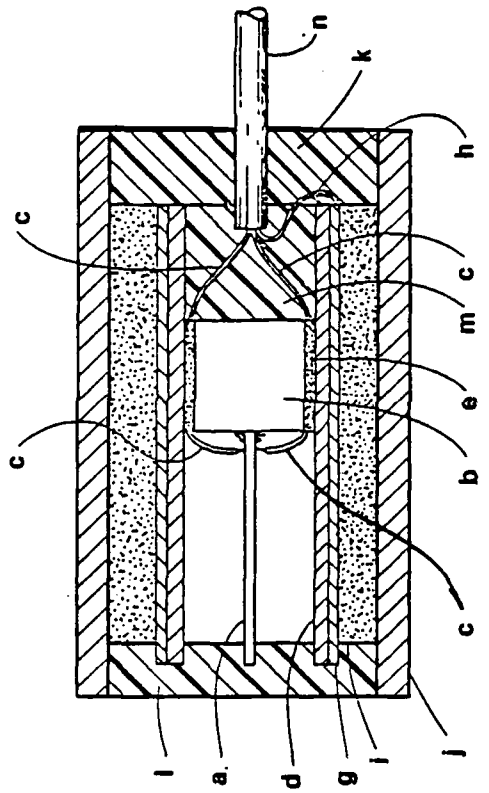

FIGURE IV-2. SHEAR WAVE TRANSDUCER (CROSS-SECTION)

feedover which can obscure the leading edge of the signal when the two transducers are in close proximity. Further isolation from compressional wave interference is obtained by placing a second, thicker layer of gasket material (i) between the inner (d) and outer (j) acrylic cylinders.

Although the bender element could be inserted into the sediment directly, this would probably result in the production of compressional wave energy by the element faces. To avoid this, while at the same time increasing the active contact area of the transducer, the end of the acrylic tube is sealed using a flexible urethane or silicon rubber potting compound (l). The end of the bender is positioned such that it extends well into the potting compound. The bond between the bender element and the potting material allows this flexible membrane to serve as the active face of the transducer, and is the source of shear waves, in the projector mode, when placed in contact with the sediment. When cured, there exists a tough flexible face suitable for efficiently coupling the transverse motion of the bender element into the transmission medium. The back of the transducer is sealed with potting compound (m) to protect the electrical leads and to make the transducer water tight. It is then capped by hard casting resin to further seal the transducer while adding strength, particularly to prevent pulling the connections apart should the power cable be placed in tension.

The transducer functions either as a projector by transforming a voltage differential across the element faces into transverse flexure, or as a receiver by transforming the motion of the active face, and hence

the piezoceramic bender element, into electrical pulses which may be detected and displayed on the cathode ray tube of an oscilloscope. In either event, direct contact between the transducer face and the propagation medium is required.

The result of these design and fabrication efforts is a transducer superior to other designs in its ability to generate and detect shear waves free from electrical or compressional wave interference. The transducer is capable of producing transverse vibrations in unconsolidated laboratory sediments; providing for shear wave attenuation measurements over at least the 1 kHz to 20 kHz frequency range. The flexible face and cantilever mount provide energy coupling in a manner and at an energy level that exceeds that of unmounted bimorph elements, allowing measurements to be made at large separations at frequencies well removed from the optimum frequency of the element itself which is inversely proportional to the square of its length. The transducer can be driven at high input voltages (typically 200 V peak-to-peak), thus permitting greater amplitude motions which translate into higher shear wave source levels for propagation studies. The flexible face response is more closely matched to the sediment particle motion which allows more efficient and repeatable coupling into the propogation medium than has been achieved with other transducer designs. The sensitivity of the cantilever mounted element allows motions imparted to the flexible face by sediment particle motion to produce relatively high electrical output for relatively small sediment particle motion. The improved sediment-to-transducer coupling achieved using this transducer allows measurements to be made

in highly absorptive media over long path lengths, a factor essential to the determination of attenuation in sediments. The details of the construction of the transducers are contained in an unpublished laboratory item.[89]

Shear Wave Measurement System

In order to perform the actual attenuation measurements, the shear wave transducers were incorporated into a shear wave measurement system consisting of the sensor system and the supporting electronics.

The sensor system, shown in Figure IV-3, consists of a vertical acrylic tube about 1.5 m long. The receiving transducer is mounted in the bottom using gasket material spacers and silicon rubber potting compound to hold it in place while providing further isolation from interfering compressional or shear energy which might be transmitted along the acrylic tube walls. The gasket spacers and silicon rubber also provide a watertight seal at the base of the acrylic tube. The projector, attached to a 1.75 m handle made from PVC pipe, is inserted into the top of the tube and allowed to rest on the air-sediment interface at the top of the sediment sample. To provide good transducer-to-sediment coupling, sufficient lead shot is poured into the PVC pipe to bring the total projector mass to 2 kg. This produces a moderate vertical stress on the sediment column. Since the inside diameter of the acrylic tube is 4.5 cm, giving a cross-sectional area of 15.9 cm^2, this results in a vertical stress of approximately 12 kPa. While not a great deal of stress, this amount of stress has been quite beneficial in decreasing the

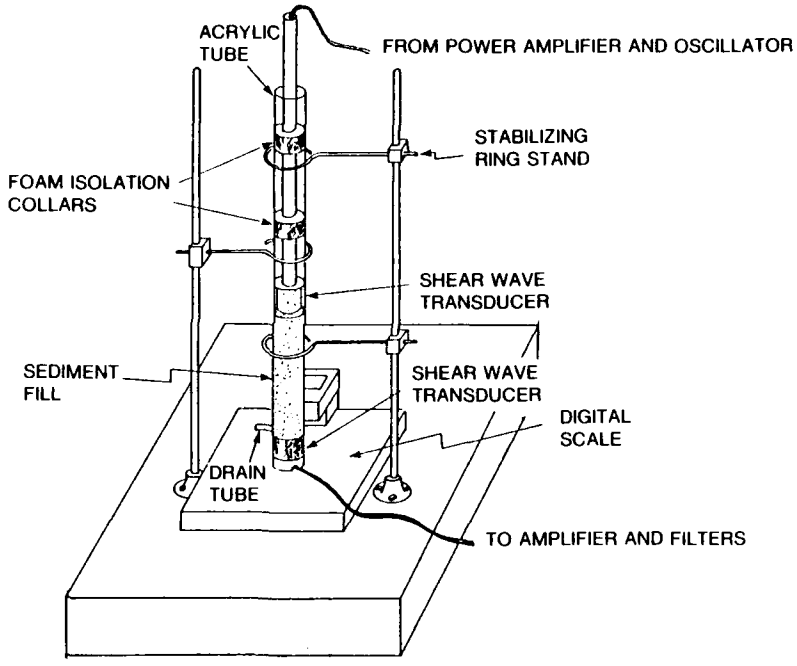

FIGURE IV-3. SHEAR WAVE SENSOR SYSTEM

sensitivity of the received levels to loads induced while manipulating the transducer handle in attempts to optimize sediment-to-transducer coupling. The outer diameter of the transducer is smaller than the inner diameter of the acrylic tube holding the sediment. There is no direct contact between the transducer and the inner wall of the sediment tube. Isolation collars made of foam rubber serve to maintain the transducer handle in a vertical position while, once again, providing no direct contact between the handle and the sediment tube. Similarly, foam isolation collars are placed at each ring stand loop to prevent direct contact between the sediment tube and the stabilizer ring stands. The tube is placed on a digital scale, isolated once again with foam rubber. This scale serves as an additional monitor of any vertical stress inadvertently imparted to the measurement assembly while manipulating the transducer handle. All of these isolation and monitoring precautions are necessary to minimize compressional interference and ensure the repeatability of the stress conditions under which the data are taken.

The upper transducer transmits a transversely vibrating wave down the sediment column where it is received by the lower transducer, amplified, and displayed on an oscilloscope cathode ray tube. The electronics which allow this to be accomplished are depicted in the block diagram of the measurement instrumentation shown as Figure IV-4.

The electronics of the system supply a pulsed sine wave of variable pulse length to the projector, while simultaneously sending a trigger pulse to start the sweep of the storage oscilloscope. The burst generator

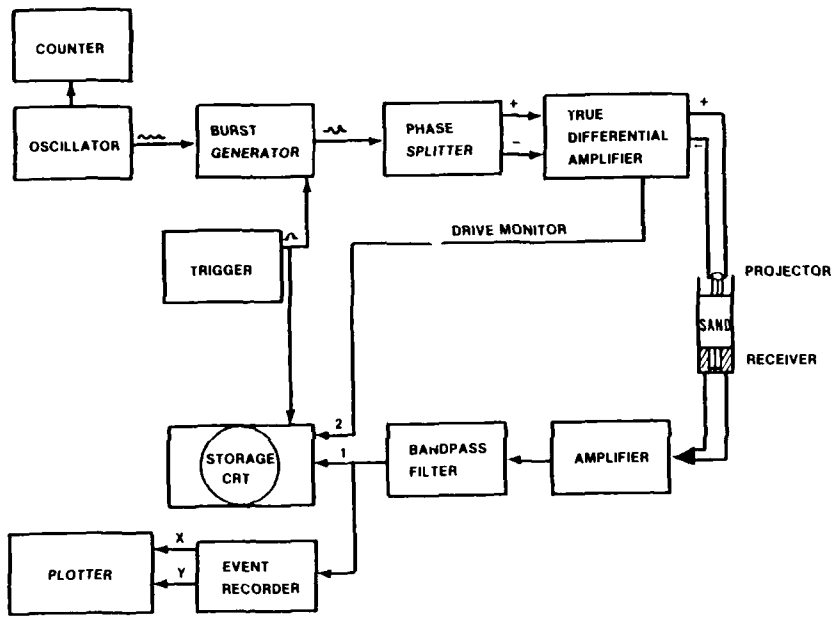

FIGURE IV-4. SHEAR WAVE MEASUREMENT INSTRUMENTATION BLOCK DIAGRAM

AD-A152 612 SHEAR WAVE ATTENUATION IN UNCONSOLIDATED LABORATORY SEDIMENTS(U) PLANNING SYSTEMS INC MCLEAN VA B A BRUNSON JUN 83 NORDA-TN-159 N00014-81-C-0275 2/3

UNCLASSIFIED F/G 8/8 NL

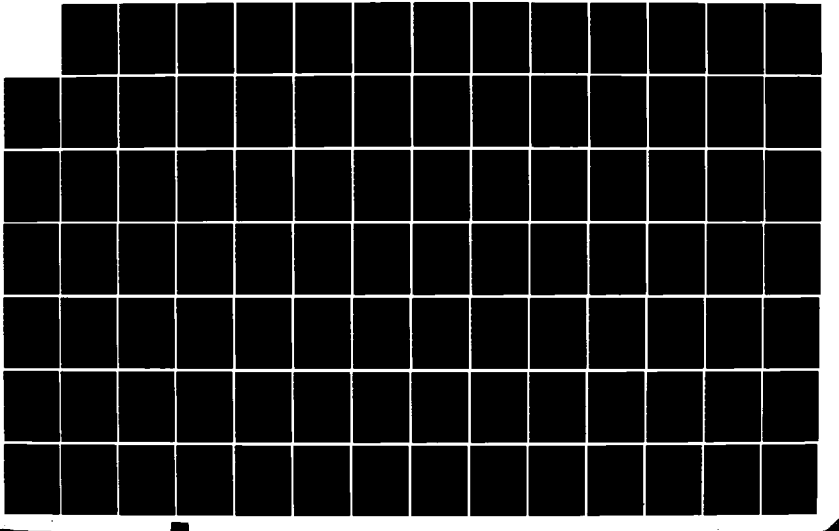

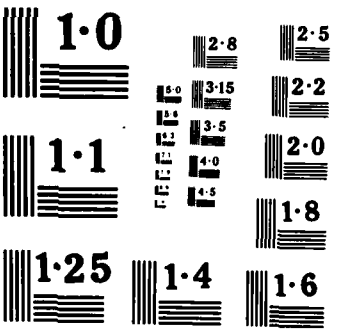
1·0
1·1
1·25
2·8
3·15
3·5
4·0
4·5
1·4
2·5
2·2
2·0
1·8
1·6

emits a pulse of an integral number of cycles of a sine wave provided at the output of an oscillator whose frequency is monitored using a digital counter. The burst generator has six settings to provide pulses of 2^n-1 cycles where n=1 to 6. Thus, the pulse length may be varied from 1 to 63 cycles of the driving sine wave. This ability to control the number of cycles in a pulse is important to ensure that the transducer is vibrating in a steady state mode at the frequency of interest established by the oscillator.

The output of the burst generator is fed into a phase splitter where a parallel but inverted pulse is produced and fed to a dual-channel amplifier. Here the pulse is amplified and fed to the signal leads on opposite faces of the bender element. The voltage across the bender is equal to the sum of the voltages output by the amplifier channels. The amplifier outputs are monitored on an oscilloscope and usually are set at 100 volts peak-to-peak, giving a balanced voltage of 200 volts peak-to-peak across the bender element. This approach was taken to achieve maximum excitation of the transmitter at a nominal drive level.

Stoll[10] has shown the log-decrement for torsionally loaded samples to be dependent on amplitude beyond a certain threshold dependent on material properties and driving frequency. In our experiments, the driving voltage was varied to test for amplitude related effects. None were observed. Calculations based on received voltage levels and the free-air response of the transducer elements indicate that displacements did not exceed 10^{-4} cm.

The transverse motion of the transducer element is coupled into the sediment column and propagates as a plane wave across the propagation path of known length to the shear wave receiver mounted in the bottom of the sediment sample tube. The transverse motion of the receiving bender element produces a voltage proportional to the amplitude of its flexure. This signal is fed via a shielded coaxial cable to a differential amplifier, amplified as required (from 0-40 dB gain in steps of 20 dB), and fed to the input of a bandpass filter. The filter settings are determined by the center frequency and the desire to maintain a constant filter bandpass quality factor, Q, defined as:

$$Q = \frac{f_C}{f_U - f_L} \qquad \text{(IV-2)}$$

where

f_C = center (signal) frequency
f_L = lower filter cutoff frequency
f_U = upper filter cutoff frequency

with

$$f_C = (f_L\ f_U)^{0.5} \qquad \text{(IV-3)}$$

$$f_L = \frac{f_C}{2}\left[\left(\frac{1}{Q^2} + 4\right)^{0.5} - \frac{1}{Q}\right] \qquad \text{(IV-4)}$$

$$f_U = \frac{f_C^{\,2}}{f_L} \quad . \qquad \text{(IV-5)}$$

The filter pass bandwidth ($f_U - f_L$) was such as to maintain a value of Q equal to ten for the discrete frequencies at which shear wave data were taken.

The filtered shear wave signals are then fed to one channel of a dual-channel, storage cathode-ray-tube, oscilloscope where the received level and signal quality are monitored. On occasion the signal is captured by a digital event recorder and displayed on an x-y plotter. In normal operations, however, the peak-to-peak voltage of the shear wave receiver output is displayed on the CRT from which the maximum received voltage level in the steady state portion of the wave form is recorded for each frequency of interest at a given transducer separation or path length. These received levels form the data for determining attenuation. For speed determinations, the time interval from the start of an oscilloscope sweep to a selected zero crossing on the CRT grid is recorded as a function of transducer separation.

This measurement system has proven to be quite adequate to produce high quality measurements of shear wave attenuation in unconsolidated sediments, whether saturated or dry. The electrical and acoustic isolation achieved has allowed repeatable measurements to be made in highly absorptive materials, with good signal-to-noise performance, even when operating at extreme separation at frequencies well removed from the optimum frequency of the transducers.

Operational Measurement Procedures

Operational measurement procedures vary somewhat depending on the material under investigation. Two basic types of attenuation measurements are made: (1) attenuation in water saturated sediment, and (2) attenuation in dry (air saturated) sediment. In addition, a

few measurements of shear wave speed have been made to obtain frame shear moduli for calculating the frame log decrements, and to provide speed data for comparison with model estimates.

For water saturated attenuation and speed measurements, a measured amount of distilled water is added to the acrylic sample tube. A measured amount of dry sediment (100-200 g) is then added using a funnel with a long throat. The funnel is used to introduce the granular material into the water gradually without entrapping air bubbles or allowing granules to stick to the sides of the tube. For the measurements discussed in this report the desire is to attain a consistent porosity, thus the sediment-water mixture is consolidated to its densest packing by mechanically vibrating the sample tube until no further rearrangement of grains is observed. For consistency, the tube is vibrated with a hand-held vibrator for one minute. When consolidation is complete the water is drained, using a drain tube at the bottom of the sample tube, until the water level coincides with the upper surface of the sediment column, resulting in 100 percent saturation. The drained fluid is retained for more precise calculation of the degree of saturation. The achievement of a reasonably consistent packing for each sediment level is assured by calculation of porosity each time an incremental sediment sample is added to the column. This calculation is made possible by knowing the total volume of saturated sediment in the tube, and the total volume of dry sediment which has been added. The difference between these volumes is the volume of the voids which are filled with water or air. The ratio of the volume of the voids to the total volume

of saturated sediment is the porosity. The total dry sediment volume is determined from the sum of the weights of the incremental sediment samples added to the column together with the grain specific gravity (or density) determined for each sediment type. The total saturated sediment volume is determined by measuring the sediment column height and multiplying by the sediment tube cross-sectional area.

Raw data from which attenuation and speed can be determined is obtained using an incremental filling method. Each measurement run consists of several incremental fillings using the procedures discussed above. Once a new transducer separation has been established, a received voltage level is recorded for each frequency being sampled. These are achieved by simply changing the frequency of the driving oscillator, the pass band of the filter, and, if necessary, the amplifier gain setting. The incremental step length is determined by the amount of dry sediment added to the sediment tube. Our experience shows that incremental steps of four to eight centimeters (100-200 grams of dry sediment) allows consistent packing to be achieved throughout a run. The number of incremental steps taken depends on the lowest frequency being sampled. Usually 10 to 15 steps make up a single run.

The transducers are pulsed at 500 ms intervals and emit a wave train of selectable length; long enough to allow the bender element to reach steady oscillation at the driving frequency. The received signal is displayed on the CRT of an oscilloscope operating in the storage auto-refresh mode. The signals "stack" on the CRT allowing the investigator to observe the amplitude and

wave-form of several recent pulses. This monitoring of the signal wave-form is an important part of the measurement process in that it permits the investigator to watch for interference effects which would render the data invalid.

When sediment is first introduced to the sample tube and consolidated, the coupling between the receiver and the sediment is fixed for the duration of the run. The upper transducer, on the other hand, is repeatedly withdrawn and reinserted for each incremental step, and merely rests upon the upper surface. The received signal level can sometimes be altered significantly by manipulation of the transducer handle. This is generally attributed to highly variable coupling between the face of the transducer and the upper surface of the sediment column. This problem has been noted by other investigators[27] and is potentially the greatest source of error in the determination of attenuation. The acquisition of repeatable data which supports high confidence in the results thus remains somewhat of an art. To allow manipulation of the transducer to optimize coupling without introducing additional non-repeatable stress, the entire sample tube and transducer assembly is placed on a digital scale. This allows the investigator to monitor the amount of pressure being applied to the sediment column during the manipulation of the upper transducer. An attenuation measurement is considered acceptable when the waveform shows constant amplitude (no scalloping), and when, by manipulating the upper transducer handle without applying additional vertical pressure, the highest achievable peak-to-peak voltage is observed on the storage CRT. This voltage is recorded together with the system gain settings for

each frequency being measured. The voltages, once converted to received levels in decibels relative to one volt, comprise the raw data from which attenuation coefficients may be determined.

Dry sediment attenuations are determined using the same procedures except that no water is introduced into the sample tube. Since many previous investigations have indicated that dry frame attenuation is linear with respect to frequency,[20,24,27,60,64] fewer frequenquencies were sampled.

Once the received voltage level at each transducer separation for each frequency is obtained, a plot is prepared similar to that shown as Figure IV-5. Here we see received level plotted against transducer separation. The slope of the line fit to the data represents the attenuation coefficient for the sediment being examined at the frequency for which the data were taken. That slope may be determined using least squares linear regression techniques to fit the data.

Several points should be noted about Figure IV-5, which is a plot of actual data observed during this investigation. First, the quality of the straight line fit to the data attests to the validity of the plane wave assumption of the measurement technique. This is quantified by the coefficient of determination, r^2, which is a measure of the degree to which the regression explains the total variation about the mean of the data. With a value of 1.00 representing a "perfect" fit to the data, the value calculated for this example is 0.97. The second point to note is that the data were taken at separations extending from less

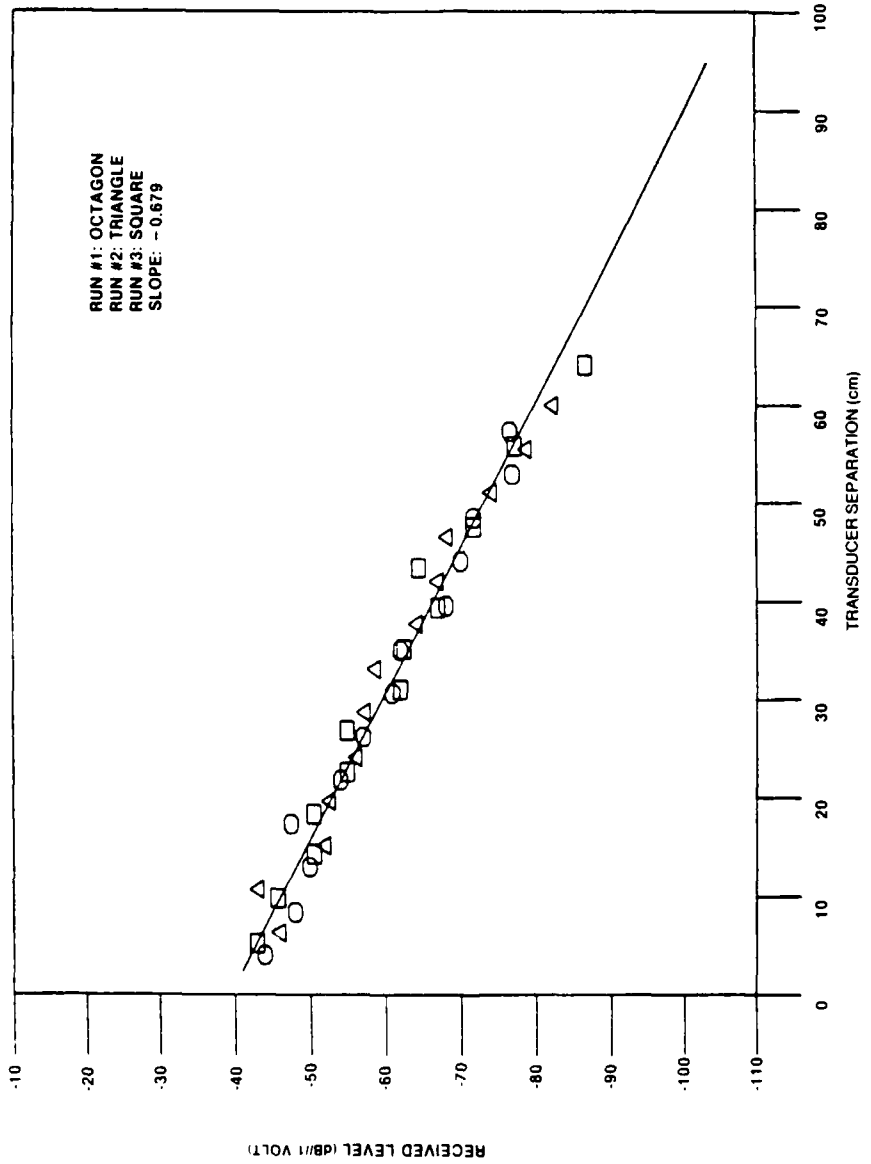

FIGURE IV-5. RECEIVED LEVEL VERSUS SEPARATION FOR WELL-SORTED ANGULAR SAND AT 4 kHz

than 5 cm to greater than 60 cm with levels varying over a 40 decibel dynamic range. This attests to the sensitivity of the transducers as well as the high signal-to-noise ratios attainable even at large transducer separations. The repeatability of the measurements is demonstrated by the fact that three independent runs, starting with an empty sediment tube each time, are displayed on the plot. This ability to reproduce previous observations is important to the building of a data set large enough to allow meaningful statistics to be calculated. The 39 observations contained in the three runs presented are not atypical. It is similar numbers of data points which together result in the estimates of attenuation assigned to each of three sediment types at each of 17 discrete frequencies betwen 1 kHz and 20 kHz. Each of these estimates has associated with it a 90 percent confidence interval. Such statistics make the results much more valuable in comparison with other data or model estimates. This confidence interval quantifies the level of uncertainty in the attenuation estimate due to all causes including measurement error, interference effects such as wave front curvature or resonance due to multiple reflections at low frequency, or physical property related variability including porosity and effective stress.

As stated previously, a few shear wave speed measurements were taken. The tube filling technique is identical to that for attenuation measurements. However, instead of recording the signal amplitude at each transducer separation increment, the elapsed time from the start of the oscilloscope sweep to a selected cycle zero crossing is noted. These observations then allow one to determine the change in time as a function

of the change in separation. Since it is generally accepted that shear wave speed in dry sediment is non-dispersive, the measurement frequencies were selected to optimize the signal-to-noise ratio with minimal use of amplifier gain.

Summary

In this chapter we have presented the experiment design considerations and the equipment and procedures used in the laboratory to determine the acoustic properties of the sediments under investigation. These have been developed with the intent to diminish the uncertainty associated with the measurement of shear wave attenuation as a function of frequency, sorting, and grain shape. It is felt that by measuring the acoustic properties under controlled conditions, the value of the resultant attenuation estimates would be enhanced. Particular care was taken to maintain constant stress and sediment packing conditions during the acoustic measurements. This allowed the measurements to be repeated, thus increasing the number of consistent data points. These in turn led to valid estimates of the mean and variance of attenuation from which confidence bounds on those estimates could be derived. These are particularly important in comparisons between the measurements and the Biot-Stoll model, and for use by other investigators for comparison with their observations or theoretical results.

In the following chapter we will detail the equipment and procedures used to obtain the very important sediment physical properties which complement the acoustic measurements.

V. PHYSICAL PROPERTIES MEASUREMENTS

Background

In the previous chapter, the basis for the development and the details of the equipment and procedures used in the acoustic properties measurements were discussed. In this chapter, the physical properties measurement equipment and procedures will be presented.

The types of physical properties measurements performed in support of the research described in this report included grain size distribution, permeability, porosity, and grain specific gravity. These, together with sediment acoustic properties, including wet and dry shear speed, as well as wet and dry attenuations as functions of frequency, allowed the complete description of the physical and viscoelastic properties of the sediments used in this study.

Sediment Properties Measurements

As mentioned above, the physical properties of the three sediment assemblages used in the shear wave measurements were determined in the laboratory. These properties are necessary to relate the acoustic measurements to similar findings reported by other investigators, to assist in establishing empirical relationships between physical and acoustic properties of the sediments, and as input parameters to the Biot-Stoll physical model. The methods and apparatus used to determine sediment physical properties, including grain size distribution, permeability, porosity, and grain specific gravity, will be described in the following subsections.

Grain Size Distribution

Size analysis of silt and sand size particles may be a controversial subject due to the fact that the methods generally used, mechanical sieving, and settling through a tube or column of fluid, measure different variables (median axis for sieving and settling velocity for the settling tube) and may result in size distributions which are not compatible in many instances. To avoid such a controversy, the size distribution of the moderately-sorted angular sand was determined using both methods.

Sediment grain size may be classified using several measures, some qualitative such as sand, silt, clay; and others quantitative such as mean grain diameter expressed in millimeters or dimensionless Phi units where:

$$\text{Phi} = -\log_2 d(\text{mm}) \qquad \text{(V-1)}$$

or conversely,

$$d(\text{mm}) = 2^{-\text{Phi}} \qquad \text{(V-2)}$$

Table V-1 represents a portion of the Wentworth scale, which is a logarithmic scale in that each size class limit is twice as large as the next smaller class limit. For detailed grain size analysis, sieves are available at $(2)^{\cdot 25}$ mm or "quarter" Phi intervals. The scale enables one to easily relate sieve size, grain diameter, Phi units, and size classes.

Sediment	Statistic	d (mm)	ϕ (%)	$kx10^{-7}$ (cm^2)	$\rho_{(sat)}$ (g/cm^3)	$\rho_{(dry)}$ (g/cm^3)	$\mu_s x10^{-8}$ ($dyne/cm^2$)	Δ_s
Angular Sand (unsieved)	mean	.372	43.2	7.245	1.94	1.51	6.30	.161
	S/SE	.136	0.7	0.68			0.97	.030
	90% CI						39	47
	n		10	11				
Angular Sand (40/45)	mean	.385	43.2	9.076	1.94	1.51	6.37	.133
	S/SE	.046	1.2	.74			0.69	.012
	90% CI						28	42
	n		10	10				
Spherical Beads (40/45)	mean	.385	35.5	11.43	1.92	1.56	9.30	.288
	S/SE	.046	0.4	1.51			1.30	.034
	90% CI						32	24
	n		11	11				

TABLE VI-1. SEDIMENT PROPERTIES

VI. SEDIMENT PROPERTIES

Introduction

A key element in the interpretation and application of acoustic data is the set of physical and environmental properties which describe the conditions under which the data were taken. For the acoustic measurements reported in this study, the physical properties of interest include those which are or may lead to inputs to the Biot-Stoll model. Additional properties may be reported, but those of primary interest include: grain size distribution, porosity, permeability, density, shear modulus and log decrement of the frame, and the derived or empirical model parameters including the sediment structure factor and pore size parameter. Table VI-1 presents a summary of the primary properties for each of the three laboratory sediments. Most of these have been measured directly, but in some instances alternative approaches are available. Each of the properties will be discussed in the following sections of this chapter.

Grain Size Distribution

The three sediments used in this study include a moderately-sorted, medium size, angular sand; a well-sorted, medium size, angular sand derived by sieving; and well-sorted, medium size, spherical glass beads. Figure VI-1 depicts the grain size distributions for the three sediments. The distribution of the moderately-sorted sand was determined using two methods. The results of the sieve analysis are shown by the bar graph of the percent of the sample falling within each

volume of the submerged body. The procedures for making this determination of grain volume are well documented, and those presented by Bowles[93] were followed to determine the specific gravity of the sands used in this study. The specific gravity used for the glass beads were those reported by the manufacturer.[95] Usually the same value is used when the application or equation calls for the grain density. Departures of water density from that at 4°C are considered negligible.

Summary

In this chapter, we have presented a brief discussion of the measurements and procedures employed to provide the physical properties of sediments used in this study. In the next chapter, we will present the results of these measurements together with the other sediment properties needed as inputs to the Biot/Stoll physical model.

A_pL = sediment sample volume
W_s = weight of sand in sample
ρ_s = unit weight of sand
W_s/ρ_s = sediment grain volume

Grain Specific Gravity

The specific gravity of any substance is defined as the density of the material divided by the density of distilled water at 4°C. This is therefore an abstract number independent of units. The term density is often used in place of specific gravity with a water density of 1.0 g/cm^3 implied.

The determination of the specific gravity usually consists of obtaining the volume of a known weight of sediment grains and dividing this by the weight of the same volume of water at the same temperature. Hence, the procedure reduces to obtaining the terms of the equation

$$G_s = \frac{W_s/V}{W_w/V} \qquad \text{(V-13)}$$

where

G_s = grain specific gravity
W_s = weight of grains
W_w = weight of water
V = volume of water or grains

The volume of a known weight of soil grains can be obtained by using a container of known volume and the Archimedes principle that a body submerged in a volume of water will displace a voume of water equal to the

k_T = permeability at temperature T, cm/sec
ρ = density of permeant at temperature T
η = viscosity of permeant at temperature T
g = acceleration of gravity

For water at 20°C, the following equation permits one to convert k_{20} in cm/sec to k in cm^2:

$$k(cm^2) = k_{20}(cm/sec) \times 1.02 \times 10^{-5} \qquad (V-11)$$

All permeabilities used in this report are in units of cm^2 unless otherwise specified.

Porosity

Porosity is the ratio of the volume of the voids in the sample to the total volume of the sample. It was measured each time additional sand was added to the sediment column in the vertical measurement tube. This provided a consistency check to confirm that the new sample had been packed to the same degree as previous samples. For purposes of reporting the properties of the sediments for this report, the porosity was determined during the permeability measurements. The permeameter afforded more precision in the measurement of the sediment column length and there were fewer sources of error involved in the permeability apparatus. In either case the porosity was determined from the equation:

$$\emptyset = \frac{A_p L - (W_s/\rho_s)}{A_p L} \qquad (V-12)$$

where

A_p = cross-sectional area of permeameter tube
L = sediment column length

quantities, is added and compacted until the sample is approximately 30 cm long. The permeameter is then assembled and the permeability of the compacted sand is measured. This method approximates the procedures used when filling the vertical sample tube for shear wave measurements, and yields permeability at the most compact or lowest porosity state of the sediment.

The secondary method of sample preparation consists of adding a measured quantity of distilled, deaerated water to the permeameter tube, then pouring a measured quantity of sand into the tube. The addition of sand and water (without vibrating or compacting) is continued until the saturated sample is approximately 30 cm long. The permeameter is assembled and the permeability of the sample is measured. After measurement, the permeameter is tapped to slightly compact the sample and the permeability is measured at the new porosity value. The result is a set of permeability versus porosity data which may be used to test the validity of the Kozeny-Carman equation for the sample. A plot of k versus $\phi^3/(1-\phi)^2$ should yield a straight line.

Both the viscosity and density of the permeant influence the value of permeability. In order to eliminate these two characteristics as variables, we have reduced the measured permeability taken at a particular temperature, T, to a specific or physical permeability, defined as:

$$k = \frac{k_T}{g} \qquad \text{(V-10)}$$

The sample was prepared for measurement by two different methods. The reasons for using two methods were (1) to reproduce the sample preparation methods used in the acoustic measurements, and (2) to allow the measurement of permeability as a function of porosity or void ratio. The latter will be used as a test of how well the permeability of the sample could be characterized by the Kozeny-Carman relationship:

$$k = \frac{1}{k_0 S_0^2} \left[\frac{\phi^3}{(1-\phi)^2} \right] \qquad (V-9)$$

where

k_0 = factor depending on pore shape and ratio of length of actual flow path to sample length (tortuosity)

S_0 = specific surface area of grain

ϕ = porosity of sample

k = physical permeability of sample, cm^2

This relationship has been used extensively in sediment modeling[17,21,27] and will be discussed in detail in Chapter VI.

The primary method of preparing a sample for permeability measurements is to add a measured quantity of distilled, deaerated water to the permeameter tube (approximately 200 ml), then add 200 grams of dry sand. The sample is then vibrated with a hand-held vibrator until the sand is well compacted and no further grain rearrangement is observed. Additional sand, in 200 g

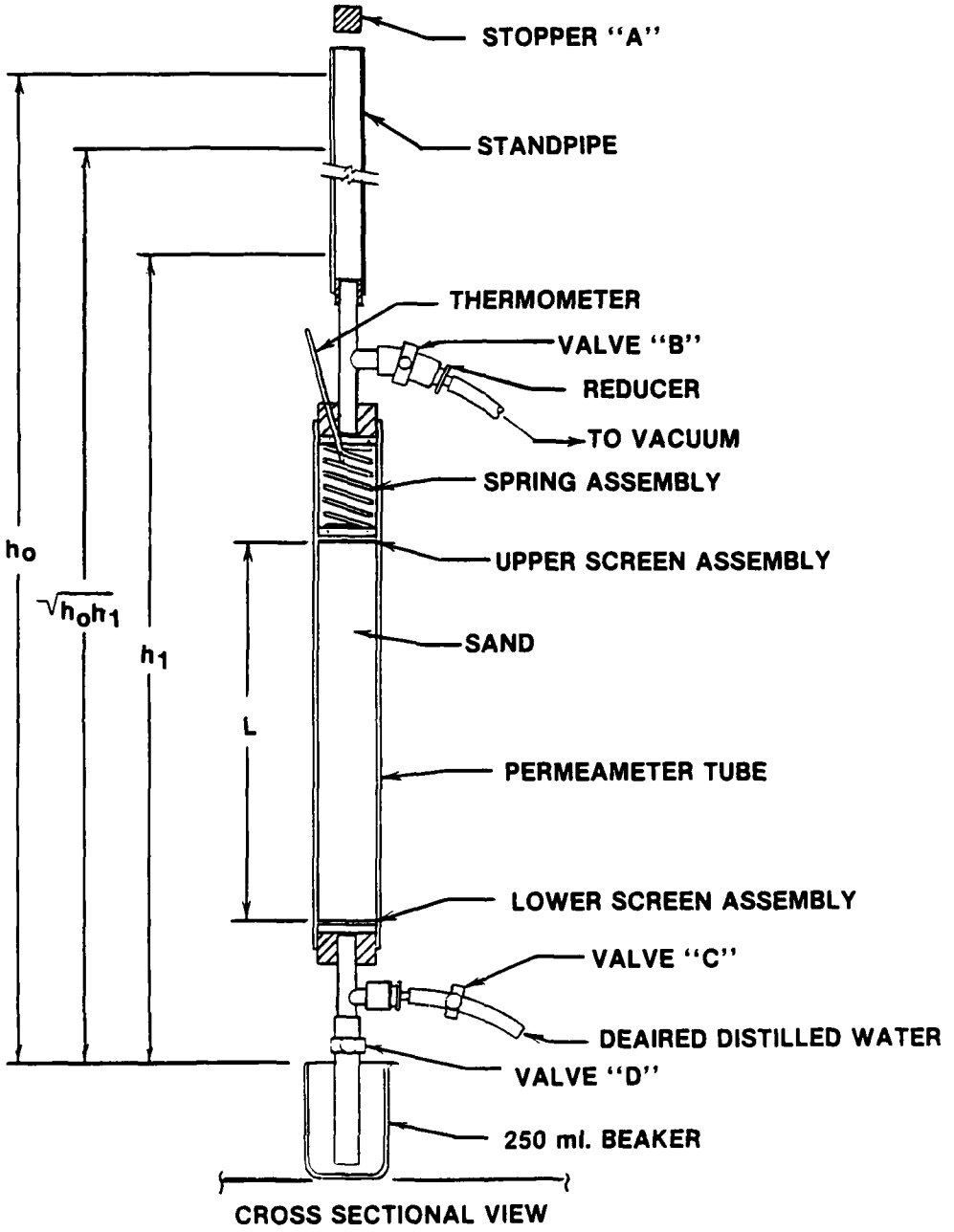

FIGURE V-1. VARIABLE HEAD PERMEAMETER (CROSS-SECTION)

sediments. The intent was to simulate the procedures and conditions prevailing during acoustic measurements of shear wave attenuation. Figure V-1 is a schematic of the permeameter.

The permeameter preparation, sample preparation, and measurement procedures are detailed in an unpublished laboratory item,[94] but the essence of the measurement and data reduction will be outlined in this subsection.

The data taken during the permeability measurement consist of those parameters required to solve the equation:

$$k = 2.3 \frac{aL}{A(t_1-t_0)} \log_{10}\left(\frac{h_0}{h_1}\right) \qquad \text{(V-8)}$$

in which

a = the cross-sectional area of the standpipe

L = the length of the sediment sample in the permeameter tube

A = the cross-sectional area of the permeameter tube

t_0 = the time when the water level in the standpipe is at h_0

t_1 = the time when the water level in the standpipe is at h_1

h_0, h_1 = the heads between which the permeability is determined.

for each standard sieve, and a cumulative distribution curve of the percent passing (also termed percent finer or percent smaller) a particular sieve represented by the size of its mesh opening.

This type of cumulative distribution (percent finer) is the opposite of the cumulative distribution used in the settling tube analysis and statistics equations (they use percent coarser). Of course, the discrepancy is easily reconciled and presented in a consistent manner. For this report, cumulative distributions derived from either method will be displayed as percent finer by weight.

Permeability

In general, all voids in a sediment sample are connected to neighboring voids. Since the pores are interconnected, any fluid contained in those pores can flow, given some finite pressure differential across the sample. The ease or rate at which that flow can occur is a function of the sediment's permeability. As pointed out in Chapters II and III, sediment permeability is an important physical property of a sediment in establishing the acoustic behavior of that sediment. In our attempt to accurately determine all those physical properties considered to significantly impact the acoustic response of the sediments used in this research, we developed the equipment and procedures needed to measure sediment permeability.

A variable head permeameter was constructed which would allow the determination of permeability of a series of permeable sands and sand-like laboratory

where ϕ_x = the Phi value for which x percent of the sample is coarser.

A second method of grain size analysis was also used. The size distribution of the moderately sorted sand was determined using standard sieves. This same procedure was used to sub-sample the sand to obtain an angular sand of uniform grain size.

The procedures for performing grain size analysis be sieving are quite straightforward for sands. The details may be obtained from any of several reference works on soil mechanics (e.g., Bowles[93]). The sieving process does not determine individual grain sizes--the test can only bracket the various ranges of sizes. This is accomplished by obtaining the quantity of material passing through a given-size sieve opening but retained on a sieve of smaller-sized openings and then relating this retained quantity to the total sample. The material retained on a given sieve consists of particles of many sizes, all of which are smaller than the openings of the sieve through which the material passed but larger than the openings of the sieve on which the soil is retained. Thus in the work presented, when we refer to the well-sorted angular sand and spherical beads as being restricted to the 40/45 sieve size range, we mean that all the particles passed through a standard sieve of mesh #40 (with rectangular opening equal to 0.42 mm) but were retained on a standard sieve of mesh #45 (with rectangular opening equal to 0.35 mm).

Information obtained from sieve analysis is generally presented as a histogram of percent retained

in distilled water at a standard temperature. Assuming a grain density of 2.65 g/cm^3, Gibbs et al.[91] gives the following equation relating sediment grain size to settling velocity:

$$r = \frac{0.055804V^2\rho_f + (0.003114V^4\rho_f^2 + [g(\rho_s-\rho_f)][4.5\eta V + 0.008705V^2\rho_f])^{0.5}}{[g(\rho_s-\rho_f)]} \qquad (V-3)$$

where

V = average settling velocity, cm/sec
η = fluid dynamic viscosity, poise
g = acceleration of gravity, cm/sec^2
r = radius of spherical particle, cm
ρ_f = density of fluid, gm/cm^3
ρ_s = density of sphere, gm/cm^3 (ρ_s=2.65)

Plotting this derived grain size against the cumulative weight of sediment results in a determination of the equivalent grain size distribution for the sediment sample. The distribution may be converted to Phi units using the relationship in Equation (V-1). The statistics of the distribution may be determined using the following equations presented by Inman.[92]

$$\text{Median} = \phi_{50} \qquad (V-4)$$

$$\text{Mean grain size} = \frac{\phi_{16}+\phi_{84}}{2} \qquad (V-5)$$

$$\text{Phi standard deviation} = \frac{\phi_{84}-\phi_{16}}{2} \qquad (V-6)$$

$$\text{Skewness} = \frac{\text{Mean-Median}}{\text{Standard Deviation}} \qquad (V-7)$$

The cumulative grain size distribution of the moderately-sorted sand was determined using a 230 cm long settling tube developed at Oregon State University. This tube, because of its 215 cm settling distance, is capable of accurately determining the grain size distribution of all size classes of sands (d>.0625 mm). A complete description of the apparatus is available as an Oregon State University, School of Oceanography report.[90] A similar system, based on the Oregon State design, is available at the Naval Ocean Research and Development Activity, Bay St. Louis, Mississippi.

The principle of settling tube sedimentation analysis is that particles with higher settling velocities will settle through a column of fluid faster than those with slower velocities. The velocity at which a sediment particle will settle through such a column is related to the size, shape, fluid viscosity, and the density difference between the particle and the fluid. Sand and coarse silt particles are commonly introduced at the top of a column of fluid of known height, separated according to their relative settling velocities, and may produce an analog record of cumulative weight versus time on a sensing and recording system. Given the known column length and settling time, an average settling velocity may be computed for a given fraction of the particles introduced.

The results of such a sedimentation analysis are directly related to the settling velocity distribution of particles in the sediment sample. They may be interpreted also in terms of the sizes of spherical particles, of uniform density, which would settle at some theoretically or empirically determined velocity

Wentworth Size Class	grain diameter (mm)	grain diameter (micron)	grain diameter (Phi)	U.S. Standard Sieve Mesh #
	2.00	2000	-1.00	10
	1.68	1682	-0.75	12
V. Coarse Sand	1.41	1414	-0.50	14
	1.19	1189	-0.25	16
	1.00	1000	0.00	18
	0.84	841	0.25	20
Coarse Sand	0.71	707	0.50	25
	0.59	595	0.75	30
	0.50	500	1.00	35
	0.42	420	1.25	40
Medium Sand	0.35	354	1.50	45
	0.30	297	1.75	50
	0.25	250	2.00	60
	0.210	210	2.25	70
Fine Sand	0.177	177	2.50	80
	0.149	149	2.75	100
	0.125	125	3.00	120
	0.105	105	3.25	140
V. Fine Sand	0.088	88	3.50	170
	0.074	74	3.75	200
	0.0625	63	4.00	230

TABLE V-1. GRAIN SIZE SCALES FOR SANDS

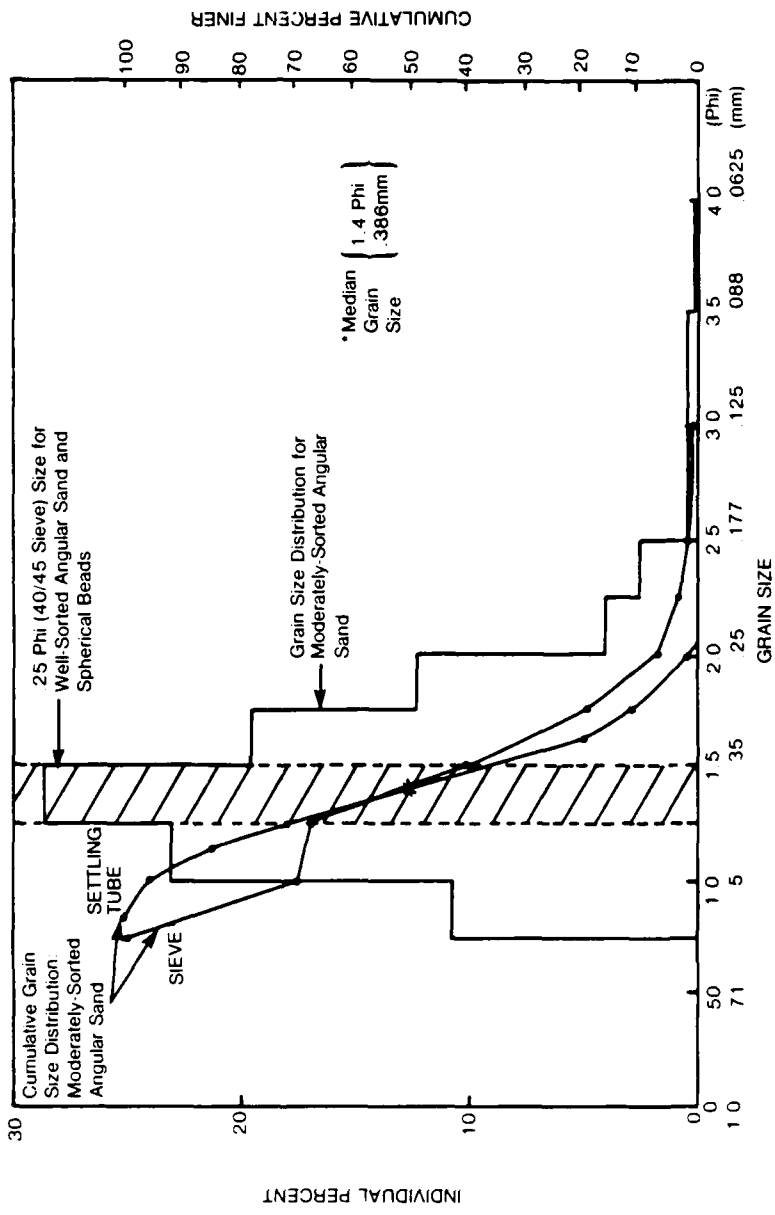

FIGURE VI-1. GRAIN SIZE DISTRIBUTIONS FOR SEDIMENTS USED IN SHEAR WAVE MEASUREMENTS

quarter Phi size bin, together with a graph of the cumulative percent of the sample finer than a given size. The settling tube results are shown as a smooth curve depicting the cumulative distribution of the moderately-sorted sand. They are very similar to the results of the sieve analysis, yielding the same median and mean grain size, 0.38 mm and 0.37 mm, respectively. There is, however, some difference between these values and the mean size of the well-sorted sand which is equal to 0.385 mm if a uniform distribution across the mesh size range (0.35-0.42 mm) is assumed.

This grain size distribution is an important parameter in the determination of permeability, and the mean and standard deviation values may be used to estimate permeability in the absence of measurements.

Given that we have achieved the goal of providing three sediments of the same mean grain size with which to assess the impact of grain shape and sorting, we may now proceed to identify how their physical properties differ.

Porosity

The porosity of unconsolidated natural (non-spherical) deposits is governed by:[96]

1. Absolute size of the grain
2. Grain size distribution
3. Grain shape
4. Method of deposition
5. Compaction during and following deposition
6. Degree of solidification

For the sediments used in this study only the first three are important factors, since there was no solidification and the method of deposition and degree of compaction were constant for all cases considered.

Theoretically the actual size of the grain has no influence on the porosity of uniform spheres. This does not hold true for assemblies of natural materials. Actually, as grain size decreases, friction, adhesion, and bridging become more important because of the higher ratio of surface area to volume and mass. This leads to an increase in porosity. Data cited by Fraser[96] showed porosities as follows: coarse sand, 39-41 percent; medium sand, 41-48 percent; fine sand, 44-49 percent; fine sandy loam, 50-54 percent.

The effect of grain size distribution is dependent upon the relative sizes of the grains involved. For spheres there exists a "critical ratio" of diameters below which the smaller sphere may penetrate the voids between the large sphere. If the conditions are right, then the porosity will be diminished from that of the uniform assemblage of either size sphere. As with size effects, this relationship may not hold for natural deposits since the pores are neither uniform in size nor shape and hence no "critical ratio" exists. For multi-component assemblages the higher porosities are obtained where one size of sphere dominates; but with increasing complexity of the mixture the porosity tends to decrease. Fraser found no consistent, reliable correlation between grain size distribution and porosity which would allow one to predict porosity given grain size distribution. This was found to be even more evident for several samples of sand in which a wide range

of grain size combinations were found to yield the same porosity.[97]

The effects of angularity on porosity are difficult to determine in natural sediments because of the difficulty of obtaining angular particles of the same size using normal sorting methods. Thus, most determinations of grain shape effects on porosity are attended by a second variable, grain size. Fraser made an attempt to determine the effects of angularity on porosity using carefully sized materials ranging in shape from lead shot to crushed mica plates. These assemblies included several sands. In general the increase in angularity lead to an increase in porosity with the coarse sands showing porosities ranging from 35-41 percent if dry, increasing to 35-47 percent when saturated in water. This increased porosity with saturation was consistent across all samples.

Thus, we see that the increase in angularity from the well-sorted glass bead to the well-sorted angular sand of the same size should result in an increase in the porosity. An examination of Table VI-1 reveals this to be true for the samples in this study. The effect of grain size distribution on porosity, as demonstrated by the well-sorted and moderately sorted angular sands, is apparently negligible for our samples.

Permeability

The permeability of the three sediments has been measured directly using equipment and techniques described in Chapter V. The physical permeabilities (in cm^2) are recorded in Table VI-1. Permeability can

also be related to porosity, grain size, and grain shape through the physical relationships of the Kozeny-Carman equation given by Carman[98] in the form [identical to Equation (V-9)]

$$k = \frac{1}{k_0 S_0^2} \left[\frac{\phi^3}{(1-\phi)^2}\right] \qquad \text{(VI-1)}$$

where k = physical permeability of sample, cm^2
k_0 = constant reflecting pore shape and tortuosity
S_0 = specific surface area of grain, cm^{-1}
ϕ = sediment fractional porosity

Since S_0 represents the ratio of the surface area to the volume of a particle, a sphere of diameter d has a specific surface area of

$$S_0 = 6/d \qquad \text{(VI-2)}$$

if we assume d_m to be diameter of a sphere with the same specific surface area as a grain with some mean size d_r in the sediment, then Equation (VI-1) can be rewritten as

$$k = \frac{d_m^2}{36\ k_0} \left[\frac{\phi^3}{(1-\phi)^2}\right] \qquad \text{(VI-3)}$$

For irregularly shaped grains, Carman has related the equivalent sphere diameter, d_m, to the mean grain size, d_r, through a shape factor ϑ such that

$$d_m = \vartheta\, d_r = 6/S_0 \qquad \text{(VI-4)}$$

The key to evaluating the shape factor is the determination of S_0. This may be done, as mentioned

in Chapter V, if we know the permeability as a function of porosity for the angular sediment. Such data were collected as part of this study. Figure VI-2 depicts plots of permeability, k, versus the quantity $\phi^3/(1-\phi)^2$. One may observe from Equation (VI-1) that if a linear relationship is obtained, then the factor $1/(k_0 S_0^2)$ may be obtained by means of a linear fit to the permeability-porosity data. For the beads, the specific surface area may be calculated from Equation (VI-2), and the factor k_0 may be calculated using Equations (VI-1) or (VI-3) if the permeability at a given porosity is known. For the sands, S_0 may be calculated if k_0 is known, and vice versa.

Bell[27] has reportedly determined k_0 using permeability and porosity data reported by Nolle et al.[18] for angular sands similar to those used in this study. This is in conflict with the statement by Carman that where the specific surface area is not known, k_0 cannot be calculated and must be assumed from values determined using non-spherical but flat-sided particle shapes for which S_0 can be calculated. Close inspection of the Nolle data and the Bell analysis reveals that Bell used the Kozeny-Carman relationship presented as Equation (VI-3), with d_m being equated to the average grain size reported by Nolle. Thus, Bell has determined the average k_0 needed to obtain the permeability observed by Nolle, assuming the grains to be spherical and of a size equal to the observed mean grain size reported. Closer analysis shows the average k_0 to be equal to 5.1, a value at the upper limit of the normal range of values for k_0 reported by Carman. While we do not feel that the spherical assumption is valid for angular sands, we will use a value of k_0 equal to

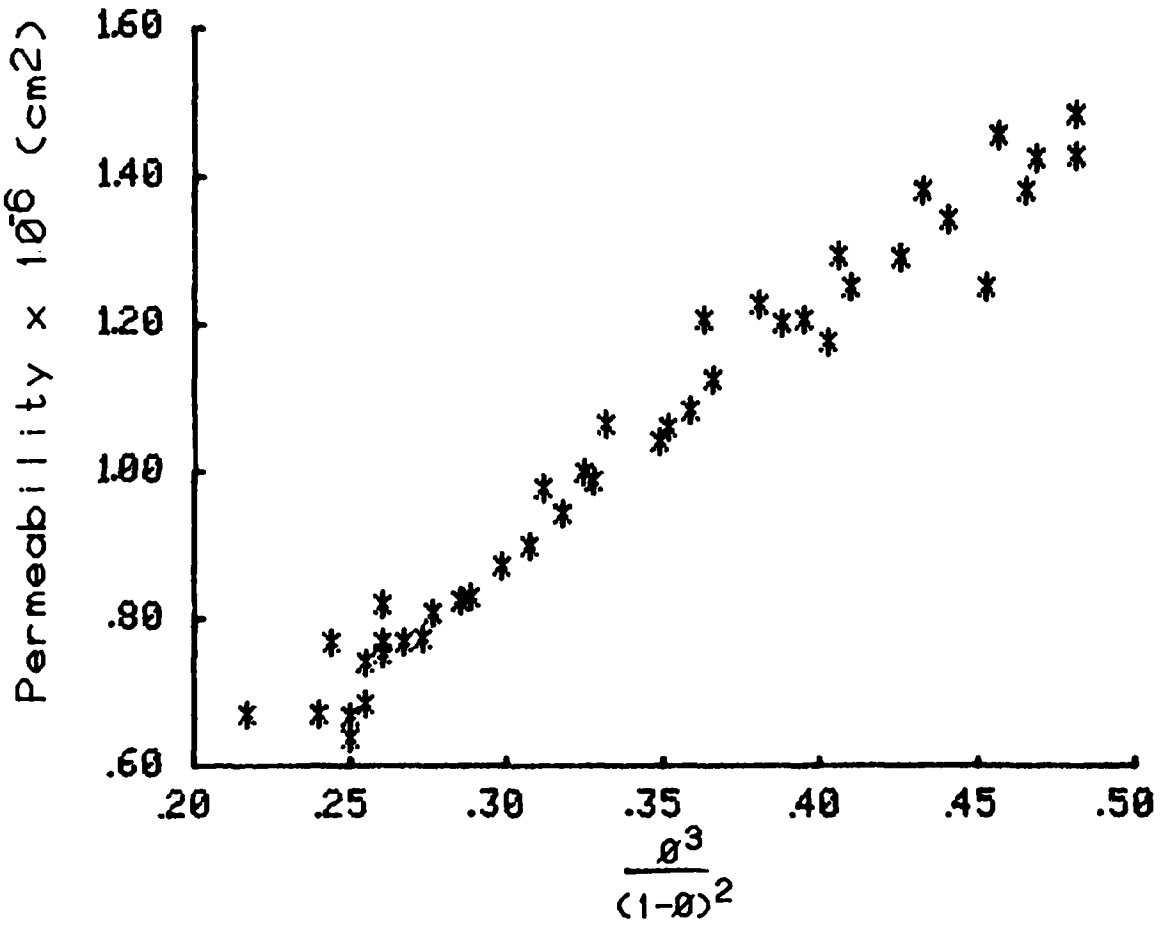

FIGURE VI-2. PERMEABILITY VERSUS $\phi^3/(1-\phi)^2$ FOR MODERATELY-SORTED ANGULAR SAND

Sediment	$\frac{1}{k_0 S_0^2}$ (cm^2)	k_0	S_0 (cm^{-1})	e	d_m (mm)
Angular Sand (unsieved)	2.92×10^{-6}	5.1	259.3	.622	.231
Angular Sand (40/45)	3.68×10^{-6}	5.1	230.8	.675	.260
Spherical Beads (40/45)	1.04×10^{-5}	3.95	155.8	1	.385

TABLE VI-2. KOZENY-CARMAN FACTORS FOR LABORATORY SEDIMENTS

5.1 for our analysis of permeability in angular sands. With this assumed value of k_0 we may now calculate the specific surface area using our values of $1/(k_0 S_0^2)$, the shape factor, and Equation (VI-4). These are presented in Table VI-2.

In addition to making provision for non-spherical grains, Carman has included a means of correcting for the distribution of grain sizes which one might find in a sediment. First consider a mixture of spherical particles, in which x_i represents the fraction, by weight, of particles of diameter d_i present. Then the specific surface area is

$$S_0 = 6 \Sigma \frac{x_i}{d_i} \qquad \text{(VI-5)}$$

in which case the mean diameter is

$$d_m = 1/\Sigma \frac{x_i}{d_i} \quad . \qquad \text{(VI-6)}$$

Next consider an irregular particle defined by some size d_r, such as a sieve size, a settling diameter, a microscope diameter, etc. The specific surface area cannot be calculated, and once again we must introduce a shape factor θ, which must be obtained empirically and which is unity for a sphere. This gives us Equation (VI-4) for each size constituent of diameter d_r.

For a mixture of particles of any shape or size distribution

$$S_0 = \Sigma x_i S_{0i} = 6 \Sigma \frac{x_i}{\theta_i d r_i} \qquad \text{(VI-7)}$$

and

$$d_m = 1/\Sigma \frac{x_i}{\theta_i dr_i} \qquad \text{(VI-8)}$$

Carman tested this relationship by mixing sands with different specific surface areas, S_{0i}. Good agreement was obtained for all cases. To test the utility of this approach we may use the knowledge which we have about S_0 for the angular sands together with the grain-size distribution data for the moderately-sorted angular sand. We have assumed the shape factor, θ, to be constant irregardless of grain size for the angular sand. Using Equation (VI-8), the shape factor for the well-sorted sand from Table VI-2, and the grain size distribution for the sand (from sieving), we obtain dm=.241 mm; S_0=249.2 cm^{-1}. Comparing this to the values of S_0 and d_m in Table VI-2, we see that these values are about four percent different from those observed from measurements. Thus, we have a reasonable approximation to the actual values for a moderately-sorted sand derived from observations of a well-sorted sand and the grain size distribution.

Empirical relationships exist from which one may estimate permeability from other physical properties of the sediment. One which has been cited in recent work by Beebe[87] was developed by Krumbein and Monk[99] to relate permeabilty in sands to their grain size distribution:

$$k = 7.6\ \bar{d}_r^{\,2} e^{-1.31\sigma\phi} \times 10^{-6} \qquad \text{(VI-9)}$$

where k = physical permeability, cm^2
$\bar{d}_r$ = mean grain size, mm
σ_ϕ = standard deviation of grain size in Phi units.

We now have discussed several methods to approximate permeability, given a sediment assemblage and some knowledge of its physical properties such as grain size distribution and porosity. Table VI-3 shows comparisons between estimates employing these methods and observations for the three sediments of this study and the well-sorted sand of the same size (40/45 sieve) reported by Nolle. The measured values are based upon the mean of observations taken using the primary method of sample preparation described in the permeability section of Chapter V, or the estimate of permeability obtained from the linear regression analysis of k versus $\phi^3/(1-\phi)^2$ obtained using the secondary method of sample preparation. The two yield nearly the same value for permeability. Two estimates are included from calculation based on Kozeny-Carman relationships. The first (K-C spherical) assumes all grains to be spherical and of a uniform diameter equal to the mean grain size reported in Table VI-1 or the Nolle paper. These estimates were made using Equation (VI-3) and the k_0 reported in Table VI-2. In all angular sands this approach overestimates the permeability. The degree of disagreement is worse in the unsieved sand; an expected result since both the spherical shape and uniform size distribution assumptions of the Kozeny-Carman relationships are violated. The second (K-C corrected) set of Kozeny-Carman estimates reflect the effect of including the shape correction factor

Sediment	Measured (Mean)	Measured (Regression)	K-C (Spherical)	K-C (Corrected)	K-M
Angular Sand (unsieved)	7.25×10^{-7}	7.29×10^{-7}	1.88×10^{-6}	7.89×10^{-7}	7.47×10^{-7}
Angular Sand (40/45)	9.08×10^{-7}	9.20×10^{-7}	2.02×10^{-6}	9.20×10^{-7}	9.06×10^{-7}
Spherical Beads (40/45)	1.14×10^{-6}	1.12×10^{-6}	1.12×10^{-6}	1.12×10^{-6}	9.06×10^{-7}
Nolle Sand (40/45)	8.5×10^{-7}	8.7×10^{-7}	9.98×10^{-7}	9.98×10^{-7}	9.06×10^{-7}

TABLE VI-3. PERMEABILITY OBSERVATIONS AND ESTIMATES FOR LABORATORY SEDIMENTS

[Equation (IV-4)], and the grain size distribution [Equation (VI-8)] to correct the permeability estimates obtained from Equations (VI-1) or (VI-3). Those estimates were calculated using either the equivalent specific surface area, S_0, from Equation (VI-7) together with Equation (VI-1) or the equivalent grain diameter, d_m, from Equation (VI-8) with Equation (VI-3). The estimate for the 40/45 angular sand is the same as the measured (regression) permeability. This is essential since the shape correction factor reported in Table VI-2 was obtained by forcing the Kozeny-Carman estimate to agree with the observations. The important improvement comes when that same shape correction factor (ϑ =.675) is assumed to hold for all sizes of angular grains included in the unsieved assemblage. While corrections for grain shape and size distribution were not able to resolve all of the difference between observed and estimated permeability, the difference was reduced from a factor of 2.58 for the uncorrected (K-C spherical) case to a factor of 1.08 for the corrected case. Thus, the ability to correct for grain size distribution in angular sands using the approach presented by Carman is effectively confirmed. A surprisingly accurate estimate of permeability for the angular sands was obtained using the Krumbein-Monk (K-M) empirical relationship between permeability and grain size distribution shown as Equation (VI-9). The grain size standard deviations (σ_{Phi}) were obtained from the Inman statistics of the grain size distribution by applying Equation (V-6) to the cumulative distributions of the sediments. In the case of the well-sorted (40/45) sediments, a uniform distribution of grain sizes was assumed across the sieve size limits. The K-M relationship was accurate to within 3 percent for

the sands of this study, 7 percent for the Nolle sands, but only 21 percent for the spherical beads. This emphasizes the care which must be taken in applying either empirical or physical relationships outside the bounds of their assumed validity.

Whether or not the observed differences are acoustically significant will be determined by the relative importance of the mechanisms which cause the observed dynamic response of a given sediment. If grain-to-fluid relative motions are important (high-permeability, low-frequency cases) then the accurate portrayal of the permeability may be quite important. If, on the other hand, grain-to-fluid relative motions are relatively unimportant (low-permeability, high-frequency cases), then inaccuracies in permeabilty estimates are not as significant. The relative importance of the permeability estimate differences shown in Table VI-3 will be demonstrated through acoustic (shear wave) predictions to be discussed in Chapter VIII.

Frame Shear Modulus (Real Part)

From Table III-1 we see that it is necessary to specify the complex shear modulus of the frame if the Biot-Stoll model is to be exercised. The real part of this modulus, μ_s, may be determined from the measurement of shear speed and total mass density for the dry sediment. Given these two parameters, assuming the imaginary part of the shear modulus is relatively small, one may calculate the real part from

$$\mu_s = \rho V_s^2 \qquad \text{(VI-10)}$$

That is how the μ_s reported in Table VI-1 was derived.

Sediment	Porosity ϕ	Exponent n	Structure Factor α
Angular Sand (unsieved)	.432	1.6	2.52
Angular Sand (40/45)	.432	1.4	1.92
Spherical Beads (40/45)	.355	1.2	1.65

TABLE VI-6. STRUCTURE FACTOR ESTIMATES DERIVED FROM SEDIMENT FORMATION FACTORS

value of the exponent n. The values varied from 1.2 for spheres to 1.9 for platy shell fragments. Natural sands showed values of n in the range 1.4 to 1.6. Grain size and grain size distribution were not significant factors. Thus, at a given porosity, increasing the angularity of the sediment grains (i.e., increasing the value of n) produces higher values of FF. The overall trend of the envelope of data showed n equal to 1.5 for natural quartz sands and 2.0 for clays, with mud and silt having intermediate values. The value for well-rounded quartz sand was 1.4

By combining Equations (VI-23) and (VI-24) we have a relationship for α dependent upon only the porosity and grain shape of the sediment. The resultant equation may be written as

$$\alpha = \phi^{-n} - \left(\frac{1-\phi}{\phi}\right) = \left[\frac{\phi^{-(n-1)}+\phi-1}{\phi}\right] . \qquad \text{(VI-25)}$$

In Table VI-6 we show the values of the structure factor calculated using this expression, the measured porosity and the exponent, n, reported by Jackson, et al.[104] for similar assemblages. Although grain size and sorting are not thought to be significant factors, different values of n were used for the two sands to indicate the range of values one might expect at the given porosity. One may see that the structure factor for the spherical beads is smaller than that for either sand. This trend of decreasing α with increasing sphericity is contrary to the trend observed by Domenico[25] or by the author. Therefore, although the values are within the theoretically acceptable bounds, they do not appear to be consistent with empirical data. The acoustic effect of these values will be demonstrated in Chapter VIII.

Combining this equation with Equation (VI-18) we obtain

$$\alpha = FF - \left(\frac{1-\phi}{\phi}\right), \qquad \text{(VI-23)}$$

an equation for the Biot-Stoll structure factor in terms of the sediment formation factor and porosity. This equation is assumed to be valid for high frequencies, but one restriction is that the wavelength divided by two should be a distance long enough to define macroscopic properties of the material. Generally this distance should be large compared to grain or pore dimensions.[103] This restriction is easily met for the frequencies and sediments considered in the present study.

In order to use the relationship in Equation (VI-23) one must establish what the formation factor is for the sediment under investigation. Recently, Jackson et al.[104] have investigated the relationships between electrical resistivity, porosity, and particle shape for sands. They report that the formation factor, defined as the ratio between the resistivity of the porous medium and the resistivity of the pore-fluid, may be related to the porosity of unconsolidated sediments by

$$FF = \phi^{-n} \qquad \text{(VI-24)}$$

where n is a constant determined by the constituent particle properties. This relationship was first constructed by Archie[104] and later modified by Winsauer et al.[105] The value of n was established for several natural and artificial sediments by varying the shape, size, porosity, and size distribution. Shape was shown to be the only parameter significantly affecting the

Other approaches have been put forth to provide estimates of the structure factor independent of acoustic data.

Brown[103] has proposed that the Biot-Stoll fluid-solid coupling factor can be related to the electrical-resistivity formation factor of a fluid-filled porous medium. He defines a coupling coefficient, λ, as

$$\lambda = \rho/\rho_f = FF\emptyset \qquad \text{(VI-18)}$$

where ρ = the bulk density of the sediment
ρ_f = the fluid density
FF = the electrical-resistivity formation factor
$\emptyset$ = porosity

He then relates this to the "apparent density," ρ_a, defined by Biot[13] as:

$$\rho_a = m\emptyset^2 - \rho_f\emptyset \ . \qquad \text{(VI-19)}$$

The factor m is defined in Equation (III-45) and contains the structure factor, α. According to Brown,

$$\rho_a = \rho_f(\lambda-1) \qquad \text{(VI-20)}$$

From Equations (VI-19) and (VI-20) we obtain

$$m\emptyset^2 - \rho_f\emptyset = \rho_f(\lambda-1) \qquad \text{(VI-21)}$$

We may substitute $m=\alpha\rho_f/\emptyset$ from Equation (III-45), resulting in

$$\alpha = \frac{\lambda+1}{\emptyset} + 1 \ . \qquad \text{(VI-22)}$$

a corrective factor, α, which is equal to or greater than one. This appears as an increase in the fluid inertia. Stoll[7] states that for uniform pores with axes parallel to the pressure gradient, α would equal one, while for a random distribution of uniform pores with all possible orientations the theoretical value of α is three. Ferrero and Sacerdote[102] have obtained a value of α=4.35 for sound propagation through an assemblage of small lead balls. This indicates that even for regular grain shapes the structure constant may equal or exceed the theoretical upper limit. In practice, α has been treated as an empirical parameter. Stoll[7,8,10] generally assigns a value of 1.25 for sands or clays, but has used values between 1.0 and 4.3 for this parameter.[6]

Domenico[25] has determined this inertia factor as a function of pressure, for shear and compressional waves, for both sand and bead specimens. For compressional waves the structure factor is between 1.0 and 1.2 for pressures below 7 MPa in both sands and beads, increasing to values between 2.0 and 3.0 at high pressures (above 20 MPa). Shear wave measurements show that for sands the structure factor remains between 1.0 and 1.2 for pressures below 10 MPA in sands, increasing to 3.0 for pressures of 35 MPa. Shear waves in beads behaved somewhat differently. The structure factor remained at a value slightly less than 3.0 to 10 MPa pressure, decreasing to 2.0 at 35 MPa. These empirical values, especially those at low pressures, are consistent with Stoll's usage of the structure factor, and the experience of the author.

Sediment	$\frac{dr}{6}$ ($\frac{dr}{7}$)	$\frac{\phi}{1-\phi}\frac{dm}{3}$	$2(\frac{kk_0}{\phi})^{0.5}$
Angular Sand (unsieved)	.0062 (.0053)	.0059	.0058
Angular Sand (40/45)	.0064 (.0055)	.0066	.0065
Spherical Beads (40/45)	.0064 (.0055)	.0071	.0071

TABLE VI-5. PORE SIZE PARAMETER ESTIMATES USING THREE DIFFERENT METHODS, a(cm).

We have at least three ways to estimate the pore size parameter. The modeler may choose the approach most appropriate to the case under investigation depending upon the sediment property data at hand. In this study, we will calculate pore size parameter estimates using each approach presented. Table VI-5 contains the results of the calculations. One can see that for these sediments the three methods give similar results. The second method, using Equation (VI-15), includes corrections for the grain shape and distribution incorporated in the equivalent sphere diameter, d_m. Without this correction, the angular sand pore size parameters would be larger by a factor proportional to the reciprocal of the shape factor, θ, in Table VI-2. The empirical grain size based estimate proposed by Stoll is quite consistent with the other two; and it appears that $d_r/6$ is most appropriate. The results of these three approaches will be compared with the empirical "best fit" estimates of the pore size parameter derived from acoustic data, and the acoustic significance of observed differences will be assessed in Chapter VIII.

Structure Factor

The structure factor appears in the Biot theory [see Equation (III-45)] in an attempt to account for the fact that not all of the pore fluid moves in the direction of the macroscopic pressure gradient because of the tortuous, multi-directional nature of the interstitial pores. This increase in effective path length results in less fluid flowing in and out of an elemental volume of sediment for a given acceleration than if all the pores were uniform and parallel. The effect is accounted for by multiplying the mass of fluid per unit volume by

$$a = 2r_h \qquad \text{(VI-13)}$$

where

$$r_h = \frac{\text{volume filled with fluid}}{\text{wetted surface}} = \frac{\phi}{(1-\phi)S_0} . \qquad \text{(VI-14)}$$

For most sediments S_0 is unknown, and we have not gained any additional information. We have simply traded one unknown parameter for another. However, if a spherical grain assumption is reasonable, then S_0 can be calculated from the grain diameter using Equation (VI-2) and the pore size parameter may be obtained using the relationship.

$$a = 2r_h = \frac{\phi}{(1-\phi)} \frac{d}{3} \qquad \text{(VI-15)}$$

In a manner similar to the approach used to calculate permeability using the Kozeny-Carman relationship, the irregular shape and non-uniform size distribution of grains may be accounted for by using Equations (VI-4) or (VI-8) to obtain an equivalent sphere diameter, d_m.

Without making an assumption about the spherical nature of the grains, we may still relate the pore size parameter to permeability, k, and porosity. Substituting Equation (VI-13) and (VI-14) into (VI-1), we see that

$$k = \frac{a^2}{4k_0} \phi \qquad \text{(VI-16)}$$

and

$$a = 2\left(\frac{kk_0}{\phi}\right)^{0.5} \qquad \text{(VI-17)}$$

Pore Size Parameter

The pore size parameter, a, appears in Equation (III-43) as a parameter with the dimension of length which depends upon both the size and shape of the intergranular pores. In Biot theory, it affects the viscous resistance to fluid flow and modifies the attenuation as a function of frequency. In the original theory it has been assumed to be a constant, thus rendering the frequency correction to be the same for all pores in a given sediment. This assumption may break down in materials where pore size is distributed over a wide range, causing a redistribution of viscous friction between the pores as the frequency is varied. Although not a physical property of a sediment in the pure sense, nonetheless, the pore size parameter serves as a measure of the effects which pore shape and size have on acoustic propagation. For modeling purposes we have included it in our specification of sediment properties.

The pore size parameter is usually considered to be an empirical constant chosen in such a way that the dispersion and attenuation curves derived from the Biot-Stoll model fit the experimental data.[12] Stoll[7] has considered it to be empirical, but has often used values between one-sixth and one-seventh the grain size in the absence of acoustic data. This determination was made based upon comparisons between the model outputs and data from which a relationship between pore size parameter and mean grain diameter could be derived.

Hovem and Ingram[17] identify the pore size parameter with twice the hydraulic radius (r_h), i.e.,

3 percent departure from the 10-kHz value is also well within the 90% confidence bounds. Thus, we may state that no significant frequency dependence is apparent for the logarithmic decrements for these dry sediments, and the 10-kHz values may be used to determine the imaginary part of the shear modulus.

Little data are available for comparison with the absolute values of dry frame log decrements. Bell[27] reported shear wave speed and attenuation values for an angular beach sand under low stress conditions similar to those of this study. His shear speed of 220 m/sec and attenuation coefficient of 63 dB/m at 10 kHz lead to a log decrement of 0.160. One may see from the values in Table VI-4 that these data are quite consistent with our observations for angular sands, falling between the sieved and unsieved cases. Hardin[60] presents log decrements for Ottawa and a subangular river sand measured at pressures between 20.7 kPa and 92.4 kPa. To reduce these values to the common pressure of 12 kPa of our measurements we used the findings reported by Drnevich, Hall, and Richart[101] which related the log decrement in sands to the negative one-third power of the confining pressure over the range from 19.2 kPa to 95.8 kPa. The average logarithmic decrement for the Hardin subangular sand, with a grain size distribution similar to the unsieved angular sand, was 0.174 after correcting for pressure. The Ottawa sand, with a well-sorted grain size between 0.59 mm and 0.84 mm, was 0.123 after correcting for pressure. Both sets of data compare well with our observations.

f is the frequency, Hz, and
8.686 is the conversion factor from nepers to decibels and is equal to 20 log e.

From Table VI-4 one can observe that the beads exhibit the greatest dry frame log decrement. This is consistent with observations reported by several investigators[24,58,59] for glass beads and sands under similar vibration amplitude and pressure conditions. Also apparent is the increase in log decrement for the moderately-sorted sand. Since the shear speeds for the sands are nearly equal, the increase is due almost totally to increased attenuation. The presence of small grains with greater specific surface areas, as demonstrated by the effective S_0 from Table VI-2, allows for greater grain-to-grain friction losses in the dry, moderately sorted sediment assemblage.

Attenuation in dry rocks or sediments is generally considered to be directly proportional to frequency, which implies [see Equation (VI-12)] that the log decrement for dry materials is indeperdent of frequency. Departure from this has large implications relative to the dominant dissipation mechanisms. To test this assumption, log decrements were computed for frequencies other than 10 kHz for the spherical beads and well-sorted sand. Attenuation in dry beads was measured at 5 kHz. The resultant attenuation coefficient of 52.4 dB/m leads to a log decrement of 0.295. This is about 2 percent higher than that at 10 kHz, but well within the 90% confidence bounds of that measurement. Similar attenuation measurements were made in the well-sorted sand at 20 kHz. The resultant attenuation coefficient of 115.9 dB/m leads to a log decrement of 0.137. The

also reported higher shear speed in dry beads than those observed in moderately-sorted Ottawa sand and a moderately-sorted angular sand. These data were also taken at low overburden pressures. Thus, our speed data are consistent with observations from other investigations once pressure differences are taken into account.

Frame Logarithmic Decrement

In order to compute the imaginary part of the frame shear modulus, μ', it is necessary to obtain the logarithmic decrement for the dry sediment. Given the logarithmic decrement, Δ_s, and the real part of the frame shear modulus, μ, one may use Equation (III-5), which may be written as

$$\mu' = \frac{\mu \Delta_s}{\pi} , \qquad \text{(VI-11)}$$

to compute the needed modulus.

For the sediments used in this study, the logarithmic decrements are calculated from the speeds and attenuation coefficients shown in Table VI-4. The reported values were obtained using shear waves at a frequency of 10 kHz. Logarithmic decrements are computed using the relationship

$$\Delta_s = \frac{\alpha_s V_s}{8.686 f} \qquad \text{(VI-12)}$$

where Δ_s is the logarithmic decrement,

α_s is the shear wave attenuation coefficient in decibels per unit length (e.g., dB/m),

V_s is the shear wave speed (m/sec),

Sediment	Statistic	V_s (m/sec)	α_s (dB/m)	Δ_s
Angular Sand (unsieved)	Mean 90% CI n	204.2 15.7 39	68.6 7.2 47	.161
Angular Sand (40/45)	Mean 90% CI n	205.4 11.1 28	56.1 2.0 42	.133
Spherical Beads (40/45)	Mean 90% CI n	244.1 17.0 32	102.5 4.8 24	.288

TABLE VI-4. MEASURED DRY FRAME SPEED, ATTENUATION, AND LOGARITHMIC DECREMENT AT 10 kHz

This property plays a key role in determining the frame logarithmic decrement, as well as being important in correcting physical model estimates or observations of wave speed and attenuation for pressure effects using the relationships derived by Richart et al.[47] discussed in Chapter II.

The shear speeds used to calculate the shear moduli were measured using the equipment and techniques described in Chapter IV. The observed speeds are shown in Table VI-4 together with the observed attenuation and the sediment frame logarithmic decrements computed at 10 kHz. We may note that the effects of sorting on dry speed appear to be negligible based upon the speeds in the sieved and unsieved sands. This is consistent with the fact that there is no change in porosity between the two samples. On the other hand there is a significant difference between the sieved sand and the spherical beads. The shear speed in the sands are approximately 16 percent lower, resulting in shear moduli approximately 32 percent lower than those for the beads. This difference in speed between the beads and the angular sand is similar to differences observed in plots of shear speeds in dry spherical glass beads and dry, crushed, and sieved glass beads presented by Murphy.[100] He showed that speeds in crushed glass beads were consistently 15 percent lower than glass spheres at pressures ranging from 0.1 to 35 MPa. The observed differences in speed between the sand and beads is also consistent with data presented by Domenico[25] when his observations are extrapolated to the pressures reported in this study. However, the magnitude of the differences reported here are greater than those obtained using Domenico's empirical pressure relationships. Bell[27]

Hovem and Ingram[17] have proposed an approach which treats the "structure constant" as a frequency-dependent factor which can be calculated from sediment properties; but, a close look reveals it to be of very limited usefulness. They write the equations of motion governing the propagation of compressional waves in the sediment as:

$$\nabla^2(He-C\zeta) = \frac{\partial^2}{\partial t^2}(\rho e-\rho_f\zeta) \qquad \text{(VI-26)}$$

and

$$\nabla^2(Ce-M\zeta) = \frac{\partial^2}{\partial t^2}(\rho_f e-\rho_c\zeta) - \frac{\eta F_r}{k}\frac{\partial \zeta}{\partial t} \qquad \text{(VI-27)}$$

Assuming solutions for e and ζ to be of the form

$$e = A_5 e^{i(\omega t-\xi x)} \qquad \text{(VI-28)}$$

$$\zeta = A_6 e^{i(\omega t-\xi x)}, \qquad \text{(VI-29)}$$

and substituting Equations (VI-28) and (VI-29) into Equations (VI-26) and (VI-27), results in two equations in A_5 and A_6. If solutions exist for A_5 and A_6, it must hold that the determinant of the coefficients for A_5 and A_6 equals zero. This determinant takes the form:

$$\begin{vmatrix} H\omega^2-C\xi^2 & \rho_f\omega^2-C\xi^2 \\ C\omega^2-\rho_f\xi^2 & \rho_c\omega^2-M\xi^2-\frac{i\omega\eta F_r}{k} \end{vmatrix} = 0 \qquad \text{(VI-30)}$$

A solution for the complex wave number ℓ will yield the phase velocity (from the real part) and the absorption (from the imaginary part) for the two kinds of compressional waves.

Stoll's[8] solution to the equations of motion governing the propagation of compressional waves in the sediment has been presented in Chapter III of this report [Equation (III-28)]. Rewriting the solution, with the substitution for m from Equation (III-45), we have

$$\begin{vmatrix} H\ell^2-\rho\omega^2 & \rho_f\omega^2-C\ell^2 \\ C\ell^2-\rho_f\omega^2 & \frac{\alpha\rho_f\omega^2}{\phi}-M\ell^2-\frac{i\omega nF}{k} \end{vmatrix} = 0 \qquad \text{(VI-31)}$$

since the constants H, C, and M may be shown to be equal [compare Stoll's[8] Equation (7) to Hovem's[17] Equations (16)-(20)] in Equations (VI-30) and (VI-31), three of the four factors in the two determinants are equal. For the determinants to be equal to one another, and zero, the factors in the lower right-hand corner of each determinant must be equal. Equating these factors we get

$$\rho_c\omega^2 - M\ell^2 - \frac{i\omega nF_r}{k} = \frac{\alpha\rho_f\omega^2}{\phi} - M\ell^2 - \frac{i\omega nF}{k} . \qquad \text{(VI-32)}$$

The coefficient F is the complex viscosity correction factor discussed in Chapter III and may be written as $F=F_r+iF_i$, where F_r is the real part and F_i the imaginary part. Substituting for F and simplifying the equation results in

$$\rho_c = \frac{\alpha\rho_f}{\phi} + \frac{i\eta F_r}{\omega k} - \frac{i\eta F_r}{\omega k} + \frac{\eta F_i}{\omega k} , \qquad \text{(VI-33a)}$$

which reduces to

$$\rho_c = \frac{\alpha\rho_f}{\phi} + \frac{\eta F_i}{\omega k} \qquad \text{(VI-33b)}$$

(A similar analysis of the equations governing shear wave propagation will result in the identical equation.) Hovem and Ingram[17] report that:

$$\rho_c = \frac{\rho_f}{\phi} + \frac{\eta F_i}{\omega k} \qquad \text{(VI-34a)}$$

or

$$\rho_c = \frac{\rho_f}{\phi}\left(1 + \frac{\eta\phi F_i}{k\rho_f\omega}\right) . \qquad \text{(VI-34b)}$$

They then define a "structure constant"

$$\gamma = 1 + \left(\frac{\eta\phi F_i}{k\rho_f\omega}\right) \qquad \text{(VI-35)}$$

and consequently,

$$\rho_c = \frac{\gamma\rho_f}{\phi} . \qquad \text{(VI-36)}$$

This "structure constant" is said to be equivalent to the structure factor presented in Stoll's[8] formulation [Equation (III-45)], and discussed by Domenico[25] as a result of his measurements on unconsolidated sediments. This statement is in error, for one can easily determine by comparing Equations (VI-33b) and (VI-34a) that the two are equivalent only in the trivial cases of $\gamma=1$. To use the Hovem and Ingram "structure constant," γ, in

place of the Biot-Stoll structure factor, α, as implied in the Hovem and Ingram paper,[17] is to commit an error. To use the Hovem and Ingram "structure constant" in the reduction of Equation (VI-30) is tantamount to solving Equation (VI-31) with $\alpha = 1$. Thus, the Hovem and Ingram proposal that their formulation of the equations of motion for the propagation of acoustic waves in sediments leads to a frequency-dependent structure factor which can be calculated from sediment properties, is invalid for all but the most trivial applications.

Berryman[107,108] has proposed that we define the structure factor to be

$$\alpha = 1 - r(1-1/\emptyset) \qquad \text{(VI-37)}$$

where r is a factor related to the particle shape which accounts for the additional mass induced in the fluid due to the oscillation of the solid sediment particles in the fluid. For spheres oscillating in a fluid, $r=0.5$; for other ellipsoidal shapes, $0 \leq r \leq 1$. Values of r for regular ellipsoidal shapes are available as functions of aspect ratio in hydrodynamics references,[109] but in general the value of r must be determined from a microscope model of the frame moving in the fluid.[107]

Given the porosity of the spherical beads from Table VI-1, one may calculate the structure factor, $\alpha = 1.80$, for $r=0.5$. No value for the angular sand is available unless one chooses to speculate on an appropriate value for r. Given the unknown nature of the shape factor r, no attempt was made to include the Berryman approach in the model-to-data comparisons.

In this subsection we have discussed various methods which have been proposed to provide estimates for the sediment structure factor. Neither the Brown, Hovem and Ingram, nor Berryman approaches appear to provide us with acceptable values. This leaves us with the requirement to determine the structure factor by empirical methods based upon acoustic model-to-data fits. In the absence of such data one may estimate the structure factor based upon theoretical and empirical insight obtained from results published by Stoll[8] and Domenico.[25]

Summary

This chapter has presented those physical properties of the sediments used in this study deemed to be important in interpretation, comparison, and modeling of their acoustic properties. We have included not only direct measurements, but also empirical and theoretical relationships from which the sediment properties can be derived. Certain of these relationships have been shown to be consistent with our observations; others have been shown to be inconsistent.

In the following chapters, we will present the results of acoustic measurements and modeling efforts using the sediments described in this chapter. The effects of using several of the relationships presented will be assessed through acoustic model-to-data comparisons.

VII. SHEAR WAVE DATA PRESENTATION AND ANALYSIS

Background

The laboratory equipment and procedures described in Chapter IV were used to determine the speed and attenuation of shear waves in three laboratory sediments. Speed and attenuation were obtained under both dry and water-saturated conditions for each sediment. The results of these measurements together with a discussion of their relationship to other observations will be presented in this chapter.

Shear Speed Measurements

As discussed in Chapter IV, shear speeds were determined using an incremental filling method to gradually increase the transducer separation while noting the incremental change in the delay time between the beginning of the oscilloscope sweep and the zero crossing of a selected cycle of the received waveform. The observed values of transducer separation and delay time may then be plotted on a graph. By fitting a straight line to the data using least squares linear regression techniques, one can determine the shear wave speed from the slope of the resultant line. The statistics of the regression analysis, in particular the standard error of the regression coefficient representing the slope, allows one to establish a confidence interval on the slope at some stated percent level. For the speeds reported in this report we have chosen to compute a confidence interval on the slope at the 90 percent level.

In Figure VII-1 we show the data and regression line from which the wet shear speeds were determined. All data were taken at a frequency of 10 kHz with a vertical stress of 12 kPa consistent with the stress conditions under which other acoustic measurements were performed. The data were taken over path lengths ranging from 2.2 to 18.6 cm. Table VII-1 summarizes the results of the shear wave speed measurements, both wet and dry. In addition, shear moduli are calculated for the three sediments from measured speed and bulk density using Equation (VI-10). It appears that the addition of fluid causes a decrease in shear speed for all three sediments. For the two well-sorted sediments the decrease is between 5.6 and 7.7 percent. The moderately sorted sand shows a speed decrease of 11.9 percent. This decrease with increased saturation is consistent with data presented by several investigators.[24,25,27] The apparent increase in shear modulus in the well-sorted sand and spherical beads is consistent with data presented by Domenico[25] for well-sorted Ottawa sand and spherical glass beads. He reported increases in shear moduli of approximately 10 percent in beads and 18 percent in Ottawa sand as the fluid content was increased from dry to brine-saturated. This is in contrast to a statement by Hardin and Richart[23] that at low confining pressures the shear modulus of Ottawa sand may be decreased as much as 15 percent by the presence of moisture. However, close examination of the data upon which this statement is based reveals a decrease in shear modulus of approximately 2 percent to be more typical. In the same paper it is stated that there was little effect of moisture on the modulus of the frame in crushed quartz sand. This is consistent with our observations for the moderately sorted angular quartz sand. The

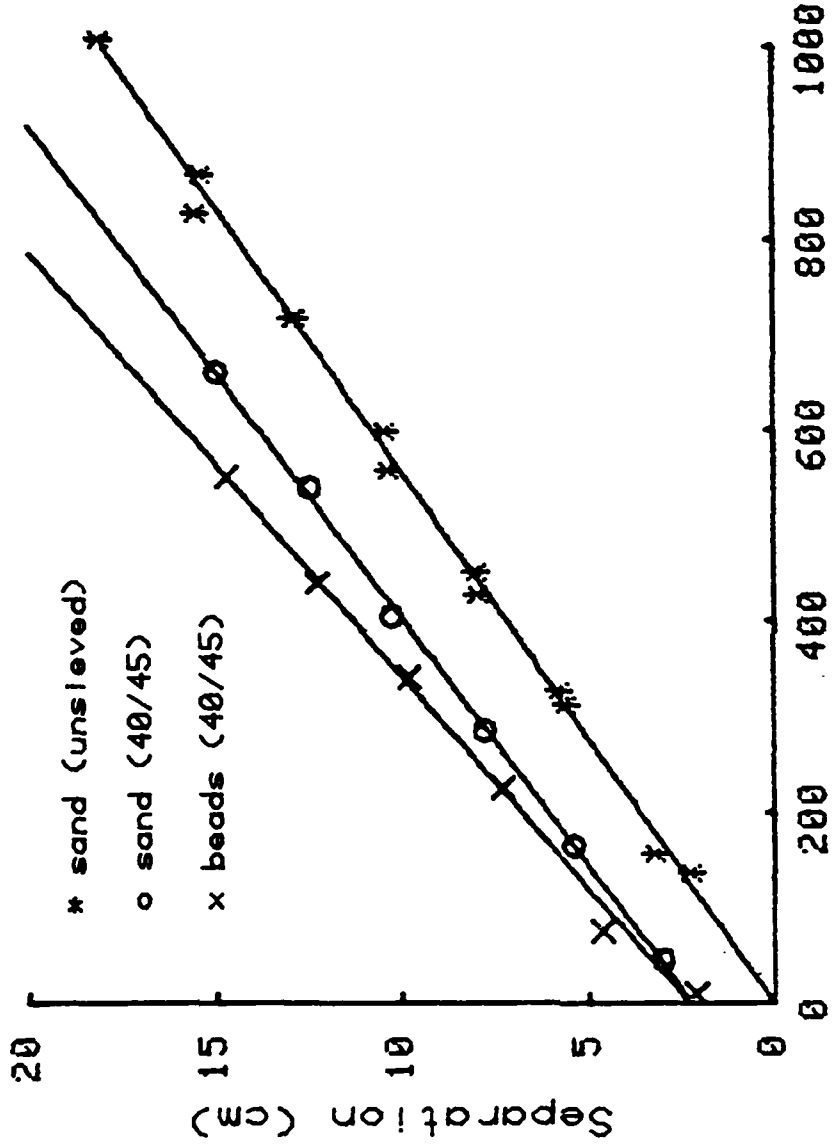

FIGURE VII-1. SHEAR WAVE SPEED DATA (SATURATED SAMPLES)

Sediment	Statistic	V_s (m/sec) dry	μ_s (dyne/cm^2) dry	V_s m/sec wet	μ_s (dyne/cm^2) wet
Angular Sand (unsieved)	Mean 90% CI η	204.2 15.7 39	6.30×10^8 0.97×10^8 39	179.8 5.6 13	6.28×10^8 0.39×10^8 13
Angular Sand (40/45)	Mean 90% CI η	205.4 11.1 28	6.37×10^8 0.69×10^8 28	193.9 6.5 6	7.30×10^8 0.49×10^8 6
Spherical Beads (40/45)	Mean 90% CI η	244.1 17.0 32	9.30×10^8 1.30×10^8 32	225.3 17.5 6	9.72×10^8 1.51×10^8 6

TABLE VII-1. SHEAR SPEED AND MODULUS AT 10 kHz, WET AND DRY SEDIMENTS

implication is that the presence of fluid has some effect on the rigidity of the frame in the case of the sieved sediments, but none in the unsieved sand. An interesting observation may be made from data presented by Pilbeam and Vaisnys.[24] When small amounts of lubricating fluid were introduced into specimens composed of dry glass beads or angular crystalline alumina, the shear speed in the glass beads increased while the speed in the alumina was unaffected. Correcting for a slight change in specimen density lead to the conclusion that the frame rigidity of the glass beads had been altered, resulting in a higher value for the shear modulus. The authors attributed this to an increased number of close contacts allowed by decreasing the contact friction. The interlocking geometry of the angular specimens, on the other hand, prohibited the making of new contacts. Thus, for the angular unsieved sand of the current study, the change in shear speed between the dry and wet conditions is attributable to the observed change in bulk density, while the well-sorted samples show a smaller change in shear speed than one would expect based on the observed bulk density change. This may be due to an increase in close grain contacts in the well-sorted sediments as lubricating fluid is introduced. The sands, having the same porosity, experience the same degree of change in the sediment bulk density, yet while the unsieved sand exhibits a 12 percent change in speed, the sieved sand speed decreases by only 6 percent. Much of the effect of the density increase is apparently offset by a 15 percent increase in the shear modulus for the sieved sand.

The values of speed are quite consistent with values reported in the literature for saturated sands with a value of 197 m/sec being reported for clean sands in shallow water off San Diego.[22] When corrected for pressure, using exponents included in their report, the shear speeds reported by Pilbeam and Vaisyns[24] vary from 150 m/sec in clean dry beads to 246 m/sec in slightly lubricated beads of a size range similar to those used in the present study.

Shear Attenuation Measurements

The attenuation of transverse vibrations excited in each of three laboratory sediments was measured at 17 discrete frequencies. The measurement techniques and equipment have been discussed in Chapter IV. Measurements were made for both dry and water-saturated samples. The dry measurements provided estimates of dry frame logarithmic decrement which is an important parameter in the Biot/Stoll physical model. The results of the dry measurements have been reported and discussed in Chapter VI in conjunction with the treatment of sediment properties. Suffice it to say that our observations are consistent with those previously reported in the literature, including our finding of a linear dependence of attenuation on frequency and constant log decrement for each dry sediment sample. Water-saturated sediments allow one to gain insight into the frequency dependence of attenuation when grain-to-fluid viscous effects are present. Attenuation measurements allow one to determine the relative importance of the various loss mechanisms postulated in the literature. The effects of grain shape and sorting may also be discerned from the attenuation data. An additional purpose for the

attenuation data is to provide well-documented measurements which can be compared with predictions from the Biot/Stoll model. These comparisons will be discussed in Chapter VIII.

In Table VII-2 we present the results of the shear wave attenuation measurements taken during this study. The attenuation values are derived from least squares linear regression fits to received level versus transducer separation data for each frequency and sediment type. We have discussed the method used to obtain the attenuation coefficients from the slope of the line fit to the data. The confidence intervals are computed from the standard error of the slope estimate. If we assume that the variations of the observations about the straight line are normal, that is the errors between our linear model and the observations are all from the same normal distribution, $N(0, \sigma^2)$, then we can assign $100(1-\gamma)\%$ confidence limits for our slope, α_s, by calculating

$$\alpha_s \pm t(n-2, 1-\frac{\gamma}{2}) \cdot SE \qquad \text{(VII-1)}$$

where $t(n-2, 1-\frac{\gamma}{2})$ is the $(1-\frac{\gamma}{2})$ percentage point of a t-distribution with (n-2) degrees of freedom, and SE is the standard error of the slope.[110] The 90% confidence intervals reported in this study were determined using this approach. The logarithmic decrements were calculated using the wet shear speed from Table VII-1 and Equation (VI-12).

The values of attenuation in Table VII-2 will allow one to compare the relative degree of energy loss exhibited by each sediment assemblage under

Frequency (kHz)	Angular Sand (unsieved)				Angular Sand (40/45)				Spherical Beads (40/45)			
	α_s (dB/m)	90% CI (dB/m)	Δs	n	α_s (dB/m)	90% CI (dB/m)	Δs	n	α_s (dB/m)	90% CI (dB/m)	Δs	n
1.0	7.2	3.0	.15	47	7.8	2.9	.17	38	9.5	2.4	.25	30
1.5	16.2	3.3	.23	47	7.9	2.5	.12	38	15.2	3.7	.26	30
2.0	39.3	2.6	.41	47	29.3	3.4	.33	38	17.2	3.2	.22	30
2.5	73.4	5.2	.61	38	53.0	6.0	.47	29	24.5	2.5	.25	30
3.0	81.0	3.7	.56	36	64.5	5.6	.48	27	32.2	2.7	.28	30
3.5	85.7	4.2	.51	36	66.9	4.5	.43	27	45.7	2.0	.34	30
4.0	97.0	9.1	.50	42	67.9	3.2	.38	39	53.3	2.5	.35	29
5.0	117.0	10.8	.48	42	83.9	3.4	.38	39	66.6	3.4	.35	29
6.0	129.4	8.8	.45	42	95.2	4.4	.35	39	78.2	3.1	.34	29
7.0	154.3	8.3	.46	42	103.2	3.9	.33	39	91.7	2.2	.34	29
8.0	174.2	13.1	.45	41	117.0	3.7	.33	38	105.6	4.6	.34	27
10.0	201.3	12.0	.42	40	133.0	3.4	.30	38	119.0	6.6	.31	27
12.0	226.4	15.4	.39	39	153.2	3.0	.29	36	135.1	6.5	.29	26
14.0	240.9	18.3	.36	37	163.7	5.9	.26	32	158.2	6.2	.29	24
16.0	262.0	26.8	.34	26	189.0	7.3	.26	30	183.3	9.4	.30	22
18.0	274.8	38.9	.32	30	214.8	8.7	.27	25	194.0	14.0	.28	18
20.0	280.9	24.7	.29	28	242.6	11.7	.27	21	216.6	11.6	.28	16

TABLE VII-2. SHEAR WAVE ATTENUATION IN WATER-SATURATED LABORATORY SEDIMENTS

similar experimental conditions. One may observe that the loss in the unsieved angular sand is always greater than that in the sieved angular sand for frequencies higher than 1.0 kHz. A similar statement may be made when comparing the well-sorted angular sand to the well-sorted spherical beads at frequencies greater than 1.5 kHz. An examination of the confidence intervals shows that those for the unsieved angular sand are usually larger, particularly at the higher frequencies (>4 kHz). In general, the most reproducible (smallest CI) estimates are exhibited by the well-sorted angular sands.

This fact is borne out visually by the plots of received level versus separation data taken at 10 kHz for each of the three sediments used in this study (Figures VII-2 through VII-4). These data were used to determine the shear wave attenuation values at 10 kHz in Table VII-2. Data from individual measurement trials for a particular sediment are indicated by different symbols on the plots. Repeatability is apparent from the trial-to-trial consistency. The well-sorted angular sand shows the least scatter about the regression lines, an observation consistent with the smaller confidence interval.

To demonstrate the nature of the observed scatter as a function of frequency, Figures VII-5 through VII-7 are shown. These figures display received level versus separation data at 1 kHz, 10 kHz, and 20 kHz for the well-sorted angular sand. As one might expect, the most scatter is apparent in the 1-kHz data. Because of the long wavelength and low attenuation at this frequency, there is a greater possibility that interference will

nature to that previously noted for the well-sorted sand data. Attempts to describe the curve with either a single power curve or linear regression line fit yield the two curves shown on the plot. While either fit yields a coefficient of determination equal to or greater than 0.9, it is easy to see that neither the linear regression line nor the power curve represents all the data well. If one desired to do so, it would be possible to state that the data yield a nearly linear frequency dependence. This could be substantiated, since the exponent of frequency from the power curve fit to the data equals 1.06. However, on closer analysis, one may identify two or three significant changes in the relationship between attenuation and frequency.

At the lower frequencies (1.0-2.5 kHz), the frequency exponent is greater than 2.0 for the power curve fit to the mean attenuation. No mechanism is known to yield a frequency exponent greater than 2.0, with the possible exception of Rayleigh scattering, and this mechanism may be ruled out at such low frequencies. If one takes into account the confidence interval surrounding the mean attenuation at each frequency, a frequency exponent of 2.0 can be supported. Biot theory predicts such an exponent for viscous losses due to fluid-to-grain relative motion at low frequency. From the transition frequency equation [Equation (IV-1)], we see that for a frequency of 2.5 kHz to be in the low frequency region according to Biot theory, the pore size must be smaller than approximately .002 cm. This is about one-third of our estimates for the average pore size from considerations discussed in Chapter VI. However, as Morse[48] has stated, given the nature of the unsieved sand it is quite reasonable to assume that a

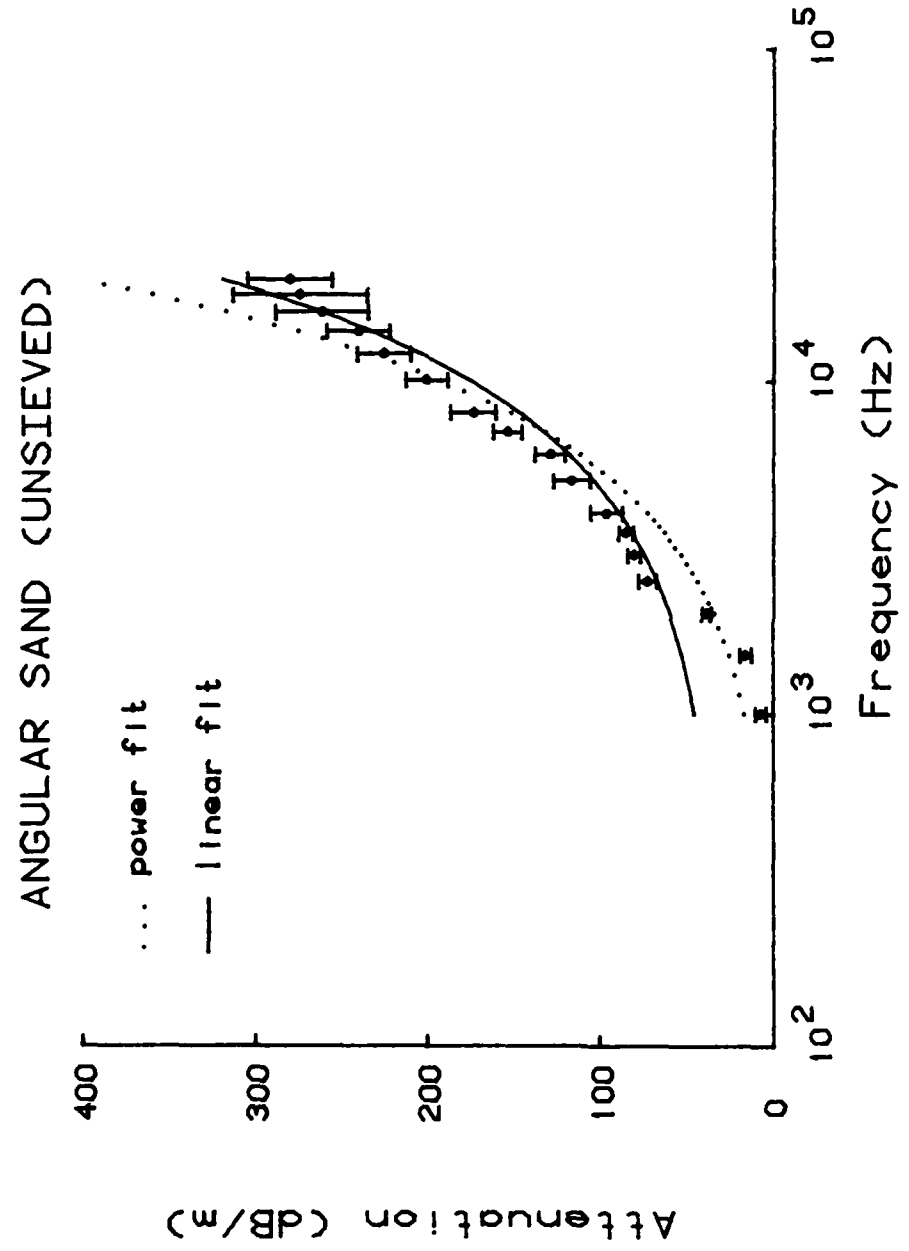

FIGURE VII-10. ATTENUATION VERSUS FREQUENCY FOR MODERATELY-SORTED ANGULAR SAND (UNSIEVED)

At the lower frequencies (1.0-2.5 kHz) the data exhibit a frequency dependence more typical of the viscous losses due to grain-to-fluid relative motion than those losses due to grain-to-grain friction. It is probable that this region is displaying the results of a complex combination of loss mechanisms resulting in both friction and viscous losses. However, it is difficult to explain the abrupt change of slope exhibited in the data above 2.5 kHz, although in shear attenuation data presented by Winkler and Nur[66] for saturated sandstone there was evidence of a similar decrease in the rate of increase of attenuation beyond 4 kHz.

As one moves beyond 2.5 kHz the slope changes to one consistent with an interaction between grain-to-grain friction losses and "high frequency" viscous losses confined to the grain boundary layer. This leads to a frequency exponent between the 1.0 and 0.5 typical of the respective loss mechanisms. A power curve fit to the data between 2.5 kHz and 20.0 kHz yields a frequency exponent of 0.70, slightly lower than that for the beads indicating a diminished role of the frame friction mechanism relative to the boundary layer viscous losses. This is consistent with the smaller frame log decrement and the decreased permeability when compared to the spherical beads.

Angular Sand (unsieved)

In Figure VII-10, we see the plot of attenuation versus frequency measured in the moderately-sorted angular sand. The most striking feature of the plot is the apparent change in slope as one proceeds from low to high frequency. This is quite similar in

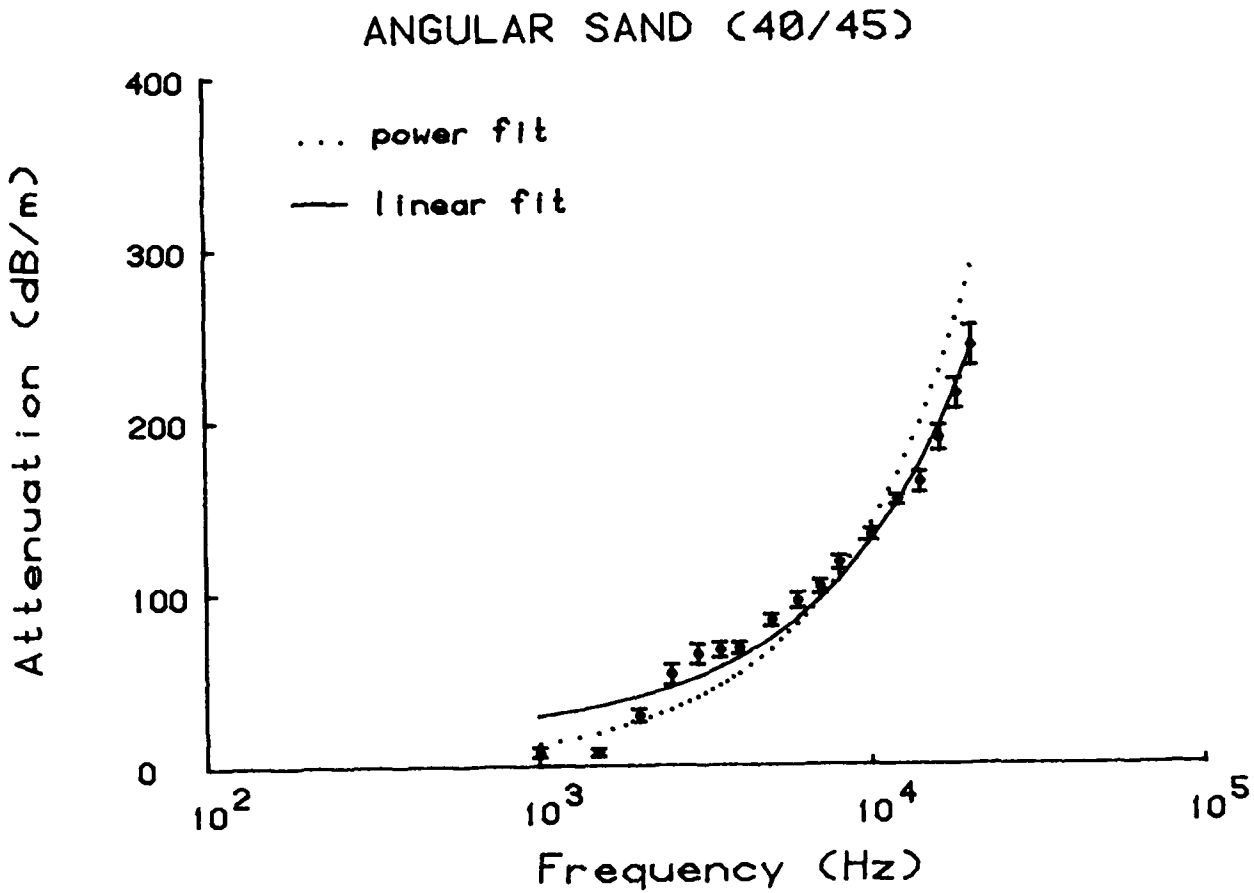

FIGURE VII-9. ATTENUATION VERSUS FREQUENCY FOR WELL-SORTED ANGULAR SAND (40/45)

for a power curve fit to data between 1.0 and 4.0 kHz is 1.24, while the exponent for frequencies between 5.0 and 20.0 kHz is 0.83.

Given the higher permeability of the beads, one would expect the transition frequency, where grain-to-fluid relative motion resulting in frequency squared loss dependence gives way to viscous losses confined to the grain boundary layer and typified by attenuation proportional to the square root of frequency, to occur at lower frequencies than in the sands.[59] This diminished effect of the frequency squared attenuation coupled with high frictional losses indicated by the large frame log decrement make the nearly linear frequency dependence understandable. So while there is some evidence that fluid viscous losses may be important, they are generally overshadowed by the grain-to-grain friction losses.

Angular Sand (40/45)

Attenuation versus frequency data are displayed in Figure VII-9 for the well-sorted angular sand (40/45). The data exhibit evidence of a significant slope change below 2.5 kHz. Least squares linear regression and power curve fits to the data are plotted in the figure. One may state, with some justification, that overall the data exhibit a linear frequency dependence. In fact, the power curve fit to the data yields a frequency exponent equal to 1.05. Visually, it is obvious that neither curve adequately reproduces the displayed frequency dependence, with several different frequency relationships apparent in the data.

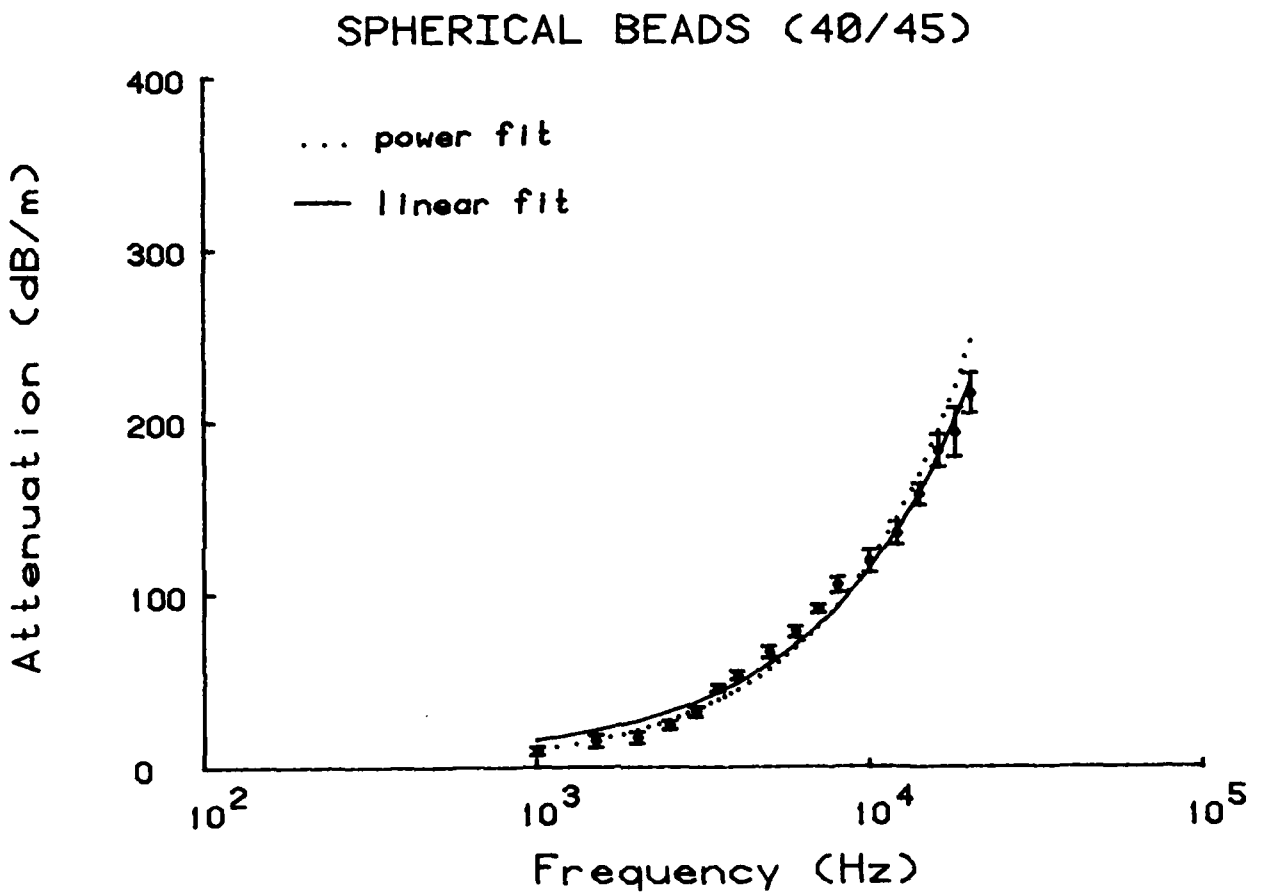

FIGURE VII-8. ATTENUATION VERSUS FREQUENCY FOR WELL-SORTED SPHERICAL BEADS (40/45)

In addition to the magnitude of the logarithmic decrements, one should examine their behavior with frequency. If the assumption that attenuation is proportional to frequency is to be sustained, then examination of Equation (VI-12) reveals that the log decrement must remain constant in the absence of velocity dispersion. If the log decrements increase with frequency, then the frequency exponent is greater than one, consistent with the grain-to-fluid viscous interaction loss mechanism. If, conversely, the log decrement decreases with increasing frequency, then the frequency exponent is smaller than one. This may be indicative of viscous loss in the boundary layer region surrounding the sediment grains. The data of Table VII-2 indicate that the loss mechanism at work in the three sediments may be a complex interaction of viscous and grain-to-grain friction since there is evidence of increasing, decreasing, and constant log decrements in all samples.

In order to better display the frequency dependence of attenuation for each sediment type, the measured attenuation values have been plotted as functions of frequency. The plots also include the 90 percent confidence intervals.

Spherical Beads (40/45)

The data displayed in Figure VII-8 are for shear wave attenuation in well-sorted spherical beads. It is apparent from the curves displayed on the figure that the data are reasonably represented by a linear fit. In fact, the exponent of the power curve fit shown is 1.06. There is, however, some evidence of non-linearity in the frequency dependence. The frequency exponent

be present in the data. This appears to be the case. However, it is felt that the interference effects are not severe enough to invalidate the attenuation estimates. They are accounted for in the confidence intervals associated with each attenuation estimate. The two higher frequency examples (Figures VII-6 through VII-7) exhibit well-behaved data which are typical of the mid-to-high frequency measurements for all three sediments.

The logarithmic decrements presented in Table VII-2 are consistent with previously reported data for sands and spherical aggregates. Kudo and Shima[29] reported shear wave attenuations in near-surface diluvial sands consistent with log decrements of 0.39. Wyllie, et al.[57] reported shear log decrements equivalent to 0.4-0.5 for well-sorted (20/30 mesh), saturated, Ottawa sands, when appropriate pressure corrections were applied in accordance with relationships included in their study. Pilbeam and Vaisnys[24] reported log decrements equivalent to 0.24 for dry spherical beads, increasing to 0.65 for lubricated spherical beads. These log decrements were obtained by correcting those reported in their study by a pressure factor proportional to the square root of the pressure ratio. These values are quite consistent with the values reported in Tables VI-1 and VII-2 for beads. Hamilton[1] concludes that, though the data are sparse, the log decrement of low-strain shear waves in most near-surface (i.e., low pressure) saturated sands should vary between 0.1 and 0.6 with most values falling between 0.2 and 0.4. The data presented in this study are in substantial agreement with Hamilton's statements.

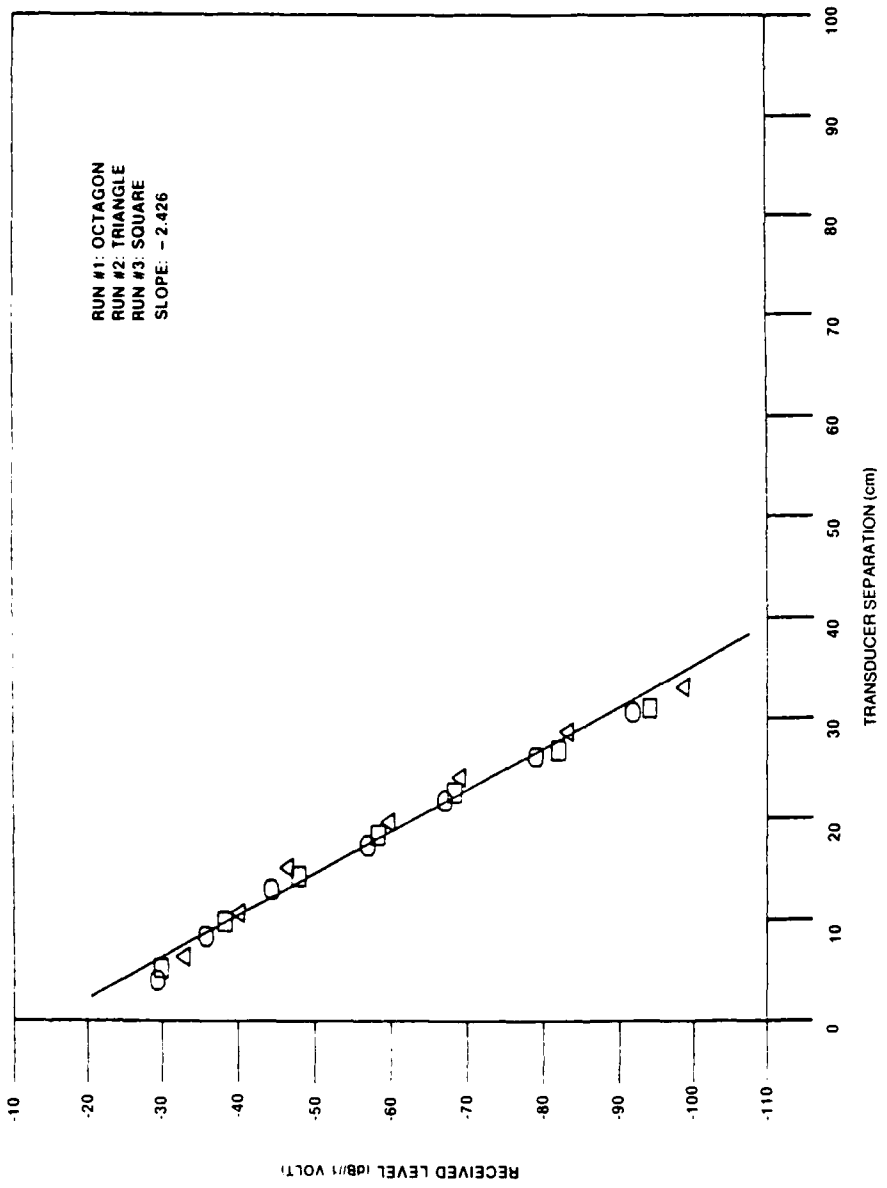

FIGURE VII-7. RECEIVED LEVEL VERSUS SEPARATION FOR WELL-SORTED ANGULAR SAND AT 20 kHz

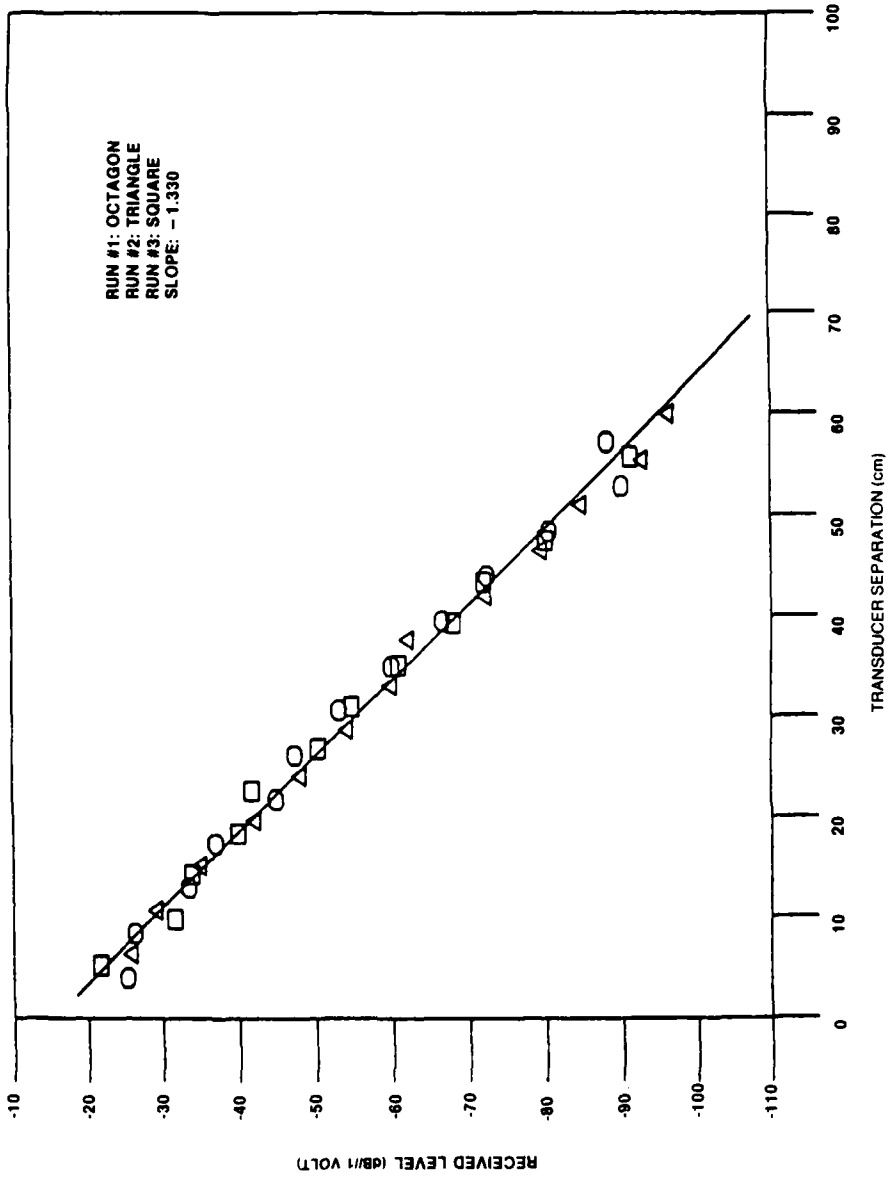

FIGURE VII-6. RECEIVED LEVEL VERSUS SEPARATION FOR WELL-SORTED ANGULAR SAND AT 10 kHz

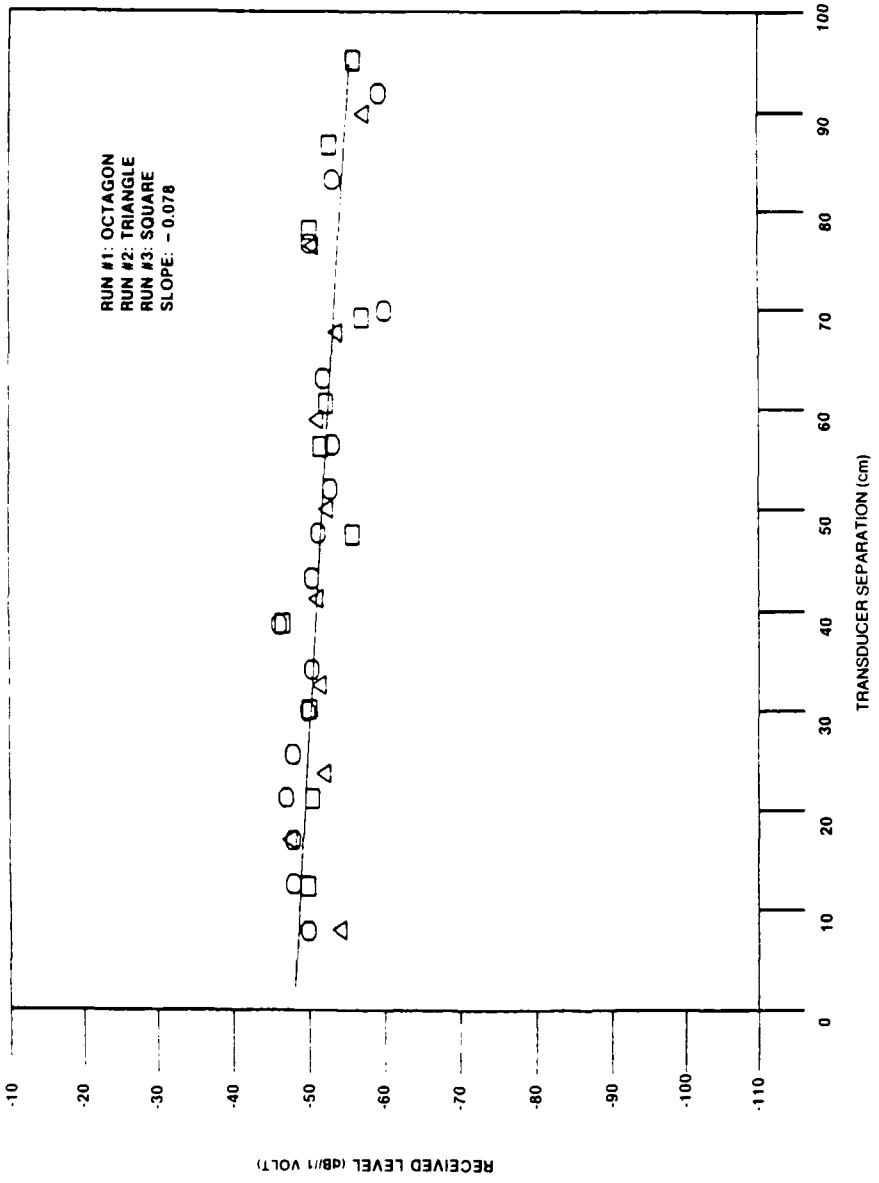

FIGURE VII-5. RECEIVED LEVEL VERSUS SEPARATION FOR WELL-SORTED ANGULAR SAND AT 1 kHz

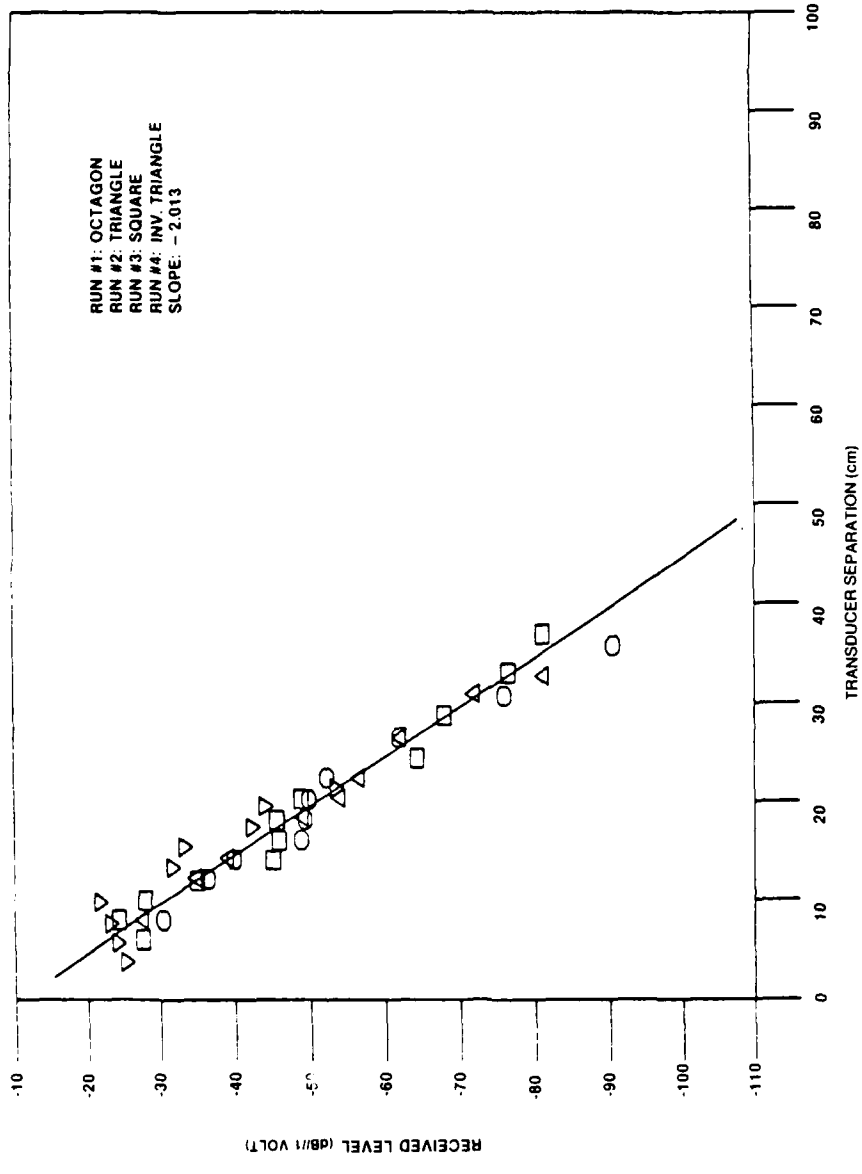

FIGURE VII-4. RECEIVED LEVEL VERSUS SEPARATION FOR MODERATELY-SORTED ANGULAR SAND AT 10 kHz

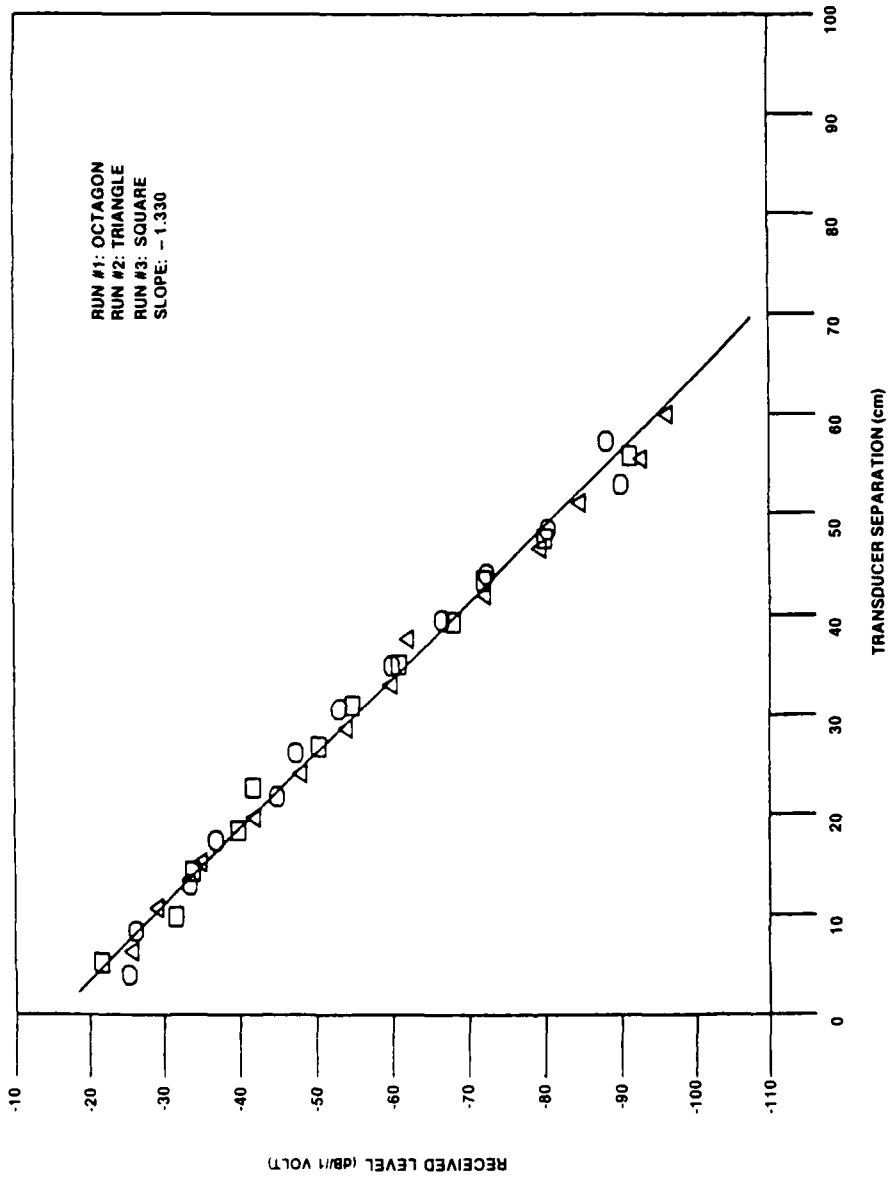

FIGURE VII-3. RECEIVED LEVEL VERSUS SEPARATION FOR WELL-SORTED ANGULAR SAND AT 10 kHz

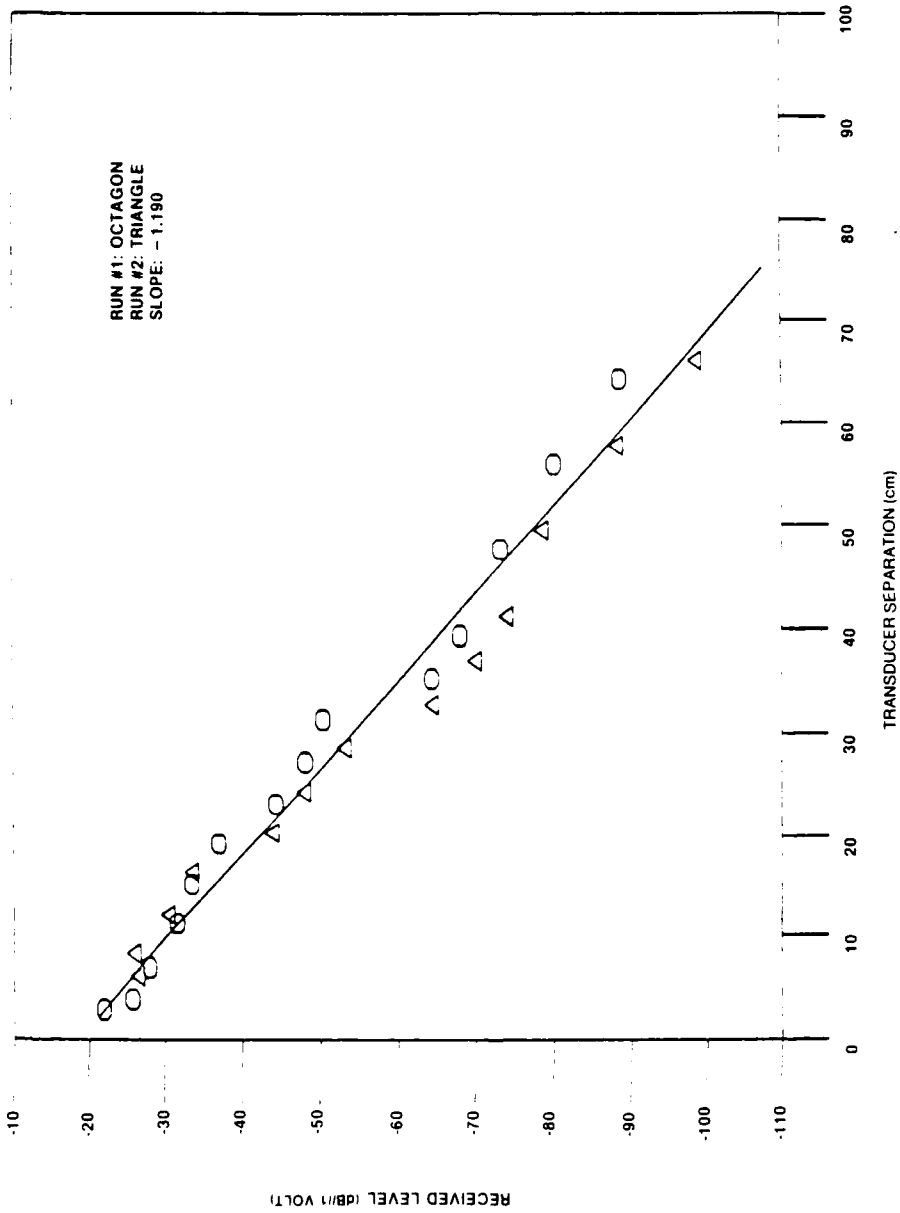

FIGURE VII-2. RECEIVED LEVEL VERSUS SEPARATION FOR WELL-SORTED SPHERICAL BEADS AT 10 kHz

significant number of intergranular pores may be smaller than the average pore size. Thus, we have some grounds, albeit tenuous, to relate the observed frequency dependence to viscous interaction between sediment grains and interstitial pore fluid. In any case, a linear relationships typical of grain-to-grain friction is not indicated in this frequency range.

As we move up in frequency, the apparent frequency exponent decreases to a value less than one, with an abrupt change above 2.5 kHz, similar to that observed in the well-sorted sand. The attenuation data between 2.5 kHz and 8.0 kHz are well represented by a power curve fit with a frequency exponent of 0.75. Between 8.0 kHz and 20.0 kHz the data may be fit by an equation with a frequency exponent of 0.53. Since we are surely beyond the low frequency regime of Biot theory, these may well be regions where the linear grain-to-grain friction mechanisms are interacting with the inertially dominated boundary layer viscous loss mechanisms represented by Biot theory as having an attenuation proportional to the square root of frequency. This type of interaction between mechanisms is consistent with previous observations and calculations reported by other investigators.[21,27,57,82,111] As a matter of interest, one may obtain a reasonable fit to the data over the frequency range from 2.5 kHz to 20.0 kHz with a single power curve yielding a frequency exponent of 0.70 with a coefficient of determination of 0.99. This behavior is consistent with that observed in the well-sorted sand, but the greater overall loss levels are probably due to the higher level of grain-to-grain frictional loss as indicated by the larger frame log decrement, and a lower viscous loss component consistent with the

lower permeability, both properties apparent from Table VI-1.

Grain Shape Effects

The effects of grain shape on the physical and acoustic properties of laboratory sediments can be determined by comparing the measurement results for the well-sorted angular sand and spherical beads. Table VI-1 reveals that though the mean grain size is the same, there are significant differences in the porosity, permeability, and complex shear modulus of the two materials. These physical differences manifest themselves as differences in the sediment acoustic properties.

The shear speed in the beads are consistently higher than the speed in the angular sand, wet or dry. Pilbeam and Vaisnys[24] noted a similar decrease in speed with increasing angularity. The relative change of speed due to saturation shows a slightly diminished effect in the angular sand. Most of the difference is attributable to the greater degree of change in the angular sediment rigidity (+14.6%) compared to that of the beads (+4.5%) which tended to offset the effect of the increased sediment bulk densities. These observations are in agreement with data presented by Domenico[25] for glass beads and Ottawa sands.

In Figure VII-11 we present plots of shear wave attenuation as a function of frequency for both saturated, well-sorted sediments. The two plots exhibit similar attenuation values at several frequencies, but they are substantially different in slope between 1.5

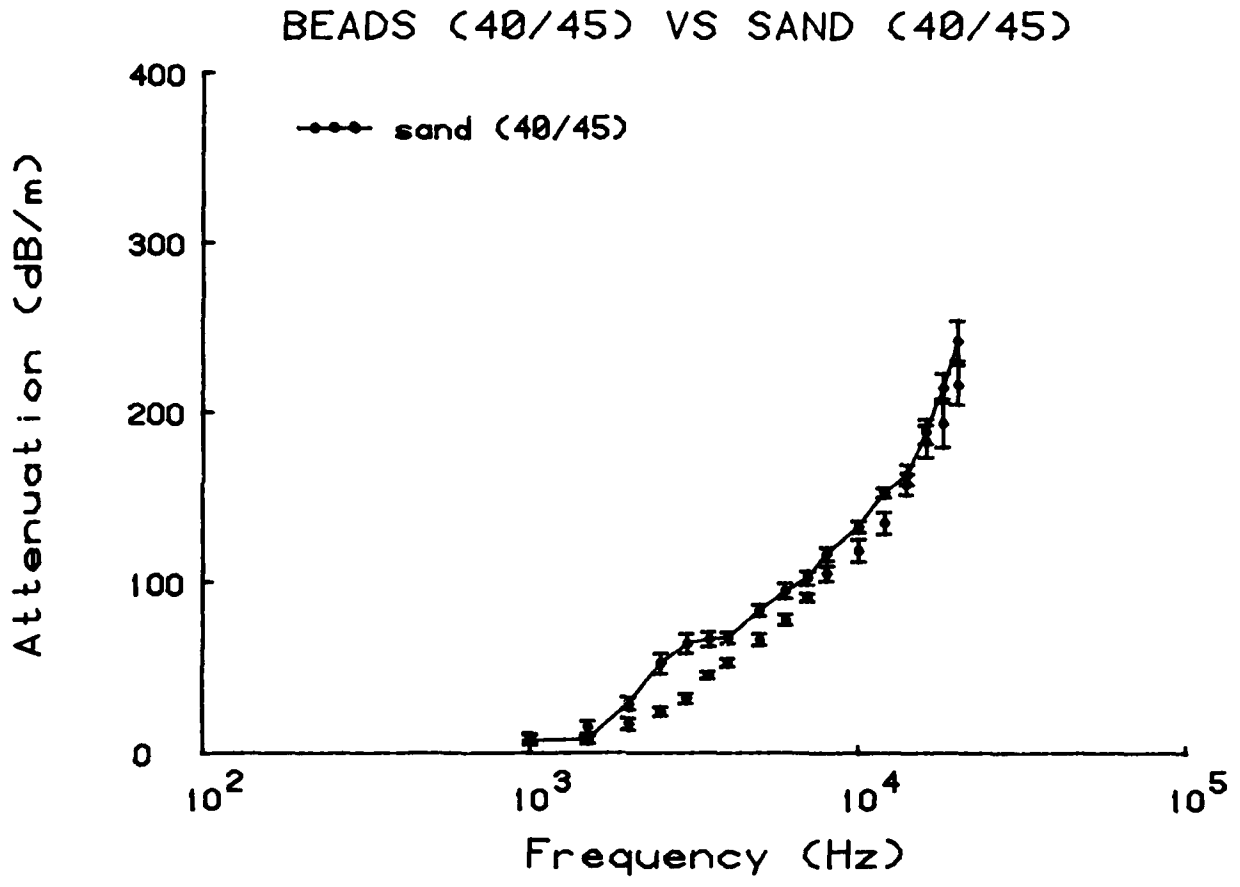

FIGURE VII-11. ATTENUATION COMPARISON BETWEEN SATURATED WELL-SORTED ANGULAR SAND AND SPHERICAL BEADS

and 4.0 kHz. The angular sand exhibits a marked change in apparent frequency dependence above 2.5 kHz. This may be due to the persistence of viscous loss attributable to the relative motion between grains and fluid, a possibility which is consistent with data presented by other authors.[66] Equation (IV-1) allows one to conclude that the transition frequency for the sand is higher than for the beads if there are smaller intergranular pore sizes present in the angular assemblage. Biot[12] has also provided another equation by which one may relate the presence of conditions appropriate to viscous loss dominance to the sediment physical properties. He gives a characteristic frequency, f_c, which may be expressed as

$$f_c = \frac{b}{2\pi\phi\rho_f} \qquad \text{(VII-2)}$$

where

$$b = \frac{\eta\phi^2}{k} \quad \text{or} \quad b = \frac{32\eta\phi}{d^2}$$

for circular pores. In the latter case, for circular pores of diameter d, the ratio f_t/f_c is equal to 0.154. This characteristic frequency was determined for low frequency or steady state friction. Biot[12] modified this characteristic frequency by a multiplicative factor related to the sinuosity and cross-sectional shape of the pores. He chose a value equal to $\sqrt{8}$ as a representative value between that for circular but sinuous pores and that for slit-like pores. The multiplicative values presented by Biot range from a low of $4/\sqrt{3}$ for aligned slits to $\sqrt{12}$ for sinuous circular pores. Given the probable presence of smaller or more sinuous pores coupled with the effects of the lower measured permeability, it is reasonable to assume that the angular sand

has a higher transition frequency. Thus, the attenuation differences at low frequency may indeed be due to the influence of different loss mechanisms in each sediment.

Once beyond 4.0 kHz the losses in the beads overtake those in the sand, becoming nearly equal at 14.0 kHz. Power curve fits show the frequency exponent to be between 1.0 and 0.5 for data between 4.0 kHz and 20.0 kHz. Since the various loss mechanisms are additive, the indication is that the beads are exhibiting a combination of grain-to-grain friction with some viscous loss in the boundary layer surrounding the spherical particles. The dominance of frame losses yields an exponent nearer to 1.0 than 0.5. This same combination is probably at work in the angular sand, but the lower degree of grain-to-grain frictional loss results in a frequency exponent closer to 0.5.

From these data we may conclude that the effect of angularity on attenuation is to increase the magnitude of fluid-to-grain losses at lower frequencies. This may be related to the decrease in permeability caused by the presence of smaller, more tortuous paths of flow through the sediment assemblage. The relative increase in loss might have been greater but for a somewhat offsetting increase in sediment rigidity in the angular sand. The difference between the two sediments narrow once the frequency is high enough for both sediments to be in the higher frequency regime. Here the interaction of boundary layer viscous losses and grain-to-grain friction result in attenuation proportional to frequency raised to some power between 0.5 and 1.0. Higher frame losses cause the beads to

exhibit a frequency exponent closer to 1.0, while the moderate frame losses of the angular sands lead to loss dominated by viscous boundary layer losses and hence a frequency exponent closer to 0.5.

Neither sediment exhibits a truly linear frequency dependence for attenuation, although linear regression fits to the data have been shown to produce reasonable estimates, particularly in the case of the spherical beads. We feel that this underscores the need to perform measurements under carefully controlled conditions with accompanying physical properties measurements which allow the sorting out of physical mechanisms at work in the specimens being examined.

Grain Sorting Effects

The effects of a broad distribution of grain sizes can be assessed by comparing the physical and acoustic properties of the two assemblies of angular sand. Measurements were performed on both sediments under very similar conditions of packing, saturation, and stress; difference should be wholly attributable to grain size sorting.

In Figure VI-1 we see the degree to which the unsieved angular sand departs from the quarter phi (40/45 sieve) size range of the well-sorted sand. There is a significant portion of the grains smaller and larger than the 40/45 size range. In fact, the sizes are split approximately equally, on a percent by weight basis, into sizes equal to, smaller than, and larger than the central 40/45 size. An important factor is the presence of a measurable quantity of sand in the

fine and very fine size ranges. These may have profound impact on the sediment permeability and attenuation.

Table VI-1 shows the two sands to have slightly different mean grain sizes. This is due to the effects of the smaller grains on the Inman statistics of the unsieved sand. The median grain sizes of all three laboratory sediments are the same. The different grain sizes do not manifest themselves as differences in porosity. There is a 2.5 percent difference in permeability. The analysis of permeability performed in Chapter VI showed this to be related to the higher specific surface area of the unsieved sand grains. The sediment rigidity is unaffected in the dry state; however, the imaginary part of the shear modulus, represented by the frame log decrement, indicates a higher degree of grain-to-grain loss in the unsieved sand. This result is not unexpected given the higher specific surface area for grain contacts to be made.

The effects of sorting on the shear modulus and speed of the saturated sediments is evident from Table VII-1. The well-sorted sand shows a 5.6 percent decrease in shear speed. This is accompanied by a 14.6 percent increase in shear modulus. The unsieved angular sand, on the other hand, exhibits an 11.9 percent decrease in shear speed with effectively no change in rigidity. Thus, the introduction of fluid has had a similar effect on the shear speeds, but in the case of the well-sorted sand there has been some effect on the sediment frame which is not apparent in the moderately-sorted sand. This larger decrease in shear speed for the unsieved sand is consistent with the larger effect of saturation

on the loss as exhibited in the wet and dry logarithmic decrements of the two sediments. The well-sorted sand shows an increase of log decrement by a factor of 2.23 from 0.133 in the dry sediment to 0.297 in the saturated sediment at 10 kHz. The unsieved angular sand shows a slightly larger 2.51 times increase from 0.166 to 0.417 at the same frequency. This apparent increase in the effect of the fluid on attenuation is consistent with statements by Shumway[53] that absorption due to fluid motion relative to the framework (viscous losses) will depend on the acoustically effective channel wall area of the sediment. This is approximated by the total surface area of particles in a given volume of sediment. If we assume the specific surface area, S_0, to be representative of this factor for the two sediments, then we have a specific surface area ratio of 1.123 between the unsieved and sieved angular sands. The ratio of the factors of increase in the log decrements for the two sediments yields 1.126. Thus, Shumway's relating the dependence of viscous loss on the particle surface area is borne out in the current measurements. However, this may only hold in cases where viscous friction is the dominant mechanism. The same ratio comparisons do not yield similar results when comparing the angular sands and the spherical beads.

Figure VII-12 graphically depicts the frequency dependence of attenuation for the two sands. Their behavior at low frequency is quite similar. Both exhibit the same marked change in the frequency dependence of attenuation above 2.5 kHz. The well-sorted sand appears to show a more rapid transition toward a 0.5 frequency exponent while the unsieved sand exhibits a

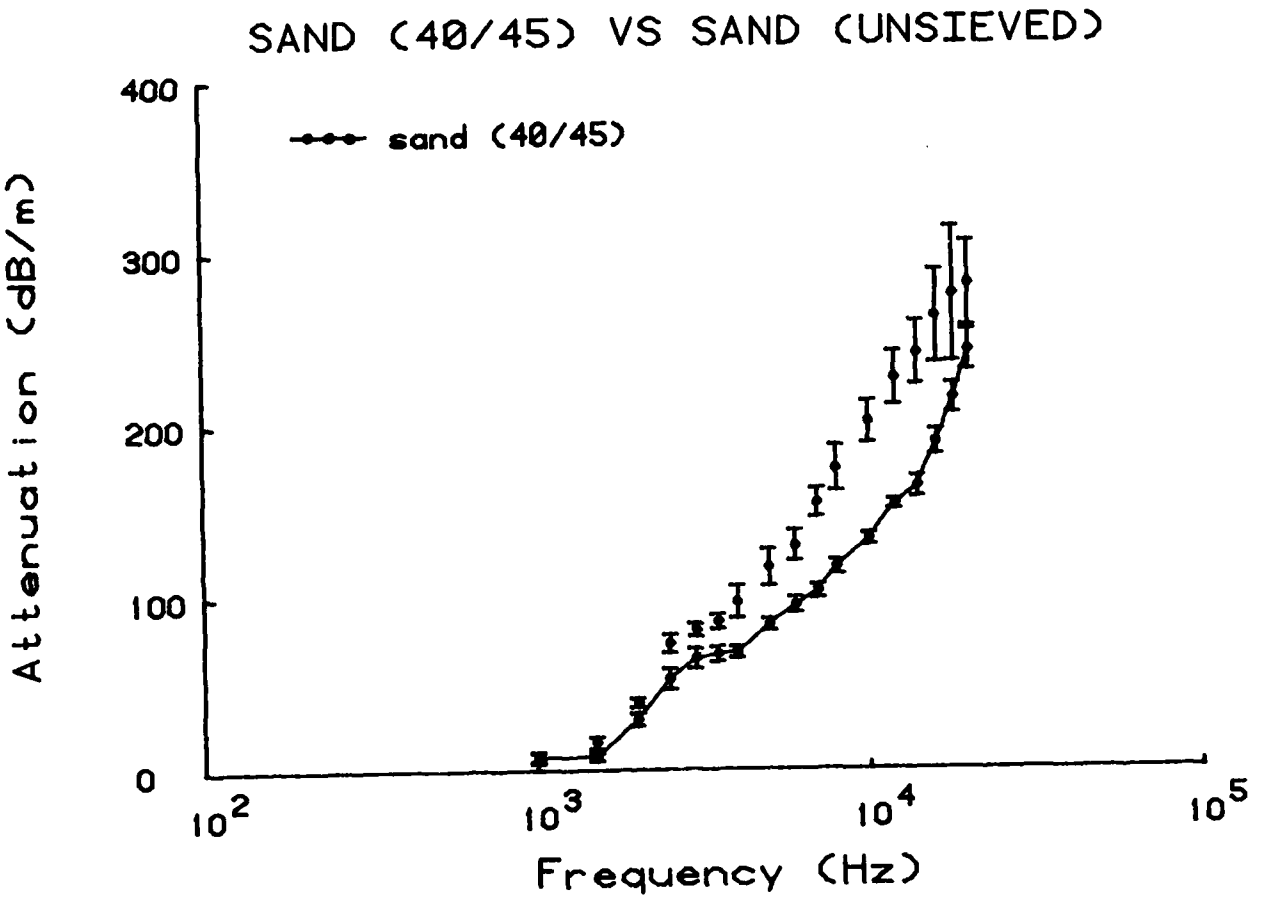

FIGURE VII-12. ATTENUATION COMPARISON BETWEEN SATURATED WELL-SORTED AND MODERATELY SORTED ANGULAR SANDS

frequency exponent of approximately 0.75 between 2.5 kHz and 8.0 kHz decreasing to 0.53 beyond. The well-sorted sand does not exhibit the same degree of slope change with increasing frequency. This may be due to a smaller more consistent distribution of pore sizes leading to a more consistent mix between the viscous and grain-to-grain loss mechanisms, an observation consistent with conclusions reached by other investigators.[62] The greater loss exhibited in the unsieved sand is probably due to the complicated interaction of higher frame losses coupled with the presence of viscous losses due to grain-to-fluid relative motion at higher frequencies than in the well-sorted sediments. Examination of Equation (VII-2) reveals that a higher transition frequency for unsieved sand is consistent with the lower permeability. In addition, the probability of a widespread distribution of pore sizes, each exhibiting loss consistent with either the grain-to-fluid relative motion mechanisms typical of large pores and "low frequency," or the loss mechanism consistent with viscous loss confined to grain boundary layers at high frequency will lead to a complicated frequency relationship for attenuation in the unsieved sediments. Morse[48] reached the same conclusion when he stated that there will be a frequency effect on attenuation dependent upon pore size (i.e., grain size) which is present in non-uniform particle distributions but not sediments composed of uniform particle assemblages. This will lead to a different transition from the frequency squared dependence to the square root of frequency dependence which will in turn be tempered by the frequency dependence attributable to grain-to-grain friction. He states further that if there are many small particles in the assemblage of non-uniform

particles then the transition to the square root of frequency dependence will occur at higher frequency with a gradual transition as more pores satisfy the conditions appropriate to the "high frequency" viscous boundary layer loss mechanism. At very high frequencies, the attenuation will become independent of sorting and the level will be proportional to the static resistance to flow and the square root of frequency. The behavior exhibited by the attenuation in the unsieved sand appears, at least qualitatively, to follow the model of behavior presented by Morse.

The data presented lead us to conclude that the effect of grain size sorting is to increase the magnitude of loss due to grain-to-fluid relative motion. This may be primarily due to an increase in the specific surface area due to the presence of small grains. An additional effect is to extend the frequency range over which the attenuation due to viscous interaction transitions from a frequency squared dependence to a dependence proportional to the square root of frequency. The actual frequency dependence is tempered by the presence of a significant degree of grain-to-grain friction present at the lower and middle frequencies. The net result is a more gradual transition as more of the interstitial pores meet the conditions consistent with a particular mechanism of viscous loss. Ultimately, the effects of grain sorting become unimportant and the loss curves become nearly parallel indicating a similar frequency dependence or attenuation mechanism at work in the sediment.

Summary

In this chapter we have presented a set of attenuation measurements spanning the frequency range from 1.0 to 20.0 kHz for each of three laboratory sediments. They represent a significant addition to the total body of shear wave attenuation data. This is particularly true when one considers the fact that confidence intervals and supporting physical properties measurements are provided to support the attenuation estimates.

In addition to increasing the body of data, the measurements provide insight into the effects of grain angularity and sorting on shear wave attenuation in fluid saturated porous media.

As we shall see in the next chapter, these acoustic and physical properties measurements should prove quite valuable in our attempts to understand the physical mechanisms responsible for the observed response of sediments to acoustic disturbances.

VIII. SHEAR WAVE MODEL PRESENTATION AND ANALYSIS

Introduction

For the present study, numerical modeling has been restricted to the shear wave formulation from Biot/Stoll theory. The appropriate shear wave solutions have been presented in determinant form as Equation (III-29). This equation has been implemented on a computer, and calculations have been made to demonstrate the various relationships and sensitivities inherent to the model. In addition, the physical properties of the laboratory sediments described in Chapter VI have been used as model inputs to predict shear wave speed and attenuation estimates for each sediment. These estimates will be compared with the direct measurements of speed and attenuation presented in Chapter VII. Such comparisons will provide some insight into the adequacy of the mechanisms included in the model to describe the observed shear wave properties of the three sediments.

The Shear Wave Model

Biot formulated his theory of acoustic propagation in porous dissipative media in terms of low frequency and high frequency viscous effects. The transition between the two regimes were said to take place near some transition frequency f_t given by Equation (IV-1). Assuming the motion in the interstitial pores of the sediment to be governed by Poisseuille flow, i.e., the frequency of vibration is less than f_t, then Biot[11] has shown the shear wave speed V_s (cm/sec) and attenuation α_s (nepers/cm) to be approximated by:

$$V_S = \left[1+\frac{1}{8}\left[4\left(\frac{\rho_{22}}{\rho}\right) - \left(\frac{\phi\rho_f}{\rho}\right)^2\right]\left(\frac{f}{f_c}\right)^2\right]V_r \qquad \text{(VIII-1)}$$

and

$$\alpha_S = \left(\frac{\phi\rho_f}{2\rho}\right)\left(\frac{f}{f_c}\right)^2\left(\frac{2\pi f_c}{V_r}\right) \qquad \text{(VIII-2)}$$

where ρ_f=fluid density; ρ=sediment bulk density; ρ_{22}=the mass of fluid per unit volume of sediment plus an additional mass due to the coupling of the fluid and solid; ϕ=porosity; f_c=characteristic frequency of the sediment defined in Equation (VII-2); V_r=the reference velocity; and f=frequency. Since the upper limit of (f/f_c) is 0.154[11], it is easily seen that Equation (VIII-1) is approximately equivalent to $V_s=V_r$. Biot chose V_r to be equal to the velocity of rotational waves for the case of no relative motion between fluid and solid. This results in shear wave velocities which are independent of frequency and equal in magnitude to the elastic case expressed in Equation (III-10). The attenuation does exhibit a direct dependence on the square of the vibration frequency. If we substitute Equation (VII-2) for f_c in Equation (VIII-2) and Equation (III-10) for V_r we obtain

$$\alpha_S = \frac{2\pi^2\rho_f^2\phi k}{\eta\rho}\left(\frac{\omega}{\rho}\right)^{-0.5} f^2 \left(\frac{\text{nepers}}{\text{cm}}\right) \qquad \text{(VIII-3)}$$

The approximation of Equation (VIII-3) is valid for the low frequency range of Biot theory. For the permeable sediments used in this study, the transition frequency may lie below the 1.0 kHz lower limit of the

AD-A152 612 SHEAR WAVE ATTENUATION IN UNCONSOLIDATED LABORATORY SEDIMENTS(U) PLANNING SYSTEMS INC MCLEAN VA B A BRUNSON JUN 83 NORDA-TN-159 N00014-81-C-0275 3/3

UNCLASSIFIED F/G 8/8 NL

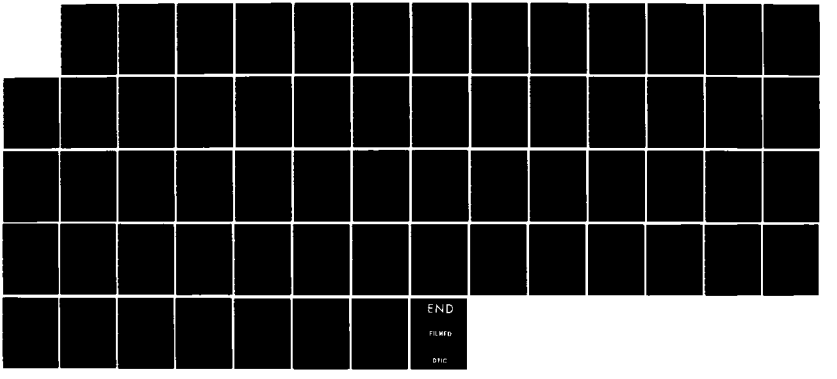

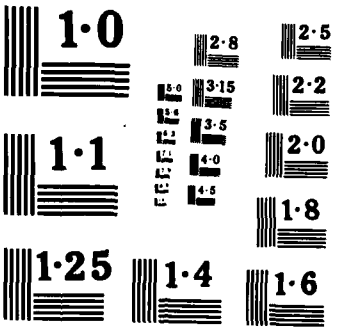
1·0
1·1
1·25
1·4
1·6
1·8
2·0
2·2
2·5
2·8
3·15
3·5
4·0
4·5
5·0

data. However, for less permeable sediments the approximation may be valid at frequencies in excess of 100 kHz, assuming the conditions appropriate to Poisseuille flow are present. Under such conditions viscous forces dominate the loss mechanisms with most of the loss being attributable to viscous interaction between the interstitial fluid and the grains. From Equation (VIII-3) we may conclude that this type of loss is proportional to frequency squared. In practice this viscous loss dominance with its accompanying frequency dependence holds true only if the friction losses due to grain-to-grain contact are less important, such as might be the case if high confining pressure or rigid frame conditions prevail.

If the observation frequency is greater than f_t, then we must assume that Poisseuille flow assumptions are no longer valid. To correct for the departure from Poisseuille flow viscous friction conditions as frequency increases, Biot[12] introduced the complex frequency correction function for the viscosity, $F(\kappa)$. The argument of this function, κ, was introduced in Equation (III-43). In a slightly different form we may write it as

$$\kappa = \left(\frac{2\pi\rho_f a^2 f}{\eta} \right)^{0.5} \qquad \text{(VIII-4)}$$

κ may be thought of as a factor analogous to the Reynolds' number of fluid mechanics. It is a formulation of the ratio of the forces of inertia to those of fluid viscosity. If we consider the porous medium to be analogous to a set of short capillary tubes, then the characteristic length term, a, may be considered to be some sort of "effective" pore radius. In application,

a characterizes both the size and geometry of the intergranular pores, being equal to the radius for circular pores and related to the width of slit-like pores. As has been stated previously, this pore size parameter may be best chosen in such a way that the dispersion and attenuation curves from theory fit a set of experimental data. The complex function $F(\kappa)$ approaches asymptotic values at low and high frequencies according to the relationships:[12]

$$F(\kappa) = F_r + i\,F_i = 1 \quad \text{as } f \to 0$$

$$F(\kappa) = \frac{\kappa}{4}\,\frac{1+i}{\sqrt{2}} \quad \text{as } f \to \infty \qquad \text{(VIII-5)}$$

Thus, the low frequency limit allows behavior identical to the case where the Poisseuille flow assumption is valid, i.e., the shear wave speed approaches that predicted for elastic materials and the viscous attenuation coefficient tends to zero in a manner proportional to frequency squared.

For large values of frequency, Biot[12] shows that

$$F_r = F_i = \frac{\kappa}{4\sqrt{2}} = \frac{1}{2}\left(\frac{f}{f_c}\right)^{0.5} \qquad \text{(VIII-6)}$$

where f_c is once again the characteristic frequency defined in Equation (VII-2). Biot[12] has used the asymptotic value for $F(\kappa)$ from Equation (VIII-6) to solve for the high frequency approximation to the shear wave speed and attenuation coefficient.

The phase speed is shown to be approximately

$$V_S = \left[\frac{\mu}{\left(\rho_{11} - \frac{\rho_{12}^2}{\rho_{22}}\right)}\right]^{0.5} \qquad \text{(VIII-7)}$$

This is equivalent to the speed of shear waves in an elastic medium containing fluid with no viscosity, assuming that the motion of the solid causes a partial entrainment of the fluid through an inertia coupling proportional to the term ρ^2_{12}/ρ_{22}. The parameter ρ_{11} in Equation (VIII-7) is the mass of the solid plus an apparent mass due to the relative motion of the solid in the fluid, ρ_{12} is the additional apparent mass, and ρ_{22} the equivalent mass of the fluid including relative motion effects. The total mass of the fluid-solid aggregate per unit volume is represented by

$$\rho = \rho_{11} + 2\rho_{12} + \rho_{22} \qquad \text{(VIII-8)}$$

The partial rotational entrainment of the fluid decreases the apparent mass of the aggregate with a corresponding increase in wave velocity, and this decrease in apparent mass may be expressed by a factor $[1-(\rho^2_{12}/\rho_{11}\rho_{22})]$. Thus, at high frequency one may neglect the influence of viscosity, velocity being driven by inertial effects. From Equations (VIII-1) and (VIII-7), we see that the velocity dispersion curves for shear waves start at $V_s=(\mu/\rho)^{0.5}$ at very low frequency and tend toward the asymptotic value of Equation (VIII-7) at high frequency. The examples shown by Biot[12] indicate velocity dispersion from slightly less than 10 percent to slightly greater than 30 percent depending on the material. For the modeling performed

in this study, the total dispersion has proven to be closer to 10 percent for an aggregate with properties simliar to a medium grain sand, assuming an elastic frame. This may be greatly affected by the anelastic frame commonly present in most sands.

The approximation, in the high frequency limit, for the shear attenuation coefficient in nepers/cm is

$$\alpha_S = \frac{1}{4}\left(\frac{f}{f_c}\right)^{0.5}\left[\left(\frac{\rho_2}{\rho_{22}}\right)^2\left(\frac{\rho_{22}}{\rho_{11}\rho_{22}-\rho_{12}^2}\right)^{0.5}\right]\left(\frac{2\pi f_c}{V_r}\right) \quad \text{(VIII-9)}$$

From this equation we see that the attenuation is proportional to the square root of frequency. If we assume the sinuosity and pore-shape modification for f_c proposed by Biot[12] to be valid, then we may replace f_c by its equivalent (assuming the correction factor to be $\sqrt{8}$),

$$f_c = \frac{4\eta}{\pi\rho_f a^2} \quad \text{(VIII-10)}$$

Then replacing V_r by Equation (III-10), we have

$$\alpha_S = \frac{\pi}{a}\left(\frac{\eta f\rho}{\pi\mu\rho_f}\right)^{0.5}\left[\left(\frac{\rho_2}{\rho_{22}}\right)^2\left(\frac{\rho_{22}}{\rho_{11}\rho_{22}-\rho_{12}^2}\right)^{0.5}\right] \quad \text{(VIII-11)}$$

We note that the increase of the attenuation factor with frequency is due to the increase of apparent viscosity with frequency, i.e., the fact that $F(\kappa)$ is not constant but becomes proportional to κ which is a function of frequency [see Equation (VIII-4)]. If we had assumed the Poisseuille law to be valid at very

high frequency, we would have found that the attenuation factor tends toward a constant value instead of increasing.[12]

The effect of equating $F(\kappa)$ to the upper or lower bounds presented in Equation (VIII-5) is shown in Figure VIII-1. Here we have displayed the Biot/Stoll model prediction of shear wave attenuation for an hypothetical sediment with properties approximating those of a permeable sand. The properties used in this "base" sediment are provided in Table VIII-1. The base case plotted in Figure VIII-1 assumes an elastic frame ($\Delta_s=0$). From Equation (IV-1) and the sediment properties from Table VIII-1, we calculate a transition frequency, f_c, between 1.0 and 1.5 kHz. We see from the plots that the curves begin to diverge slightly beyond 1.0 kHz. However, the base base appears to show influences of the Poisseuille flow conditions until approximately 8 kHz. This corresponds to the critical frequency, f_c, which is approximately 8 kHz for the base sediment properties. Graphically then we see that the transition from Poisseuille flow to the high frequency regime dominated by boundary layer viscous losses appears to take place between f_t and f_c. The attenuation plot for the low frequency assumption that Poisseuille flow conditions prevail begins to level off above 10 kHz becoming essentially constant above 40 kHz. This demonstrates graphically the importance of including a frequency dependent viscosity correction factor in the theory.

Up until now our discussions have been concerned with viscous effects, ignoring the possibility that grain-to-grain friction could be an important loss

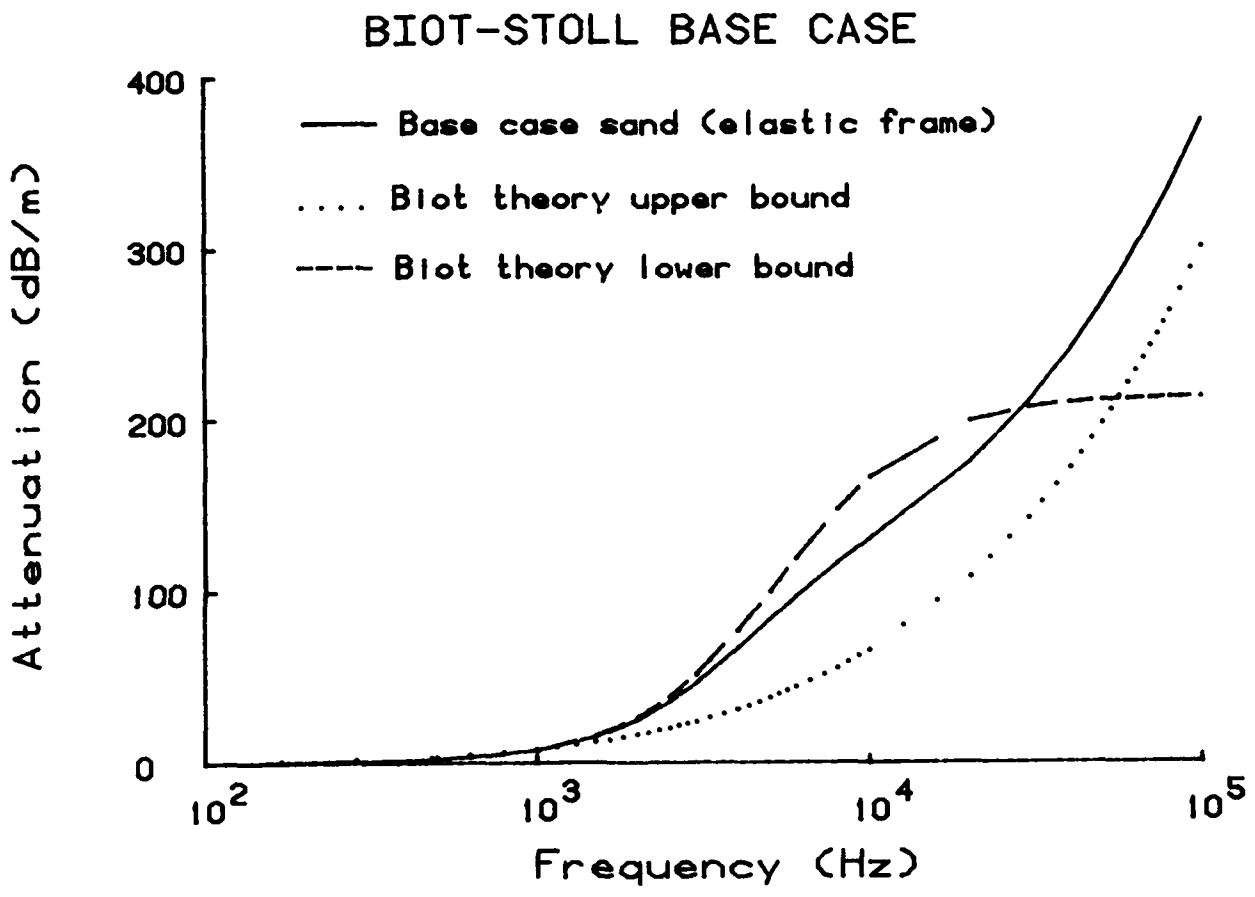

FIGURE VIII-1. BIOT/STOLL MODEL ATTENUATION PREDICTIONS FOR BASE CASE SAND WITH THEORETICAL UPPER AND LOWER BOUNDS

Physical Property	Value	Units
Density of sediment grains	2.65	$g \cdot cm^{-3}$
Bulk modulus of grains	3.60×10^{11}	$dyn \cdot cm^{-2}$
Density of fluid	1.0	$g \cdot cm^{-3}$
Viscosity of fluid	1.0×10^{-2}	$g \cdot cm \cdot s^{-1}$
Bulk modulus of fluid	2.0×10^{10}	$dyn \cdot cm^{-2}$
Bulk modulus of frame	4.36×10^{8}	$dyn \cdot cm^{-2}$
Shear modulus of frame	2.6×10^{8}	$dyn \cdot cm^{-2}$
Porosity	0.40	-
Permeability	1.0×10^{-7}	cm^2
Bulk log decrement	0.1	-
Shear log decrement	0.1	-
Structure factor	1.25	-
Pore size parameter	0.0012	cm

TABLE VIII-1. BASE SEDIMENT PHYSICAL PROPERTIES

mechanism. This assumption may be invalid for unconsolidated sediments under low confining pressure or with restricted flow paths resulting in low permeability. The concept of including internal solid dissipation as an additional mechanism in the model was presented by Biot[13,14] in papers published subsequent to his initial presentation of the theory. However, Stoll[6-8] was the first to implement the concept in a practical manner. He included frame losses as a contributory mechanism by assuming the frame moduli to be complex operators. This was done in a manner consistent with the linear frequency dependence of attenuation observed in many particulate or granular assemblages, leading to shear and bulk frame moduli which are complex constants independent of frequency. Once included in the model they produce additive losses which are linear in frequency with magnitudes related to the frame logarithmic decrements. In Figure VIII-2, one may see the relative importance of accounting for both viscous and frame losses even for a sediment with a moderate frame shear log decrement. Neither the viscous nor the frame losses adequately describe the total sediment attenuation. While both mechanisms are important, the viscous losses are dominant from approximately 1 kHz to 30 kHz, with frame losses dominating beyond. The frequency range over which a given mechanism dominates is of course dependent upon the fluid viscosity and the frame logarithmic decrement. For constant values of these two properties, the relative importance of mechanisms is determined by other sediment parameters. Of these, permeability, pore size parameter, and structure factor are quite important. In the following sections we will examine how the predicted attenuation changes relative to the base case as these three parameters are varied.

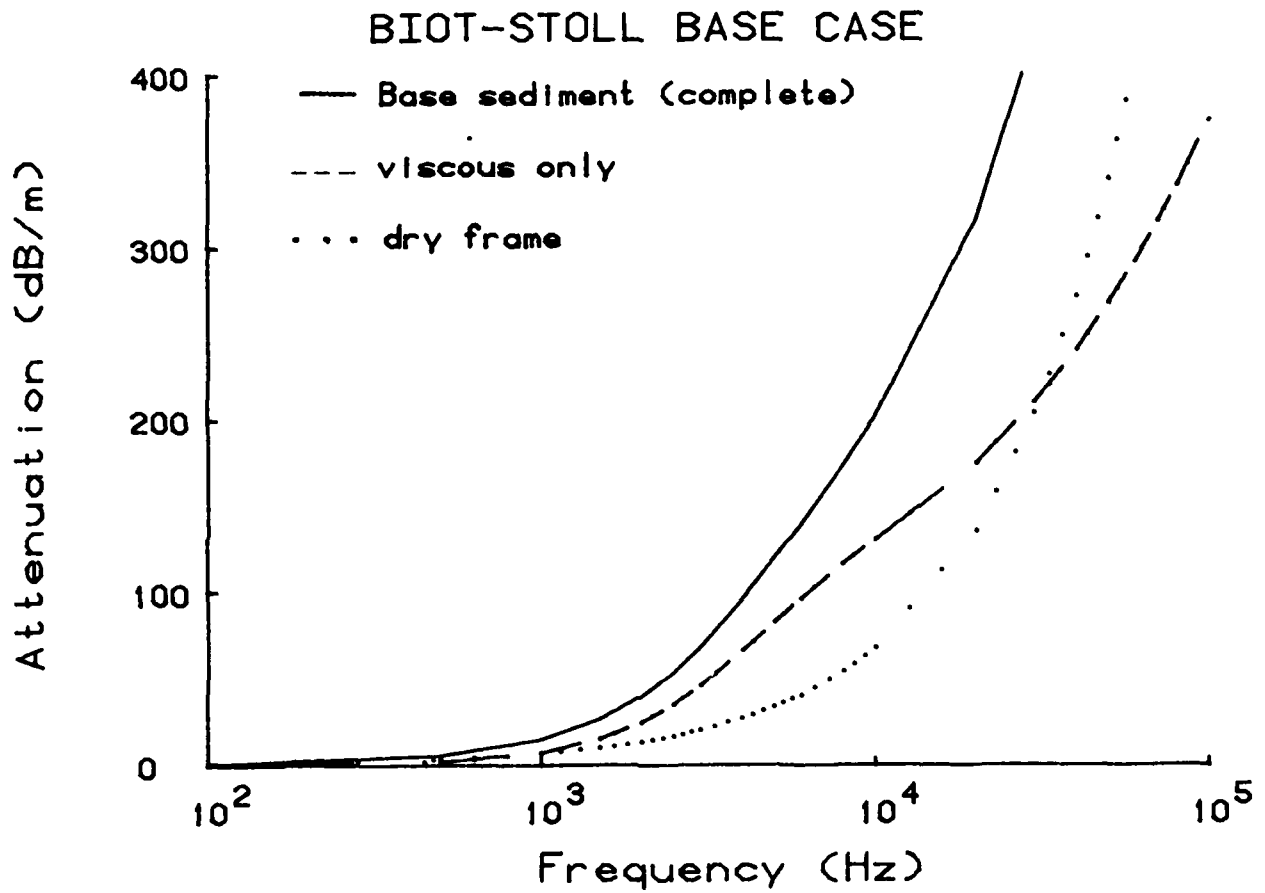

FIGURE VIII-2. ATTENUATION PREDICTIONS SHOWING CONTRIBUTIONS OF FRAME AND VISCOUS LOSSES TO TOTAL SEDIMENT LOSSES FOR BASE CASE

In each comparison, the properties of the sediment will be those listed in Table VIII-1, with the exception of the parameter being examined.

Permeability Sensitivity

In Figure VIII-3 we present model predictions of shear wave attenuation as a function of frequency for the base case ($k=1.0 \times 10^{-7} cm^2$) and for cases with permeabilities an order of magnitude larger and smaller. The relative magnitude of the various cases changes with increasing frequency. This is due to the change of importance of friction relative to viscous losses as the frequency changes for a given permeability. The frame friction loss maintains a constant linear dependence on frequency and is the same magnitude for each case since each has the same frame logarithmic decrement. The viscous loss, on the other hand, shows a frequency dependence which varies with sediment permeability, among other things. This change of frequency dependence may be demonstrated by observing the apparent change of slope in the viscous loss curve of Figure VIII-2. The slope appears to decrease slightly below 10 kHz, and the frame attenuation becomes dominant at a slightly higher frequency. This change of dominant mechanism indicates that the rate of change of attenuation with increasing frequency for the viscous loss mechanism is less than that for the frame loss mechanism. Model studies show that the frequency at which the viscous loss rate of increase becomes smaller than that for frame losses is a function of permeability, all other properties being equal. As the permeability decreases, the viscous losses dominate to higher frequencies.

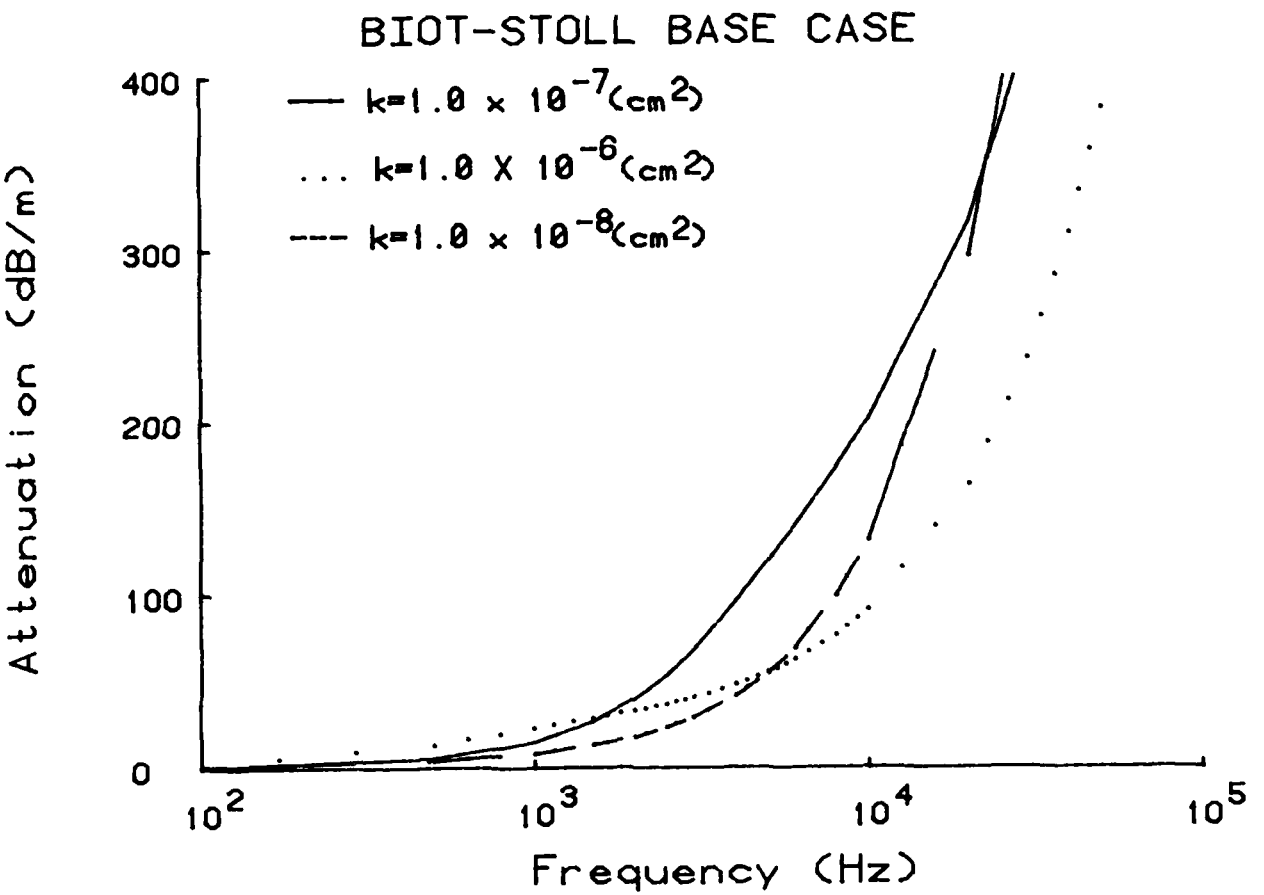

FIGURE VIII-3. SENSITIVITY OF BIOT-STOLL MODEL ATTENUATION PREDICTIONS TO VARIATIONS IN PERMEABILITY

This accounts for the observed crossings of the attenuation curves for various permeabilities in Figure VIII-3. The more permeable case is successively overtaken by the base case and then the low permeability case, each of which maintains a steep frequency dependence to a higher frequency. Eventually, the base case is overtaken by the low permeability case as viscous losses cease to dominate friction losses. Comparison of the high permeability case with the frame loss curve from Figure VIII-2 shows the effects of viscous losses to be minimal beyond about 10 kHz. A comparison of viscous to frame losses as a function of frequency shows the viscous loss mechanism to dominate to frequencies beyond 100 kHz for the low permeability case. Thus, we may conclude that the effect of permeability on total shear wave attenuation is to change the frequency beyond which the dry frame losses dominate. That is to say that the transition frequency, f_t, of Biot theory is inversely proportional to permeability, all other factors being equal. This is consistent with Equation (VII-2) which relates the Biot characteristic frequency, f_c, to the inverse of permeability.

Pore Size Parameter Sensitivity

The pore size parameter, a, has been varied over three orders of magnitude to show the effect of this parameter on the amplitude and shape of the attenuation curves. From Figure VIII-4, we see that decreasing the pore size parameter from .012 cm to .0012 cm has a more profound effect on the attenuation than the reduction from .0012 cm to .00012 cm. The parameter is of course related to the average size of the interstitial pores, but Stoll[6] states that the pore size parameter as

that derived through porosity and grain size relationships, is to invoke the observation by Stoll that the pore size parameter, though related to mean grain size, must also include allowances for the size, shape, and sinuosity of the pores. This is equivalent to multiplying the pore size by a factor $(\xi)^{0.5}$. To reconcile the values in Table VI-5 with the pore size parameter derived from the model-to-data fit requires a value for ξ of approximately 25. While Biot[12] uses such a sinuosity correction factor, albeit much smaller, he does so arbitrarily, stating that the true value must be that which reconciles the model to data. This leaves us no closer to an independent estimate for the pore size parameter than we were before invoking such a sinuosity correction. As with the structure factor, the pore size parameter remains a free parameter which must be determined through comparisons between data and model predictions. The only relief from this is if the sediment in question is uniform in size, can be represented by spherical shapes, and the relationship in Equation (VIII-13) is borne out by further investigation.

Another issue which is important to the application of the model is whether the permeability can be obtained apart from direct measurement and what effect this approach will have on the model's ability to reproduce observations. For beads the Kozeny-Carman relationship between permeability, grain size, and porosity has proven to be quite accurate (see Table VI-3). As expected, there is no discernible difference between attenuation values derived from either measured or predicted permeability. The Krumbein-Monk prediction for permeability proved to be about 21 percent lower than that observed. Even so, the attenuation predicted

for the pore size parameter. The best estimates are obtained using relationships which rely on porosity or permeability rather than mean grain size. One problem with such approaches is that they assume that the intergranular voids have a circular cross-section with some relationship to the size of the spherical grain (e.g., the hydraulic radius assumption of Equation (VI-15) or the equations relating transition frequency to pore radius. From spherical packing models similar to those used by Graton and Fraser,[112] one may see that voids have cross-sections which have been described as spherical-triangles or concave-squares. The void as a whole may be called a concave-octahedron since its sides are formed by the converging cuspoid surfaces of eight tangent spheres. The volume of this pore represents the porosity when compared to the volume of the unit sediment cell made up of the spheres that contain it. The "equivalent" radius, r_e, of this pore for the most stable pack is related to the spherical grain radius, R, by the relationship:[111]

$$r_e^3 = \frac{4.25}{\pi\phi} R^3 \qquad \text{(VIII-13)}$$

Using the mean grain radius and sediment porosity for the spherical beads we calculate a value of r_e=.030 cm, a value equal to the optimum pore size parameter. This radius will change slightly with packing, but for a constant porosity there is only a 12 per cent variation in r_e. Unfortunately this, like other geometrical relationships, is probably valid only if the grains are uniform in size and spherical. Thus it offers little aid in estimating the pore size parameter of angular or non-uniform sized grains. The other alternative to reconcile the empirically derived pore size parameter to

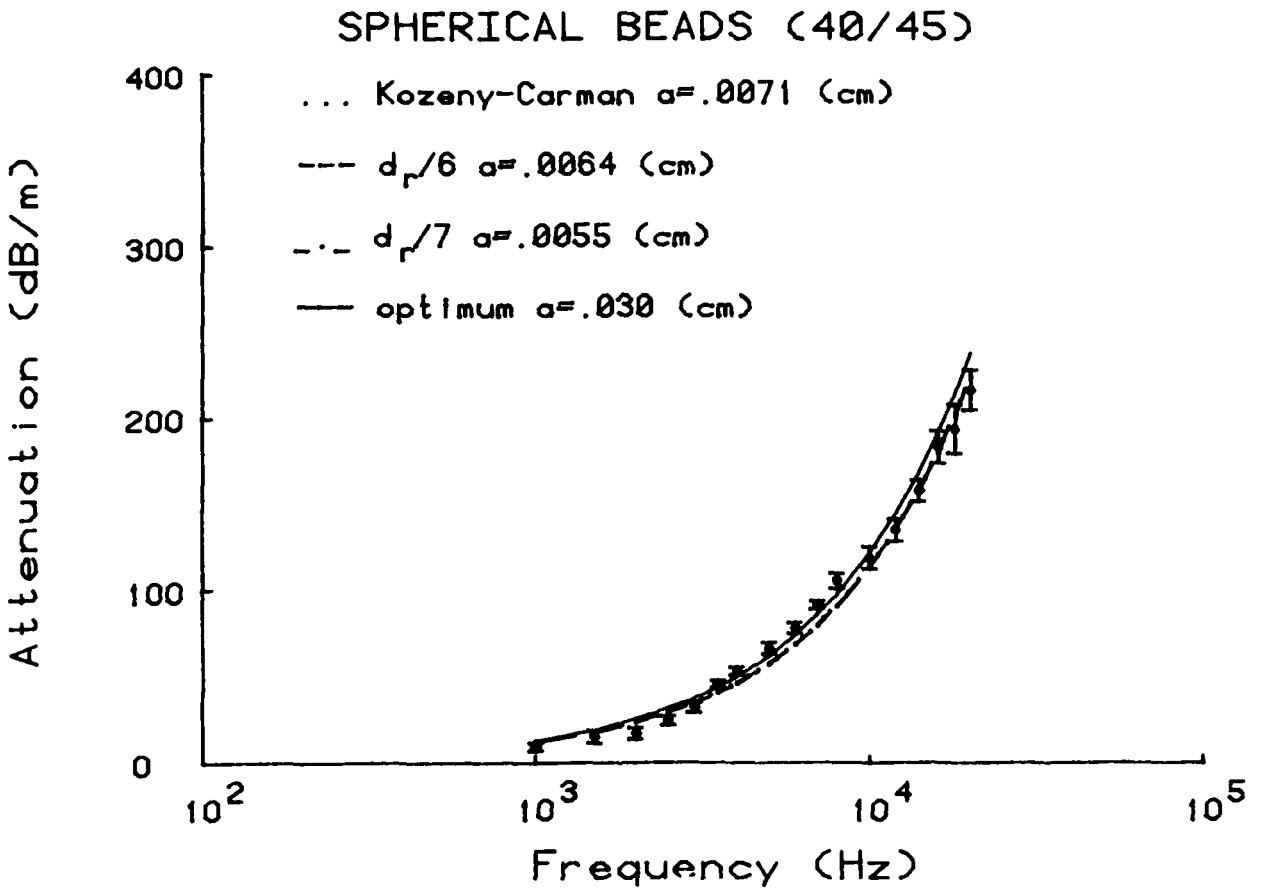

FIGURE VIII-8. COMPARISON OF PORE SIZE PARAMETER EFFECTS ON ATTENUATION PREDICTIONS FOR SATURATED BEADS (40/45)

but more severe mismatch results from using the Hovem and Ingram approach. As mentioned in Chapter VI, this is tantamount to using a structure factor equal to 1.0. The consequences of comparing the model predictions based on their structure factor to the data is a χ^2 equal to 36.6; a much worse fit with a general over-estimation of the observed attenuation. The conclusion from these comparisons is that although the Brown approach is better than the Hovem and Ingram approach, neither yields an acceptable estimate for the structure factor. In fact an estimate based on Domenico's[25] findings yields a much better fit to the data. We are left with the situation that, despite claims to the contrary, the structure factor is an empirical parameter to be determined by direct comparison of model and data. However, we have established that for spherical grains the findings of *Domenico are consistent* with observations, and in the absence of acoustic data one may specify a value of 3.0 for the structure factor.

We have also produced comparisons between the data and model predictions made with pore size parameter estimates from Table VI-5. The results are displayed in Figure VIII-8. All of the non-optimum pore size parameters are smaller than the optimum value of a=0.030 cm, and all are nearly equal to 0.006 cm. In fact the spread of estimates for the various values of pore size parameters are not discernible in the attenuation plots. They uniformly lead to underestimation of the attenuation in the mid-frequency (3.5 kHz to 10 kHz) range, but appear to do well beyond that frequency. Although the χ^2 ranges from 4.63 for a=.0071 cm to 5.02 for a=.0055 cm, these estimates offer reasonably good comparisons with data, especially in the absence of other sources

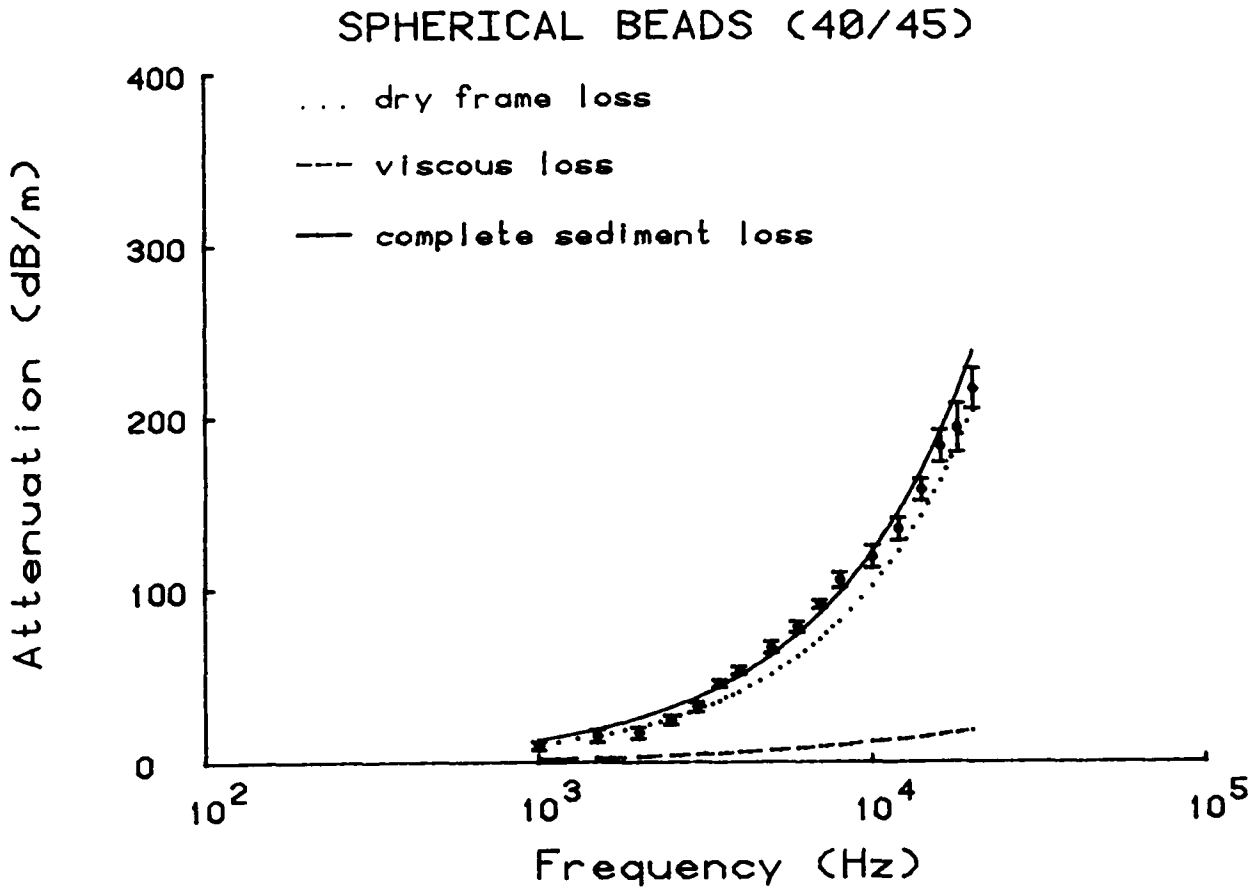

FIGURE VIII-7. COMPARISON OF FRAME, VISCOUS, AND TOTAL ATTENUATION PREDICTIONS TO BEAD (40/45) DATA

structure factor was tested over a range from 1.0 to 3.1, while the pore size parameter was tested over the range 0.0001 cm to 0.1 cm. As we have seen from our sensitivity studies performed on the base sediment, large values of either parameter tend to indicate that viscous effects will be dominated by frame friction losses at lower frequencies than if these parameters were smaller. The fact that for this sediment both parameters are large, indicates that the attenuation is primarily due to grain-to-grain friction. Figure VIII-7 confirms this. It is obvious that the dry frame losses contribute much more than the viscous losses, the difference increasing with frequency. This is, of course, consistent with the large frame log decrement measured for the dry beads.

The derived value of 3.05 for the structure factor is quite consistent with the findings of Domenico[25] that spherical grain assemblages tend to have structure factors approaching 3.0 for all pressures below 10 MPa. The fact that the bead structure factor exceeds the theoretical upper limit of 3.0 (for cylindrical pores) is supported by the work of Ferrero and Sacerdote[102] who found that a structure factor of 4.35 was indicated for spherical lead balls. In contrast to these consistencies are the empirical or theoretical approximations to the structure factor proposed by Brown[103] or Hovem and Ingram.[17] Brown's approach, as outlined in Chapter VI, leads to a structure factor equal to 1.65. Using this value in place of the optimum value yields an overestimation of the loss, particularly at the higher frequencies. Exemplary of the degree of error introduced is the χ^2 value of 8.8 resulting from the comparison between the model prediction and the data. A similar

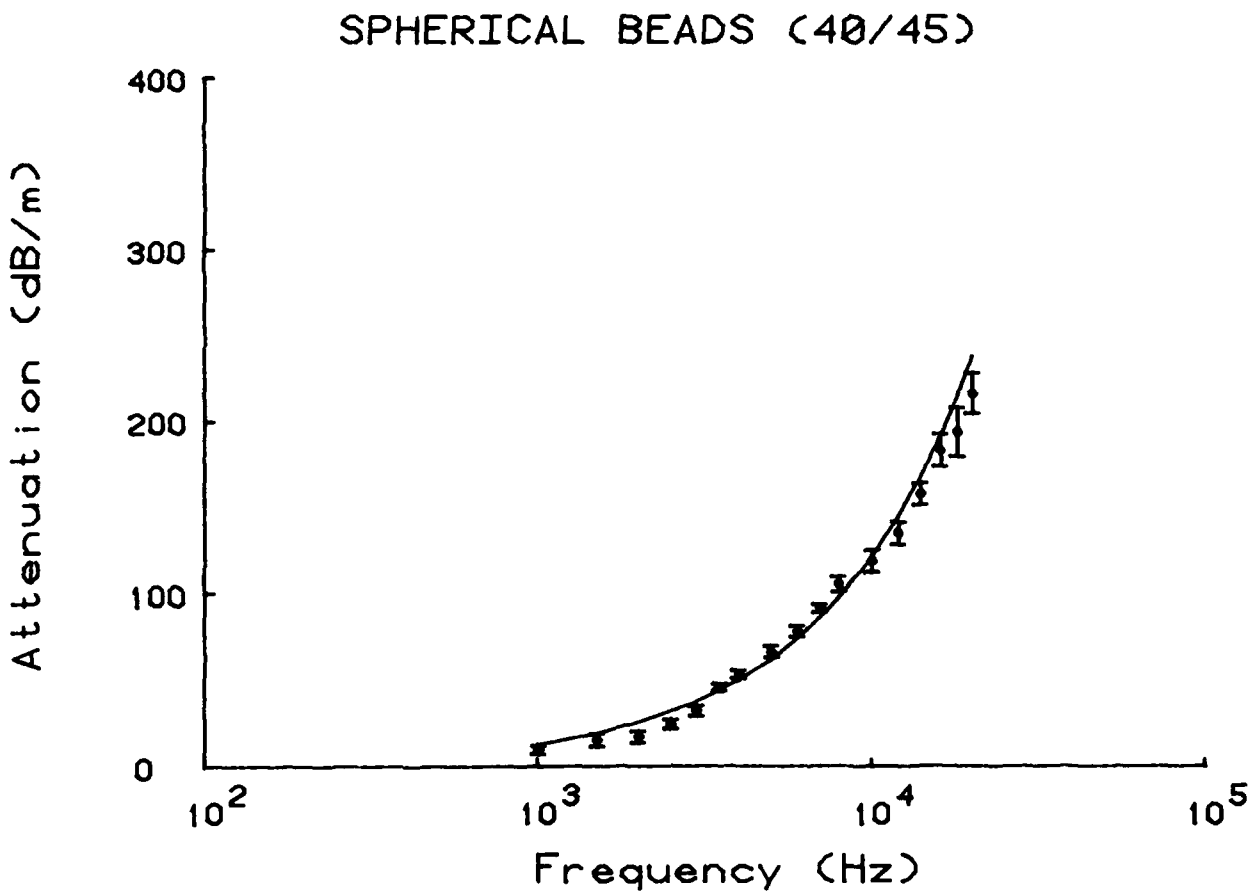

FIGURE VIII-6. COMPARISON OF BIOT-STOLL MODEL ATTENUATION PREDICTIONS TO BEAD (40/45) DATA FOR OPTIMUM VALUE OF PORE SIZE PARAMETER AND STRUCTURE FACTOR

approach was used to arrive at a "best fit" between the Biot/Stoll model and the attenuation data for each sediment. The values of the two parameters have been determined to three significant digits. That is the precision required to affect the χ^2 value to the same degree. A change of pore size parameter by .001 or a change of structure factor by .01 leads to a change in χ^2 in the first decimal place. A lower bound of 1.0 has been placed on the value of the structure factor to maintain its physical significance as a modifier to the fluid density. For the perfectly aligned tubes consistent with a structure factor of 1.0 there is no density modification. To allow the structure factor to assume values less than 1.0 is to assume better than perfect alignment of the interstitial pores. This is not physically realizable, hence the lower bound.

For the remainder of this chapter, we will discuss the model-to-data comparisons for the beads, the well-sorted sand, and the moderately sorted sand.

Spherical Bead (40/45) Data Versus Model

Since an assemblage of spherical beads of uniform size is as close to an ideal sediment as one is likely to find, it is expected that the Biot/Stoll model should prove quite capable of reproducing the observed data. In Figure VIII-6, we present the results of optimizing the Biot/Stoll model fit to the shear wave attenuation data. The best fit was obtained using a structure factor of 3.05 and a pore size parameter of .030 cm together with the other physical properties of Table VIII-2. This resulted in a $\chi 2$ equal to 2.9. The

Physical Property	Units (cgs)	Beads (40/45)	Angular Sand (40/45)	Angular Sand (unsieved)
Density of grains	$g \cdot cm^{-3}$	2.42	2.65	2.65
Bulk modulus of grains	$dyn \cdot cm^{-2}$	3.60×10^{11}	3.60×10^{11}	3.60×10^{11}
Density of fluid	$g \cdot cm^{-3}$	1.0	1.0	1.0
Viscosity of fluid	$g \cdot cm\ s^{-1}$	0.01	0.01	0.01
Bulk modulus of fluid	$dyn \cdot cm^{-2}$	2.0×10^{10}	2.0×10^{10}	2.0×10^{10}
Bulk modulus of frame	$dyn \cdot cm^{-2}$	4.36×10^{8}	4.36×10^{8}	4.36×10^{8}
Shear modulus of frame	$dyn \cdot cm^{-2}$	9.295×10^{8}	6.371×10^{8}	6.296×10^{8}
Porosity	-	0.355	0.432	0.432
Permeability	cm^2	1.143×10^{-6}	9.076×10^{-7}	7.245×10^{-7}
Bulk log decrement	-	0.1	0.1	0.1
Shear log decrement	-	0.288	0.133	0.161
Structure factor	-	3.05	1.00	1.00
Pore size parameter	cm	0.030	0.012	0.010

TABLE VIII-2. PHYSICAL PROPERTIES OF LABORATORY SEDIMENTS
(MEASURED AND DERIVED FROM BIOT/STOLL MODEL FITS)

factor and pore size parameter derived from empirical relationships or by best fits to the attenuation measurements. The best fit model inputs are summarized in Table VIII-2.

Although visual fits to the attenuation data are helpful in arriving at optimal values for the structure factor or the pore size parameter, they can be misleading. In order to provide an objective measure of the "goodness" of a particular fit to the attenuation data, a goodness of fit χ^2 was defined as

$$\chi^2 \equiv \frac{1}{n}\sum_{i=1}^{n} \left\{\frac{1}{CI_i^2}\left[\alpha_S(f_i) - \hat{\alpha}_S(f_i)\right]^2\right\} \qquad \text{(VIII-12)}$$

where the CI_i are the confidence intervals associated with each of the shear wave attenuation data points $\alpha_S(f_i)$, $\hat{\alpha}_S(f_i)$ are the Biot/Stoll model estimates of attenuation at a particular frequency f_i, and f_i are the seventeen discrete frequencies at which data were taken. The value of χ^2 is dependent upon the structure factor and the pore size parameter, since these are the only parameters regarded as "free" in the model-to-data fits. Given Equation (VIII-12), one may see that χ^2 equals zero if the model estimate equals the observed attenuation values. This is the optimum fit, but it is not realizable in practice. A more realistic standard value for χ^2 is obtained if the difference between the model and data is equal to the confidence interval at each frequency. In that case, the χ^2 goodness of fit measure equals one. In any case, the calculation of χ^2 allows one to objectively test various combinations of structure factor and pore size parameter in terms of the data, taking into account the confidence one has in a particular attenuation measurement. This

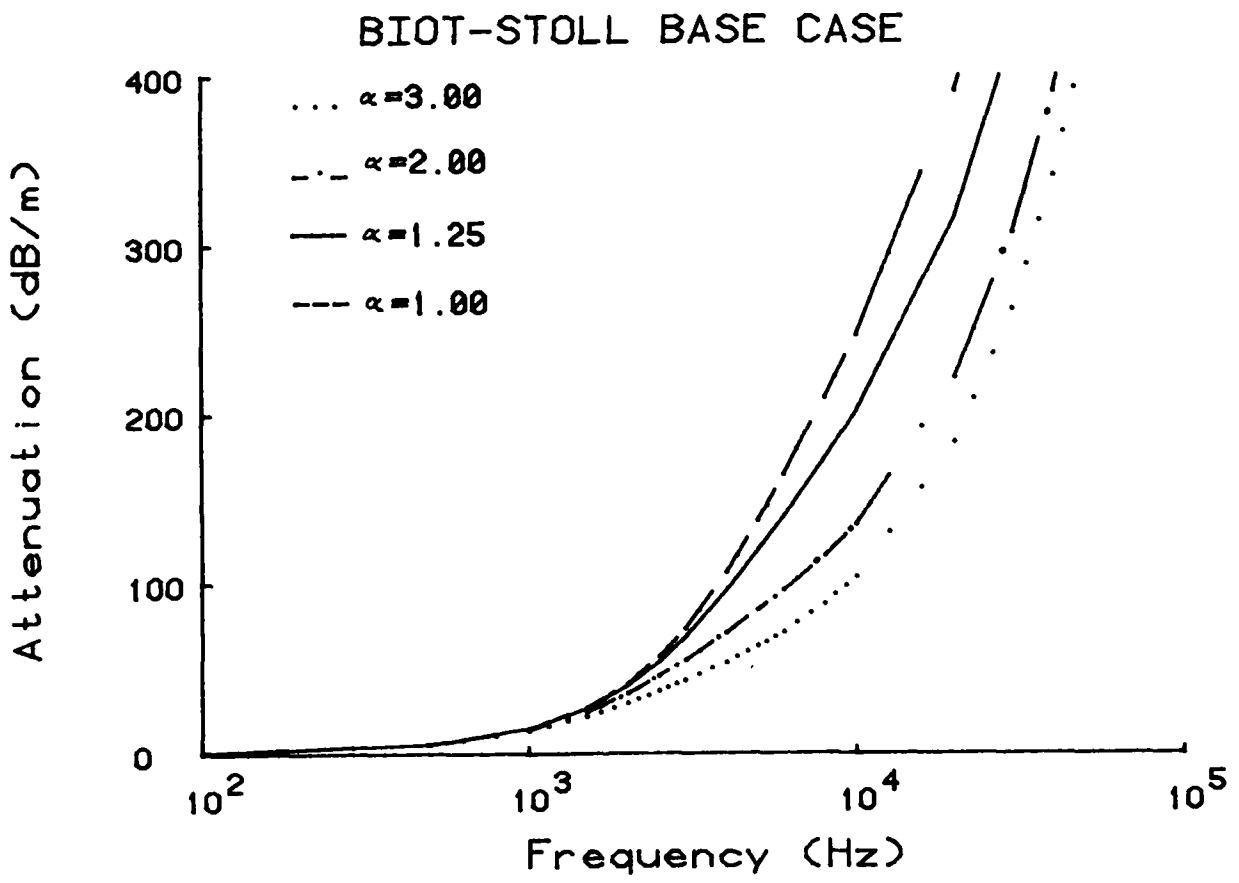

FIGURE VIII-5. SENSITIVITY OF BIOT-STOLL MODEL ATTENUATION PREDICTIONS TO VARIATIONS IN THE STRUCTURE FACTOR

attenuation, particularly at the mid to higher frequencies. These effects are demonstrated graphically in Figure VIII-5. As stated previously, the structure factor acts to increase the fluid inertia, effectively accounting for the restriction in the fluid's ability to flow in or out of an element of sediment for a given acceleration due to the macroscopic pressure gradient. The degree of restriction is proportional to the tortuosity of the intergranular pores, this being in turn represented by the structure factor. For the lower values of the structure factor, the flow is less impeded, resulting in a greater degree of fluid mobility. This fluid motion leads to a higher degree of fluid-to-grain interaction at the lower frequencies. In Figure VIII-5, we see the case where the structure factor equals 1.0, rising more rapidly than the others. In this case the flow is unimpeded and the full effect of the viscous loss mechanism is felt. On the other hand, the tortuosity represented by a structure factor of 3.0 leads to a slowly increasing attenuation which is dominated by the grain-to-grain friction loss mechanism since viscous loss effects are not well developed under such conditions. The differences between the cases, once manifest at mid-frequency, continue to grow in magnitude as the frequency increases.

Biot/Stoll Shear Wave Model-to-Data Comparisons

In order to evaluate the applicability of the Biot/Stoll shear wave model, we have made several comparisons of model predictions with the observations discussed in Chapter VII. The model inputs were those mean values of the physical properties of the sediment presented in Table VI-1, together with estimates of the structure

used in the present version of the model incorporates the Biot correction factor for the sinuosity of the pores in addition to allowances for the pore size and shape. The effect of the pore size variation is similar to the effects observed in the permeability variation study. The larger pore size becomes dominated by friction at a lower frequency, and thus this case shows a lower rate of loss increase consistent with the interaction of the linear friction loss mechanism and the high frequency boundary layer viscous loss mechanism with its $f^{0.5}$ frequency dependence. However, as frequency increases the attenuation becomes more dominated by grain-to-grain friction which steepens the curve allowing the large pore size parameter case to overtake the others. Model studies show this to take place in the vicinity of 30 kHz. The same holds true for the .0012 cm pore size parameter case relative to the smallest pore size parameter case. Thus the pore size parameter and the permeability work in a similar manner to determine the frequency range over which a particular loss mechanism dominates. Both show an inverse relationship to the Biot transition or characteristic frequency. Attenuation shows more sensitivity to a given magnitude of change in the pore size parameter since the two Biot frequencies f_t and f_c are inversely proportional to the square of the pore size.

Structure Factor Sensitivity

Examination of structure factor variation over the entire theoretical range of values (for cylindrical pores) from 1.0 to 3.0 reveals little effect on curve shape but a significant effect on the magnitude of

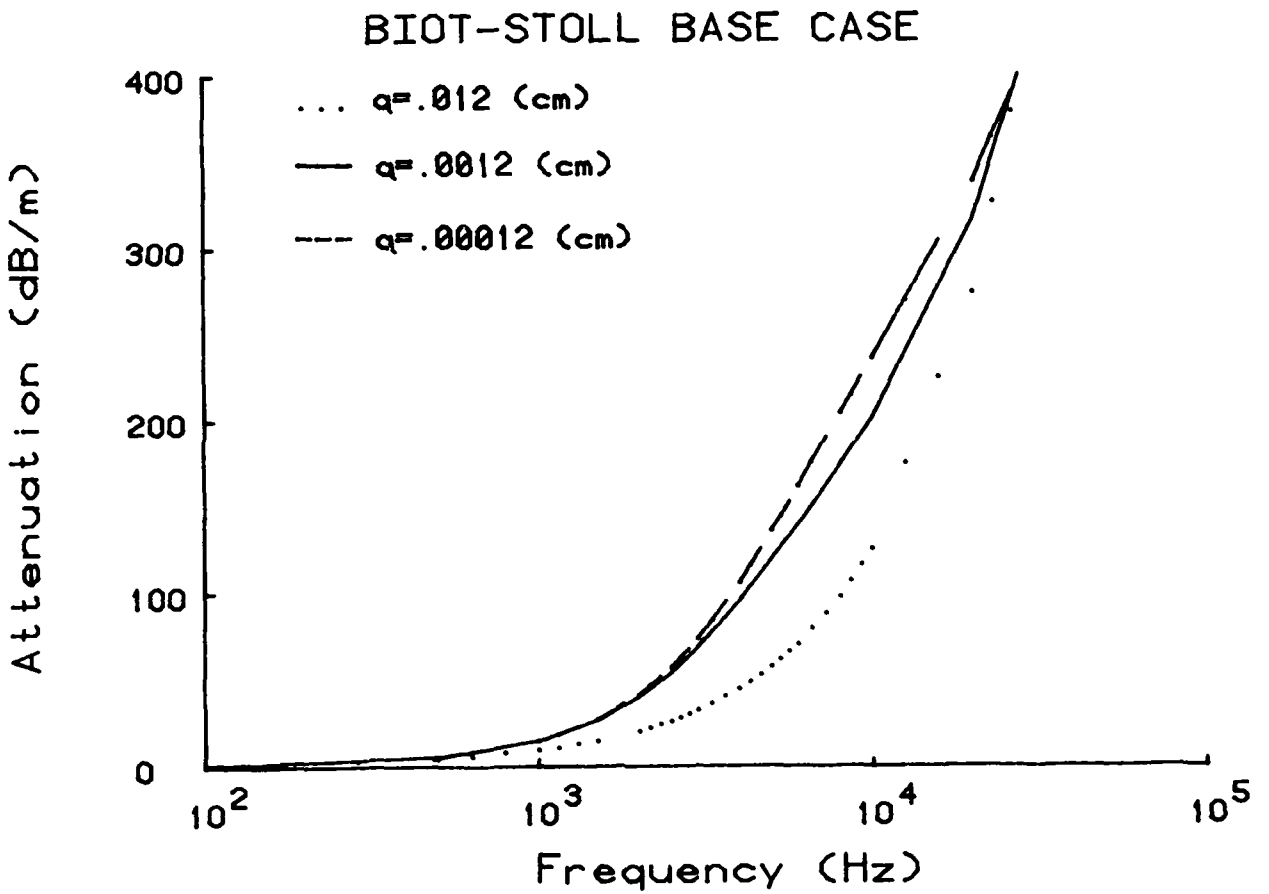

FIGURE VIII-4. SENSITIVITY OF BIOT-STOLL MODEL ATTENUATION PREDICTIONS TO VARIATIONS IN PORE SIZE PARAMETER

using that permeability showed only a maximum departure of one percent from the attenuation predicted using the measured permeability.

As a separate test of the model, we compared predicted and measured shear speeds. As expected, the dry frame speeds were virtually identical. The wet speed measured at 10 kHz is reported in Table VII-1 as 225.3 $\pm$17.5 m/sec. The predicted speed of 10 kHz is 226.6 m/sec. The discrepancy is less than one percent. The model does show approximately one percent dispersion from the speed at 10 kHz with most of it confined to frequencies below 4 kHz. The overall agreement between the model and measurements is quite good.

We have compared the model predictions to both attenuation and speed data. The model has proven to be quite capable of reproducing both types of data, even using empirically determined permeability. The structure factor and pore size parameter remain as empirical parameters since none of the proposed empirical or theoretical approaches appear to be adequate. The structure factor is least worrisome in that the work of Domenico[25] appears to provide a good estimate in the absence of data. The pore size parameter, on the other hand, defies our attempts to predict it adequately, unless the relationship expressed in Equation (VIII-13) is borne out by further data. Fortunately, in the case at hand, the model predictions were not critically sensitive to pore size, being dominated by frame losses.

Angular Sand (40/45) Data Versus Model

One of the objectives of this research is to test the Biot/Stoll model's ability to predict shear wave

attenuation in both simple and complex sediments. It is appropriate, then, to compare model predictions to observations of shear wave attenuation in the well-sorted angular sand. This sediment introduces the complicating factor of grain shape. We saw in Chapter VII that the apparent effect of grain angularity is to increase the magnitude of fluid-to-grain losses at the lower frequencies. The question remains whether the differences in physical properties between the beads and the angular sand can account for the attenuation differences when used as inputs to the Biot/Stoll model. In Figure VIII-9, we have plotted the attenuation versus frequency predictions resulting from optimizing the Biot/Stoll model fit to the shear wave attenuation data. A best fit was attained by using a structure factor of 1.00 and a pore size parameter of .012 cm with the other physical properties of Table VIII-2. The resultant χ^2 goodness of fit value is 7.8. The structure factor was tested over a range of values from 1.0 to 3.0, while the pore size parameter was varied from 0.0001 cm to 0.1 cm. The comparison plot of model predictions versus data shows that the model has not been able to reproduce the sudden increase in attenuation between 2 kHz and 3 kHz, and generally underestimates the loss in the 2.5 kHz to 10 kHz range. Beyond 10 kHz, the model does an excellent job of reproducing observed attenuation.

The fact that the physically realistic optimum value of the structure factor is 1.0 indicates that viscous losses are relatively important contributors to the total loss. The moderately large pore size parameter was shown to be an indicator that frame losses will also be important since the viscous loss mechanism will

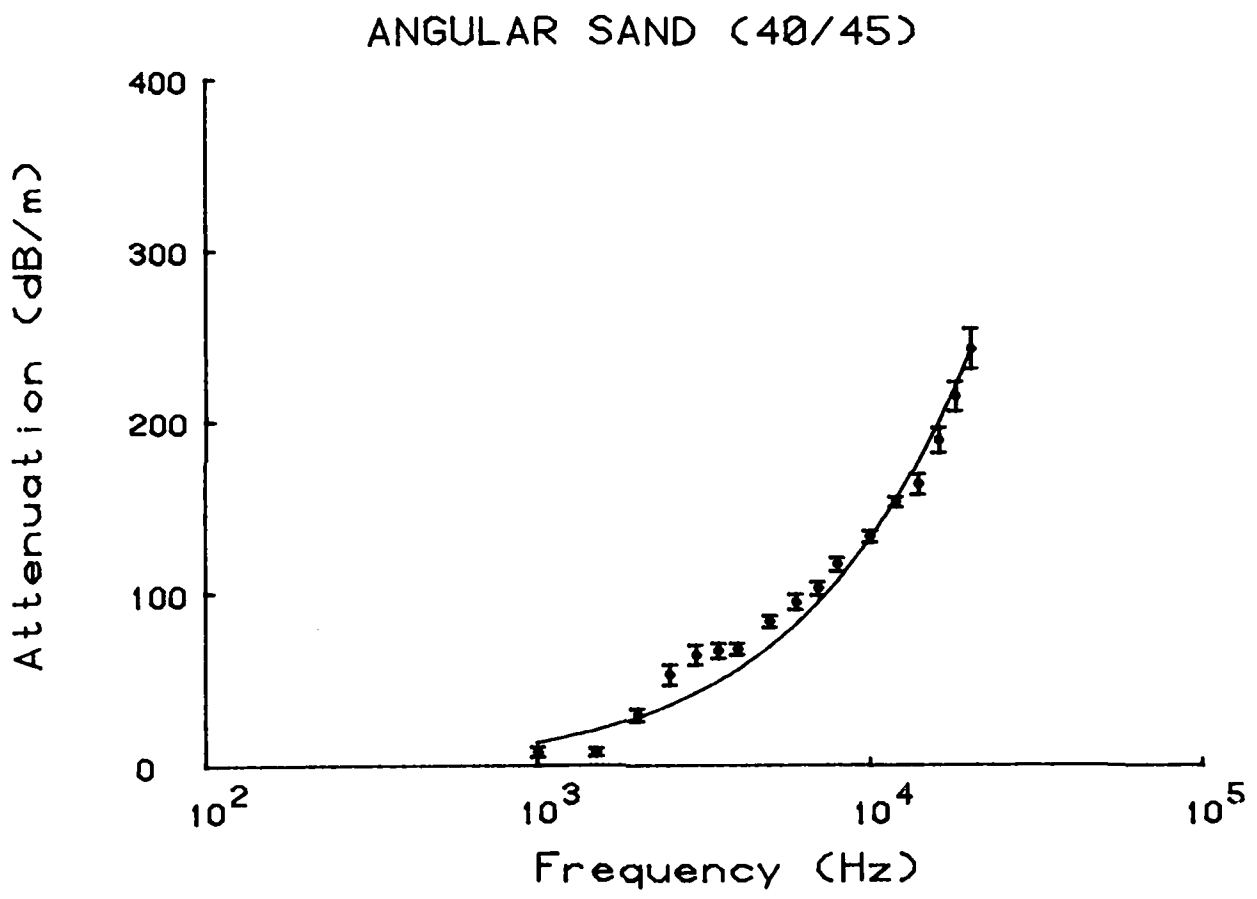

FIGURE VIII-9. COMPARISON OF BIOT-STOLL MODEL ATTENUATION PREDICTIONS TO ANGULAR SAND (40/45) DATA FOR OPTIMUM VALUE OF PORE SIZE PARAMETER AND STRUCTURE FACTOR

transition from an f^2 to an $f^{0.5}$ dependence at lower frequency than if the pore size parameter were small. Figure VIII-10 shows this analysis to be supported by the relative magnitudes of the predicted attenuation due to viscous and frame friction losses. The viscous losses dominate at all frequencies displayed, but the frame losses play a significant role in the total attenuation. It appears that the frame losses would overtake the viscous losses at frequencies below 1 kHz or slightly above 20 kHz. This domination of viscous losses is in sharp contrast to the domination of frame friction losses in the spherical beads. Thus, though the model does not fit the angular sand data as well as it did the bead data, it is quite useful as a diagnostic tool to confirm the indications in the data that the grain angularity leads to an increased viscous loss contribution to the total shear wave attenuation.

The value of 1.0 for the structure factor is in keeping with the findings of Domenico[25] that the structure factor is between 1.0 and 1.2 for sands at pressures below 10 MPa. The structure factor which one would expect from the porosity and formation factor approach proposed by Brown[103] as modified by grain shape considerations reported by Jackson, et al.,[104] takes values between 1.92 and 2.52. Model studies have shown such values for the structure factor to lead to underestimation of the viscous losses resulting in low overall attenuation. As stated previously, the Hovem and Ingram[17] structure constant is equivalent to setting the Biot/Stoll structure factor to 1.0. In the present case that value is the same as the optimum. However, as we have seen from the spherical beads, the approach does not apply in general and any agreement between the

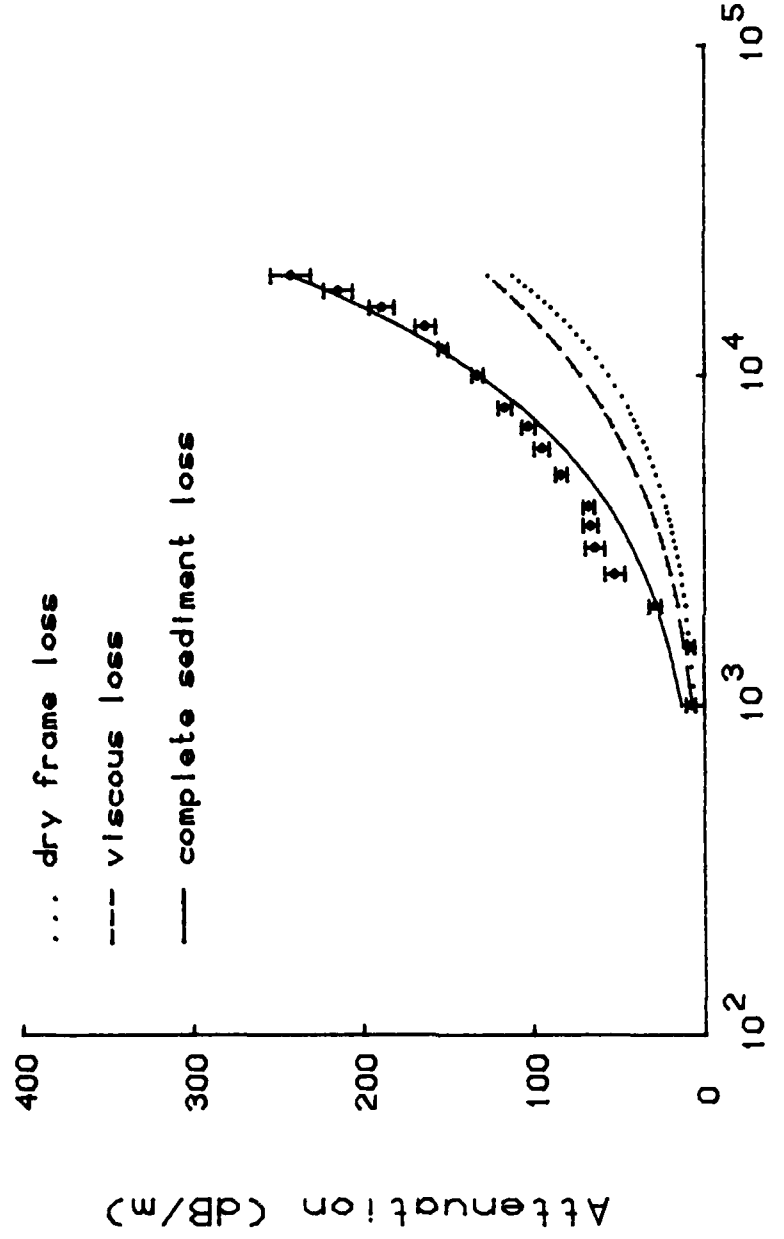

FIGURE VIII-10. COMPARISON OF FRAME, VISCOUS, AND TOTAL ATTENUATION PREDICTIONS TO ANGULAR SAND (40/45) DATA

two is fortuitous. As in the case of the beads, we are left without a theoretical or empirical relationship which yields a generally acceptable value for the structure factor. The only means we have of obtaining the structure factor is by fitting the model to observations. This shortcoming is tempered by the apparent validity of Domenico's findings. In the absence of evidence to the contrary, a value of 1.0 should be used for the structure factor when modeling shear attenuation in angular sediments. This is curious, however, since Stoll[7] has equated this value with the condition of perfectly aligned cylindrical pores. This degree of alignment does not seem compatible with what one might expect to be the arrangement of pores in a complex sediment.

Several theoretical or empirical relationships used to obtain estimates for the pore size parameter have been discussed in Chapter VI. Both approaches based on Kozeny-Carman relationships [Equations (VI-15) and (VI-17)] assume that the pore size parameter is equal to twice the hydraulic radius [Equation (VI-13)]. If this relationship is not valid, then neither is the resultant pore size parameter. Stoll[7] has taken an empirical approach to approximating the required parameter. He related permeability, pore size, and attenuation at 30 kHz using the Biot model, then compared the observed attenuation at the same frequency. As a result he was able to relate the sediment grain size to the pore size parameter. This analysis yielded the empirical estimates discussed in Chapter VI. From Figure VIII-11, one can see the effect of using the pore size parameter estimates calculated using the Kozeny-Carman and Stoll

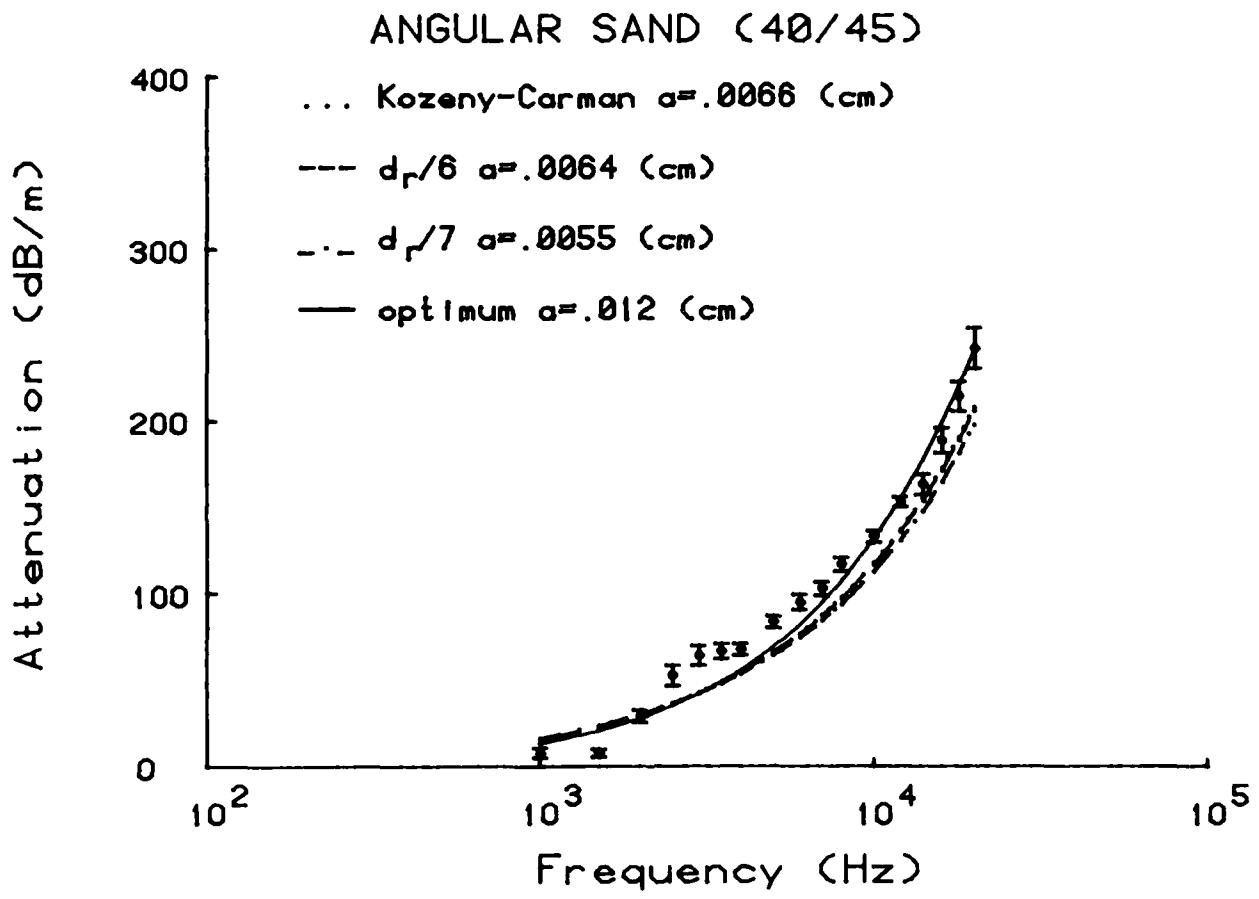

FIGURE VIII-11. COMPARISON OF PORE SIZE PARAMETER EFFECTS ON ATTENUATION PREDICTIONS FOR SATURATED ANGULAR SAND (40/45)

approaches. All fail to reproduce the observed attenuation values. Several structure factor combinations were tried for each pore size parameter, but no improvement in fit was obtained. We can see that the parameter values are approximately one-half the optimum value. Using the Biot sinuosity correction factor, ξ, to achieve the observed pore size parameter by correcting the grain-size based estimates requires a value for ξ of approximately four. While more reasonable than the value required for the beads, we are still left without a relationship with which we can estimate the pore size parameter in the absence of acoustic data. Unfortunately, for this case where viscous losses are significant, the model-to-data fit is more sensitive to the pore size parameter than was true with the beads. The χ^2 for a=.0066 cm is 15.4, for a=.0064 cm, χ^2=16.3; and for a=.0055 cm, χ^2=21.5. This is a substantial increase over the χ^2 for the optimum value of a=.012 cm.

We also attempted to predict permeability values for the angular sand. The results of applying the Kozeny-Carman premeability formula to angular sand was discussed in Chapter VI. Figure VIII-12 displays the predicted shear wave attenuation using the permeability values from Table VI-3. The result of using the Krumbein-Monk empirical grain size relationship [Equation (VI-9)] or the Kozeny-Carman relationship corrected for grain shape [Equation (VI-3)] to provide permeability estimates to the model is a predicted attenuation virtually identical to that obtained using the measured permeability. If the Kozeny-Carman relationship is not corrected for grain shape [Equation (VI-1)], then the model greatly underestimates the shear wave attenuation since the overestimation of permeability resulting from

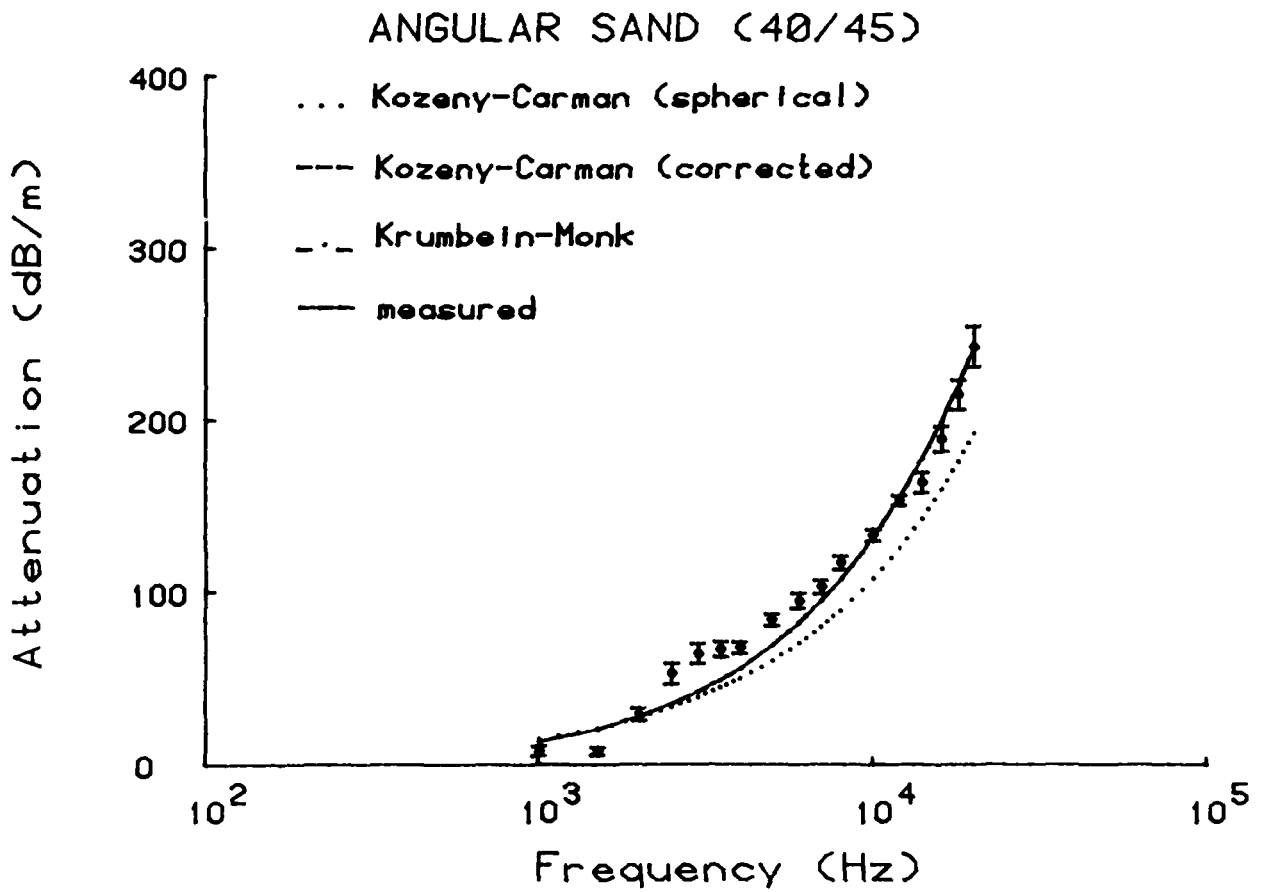

FIGURE VIII-12. COMPARISON OF PERMEABILITY ESTIMATE EFFECTS OF ATTENUATION PREDICTIONS FOR SATURATED ANGULAR SAND (40/45)

the spherical grain assumption does not allow for sufficient grain-to-fluid viscous interaction in the model.

The model also provided predictions of wave speed. These predictions can be compared with observations at 10 kHz to provide another test of model adequacy. The observed dry frame speed was 205.4 $\pm$11.1 m/sec while the wet shear speed was 193.9 $\pm$6.5 m/sec. The model prediction for the dry frame should yield a nearly identical value, and it does with a value of 205.9 m/sec. The wet shear wave speed was predicted to be 197.0 m/sec, a discrepancy of less than two percent; well within the 90 percent confidence interval about the measured speed. This is not too surprising in light of the apparently good agreement between the predicted and observed attenuation at 10 kHz. Given the agreement in both speed and attenuation at 10 kHz, it follows that the logarithmic decrements should agree. They do, both prediction and measurement showing a value of 0.297 for the saturated log decrement. Given the importance of viscous losses one would expect some dispersion in the predicted speed. The total dispersion relative to the 10 kHz speed is about five percent. Most of the shear speed changes occur below 4 kHz. Overall, the speeds and log decrements agree quite well where model estimates and data are available for comparison.

We have now compared Biot/Stoll model predictions to shear wave speed and attenuation data for the angular (40/45) sand. The comparison reveals that the model is not successful in accurately reproducing the observed attenuation between 2.5 kHz and 8 kHz. The model underestimates the observed loss and does not predict

the increased rate of attenuation apparent in the data between 2 kHz and 4 kHz. Attempts to reconcile the discrepancy by decreasing the pore size parameter to increase the viscous loss lead to poorer fits overall. Increasing the frame loss by increasing the frame log decrement allows one to get a better match at the mid-frequencies, but overestimates the high frequency loss. An interesting point is that a better fit to the data is obtained if the structure factor is allowed to assume values less than one. While physically unrealistic, given the role which the structure factor plays as a modifier of fluid density, there exists the possibility that the two loss mechanisms included in the model are inadequate in the mid-frequency range, and this non-physical structure factor leads to an equivalent substitution for a missing mechanism.

There appears to be no theoretical or empirical relationship which allows one to calculate either the pore size parameter or the structure factor in the absence of acoustic data. The structure factor, however, may be estimated to have a value between 1.0 and 1.2 based on the work of Domenico[25] in sands at low pressure.

Thus we conclude that while changes in physical properties attributable to grain shape such as porosity, permeability, complex frame shear modulus, pore size parameter, and structure factor lead to a modification of the relative importance of viscous and frame friction losses, the model is still incapable of accurately reproducing the observed attenuation at all frequencies.

Angular Sand (Unsieved) Data Versus Model

We have seen the effect of adding the complicating factor of grain shape on the ability of the Biot/Stoll model to reproduce observed attenuation. We will now investigate the effect of a further complication, grain size distribution, on the model's ability to predict measured shear wave attenuation. This aspect of our investigation may be particularly important in practice since natural sediments rarely if ever occur as uniform size assemblages.

In Chapter VII we saw that adding grain size distribution as a complicating factor to the angular sand assemblage led to an apparent increase in attenuation. Some of the increase may be attributable to additional grain-to-grain friction as demonstrated by the larger frame log decrement. In addition, a 20 percent decrease in permeability should account for some of the difference at higher frequency. Other than these two physical properties, little was changed by adding additional sizes of grains to the angular assemblages. Given that the Biot/Stoll model was not formulated for mixed grain sizes, the question remains whether these physical property changes together with appropriate changes in the pore size parameter and structure factor are sufficient to obtain a good model-to-data fit for the angular unsieved sand.

In Figure VIII-13, we have displayed the results of calculating shear wave attenuation using the physical properties of Table VIII-2 together with the optimum structure factor, α=1.0,and pore size parameter, a=.010 cm. The goodness of fit parameter, χ^2, is equal to 20.5. Visually, the best fit is not too good. The

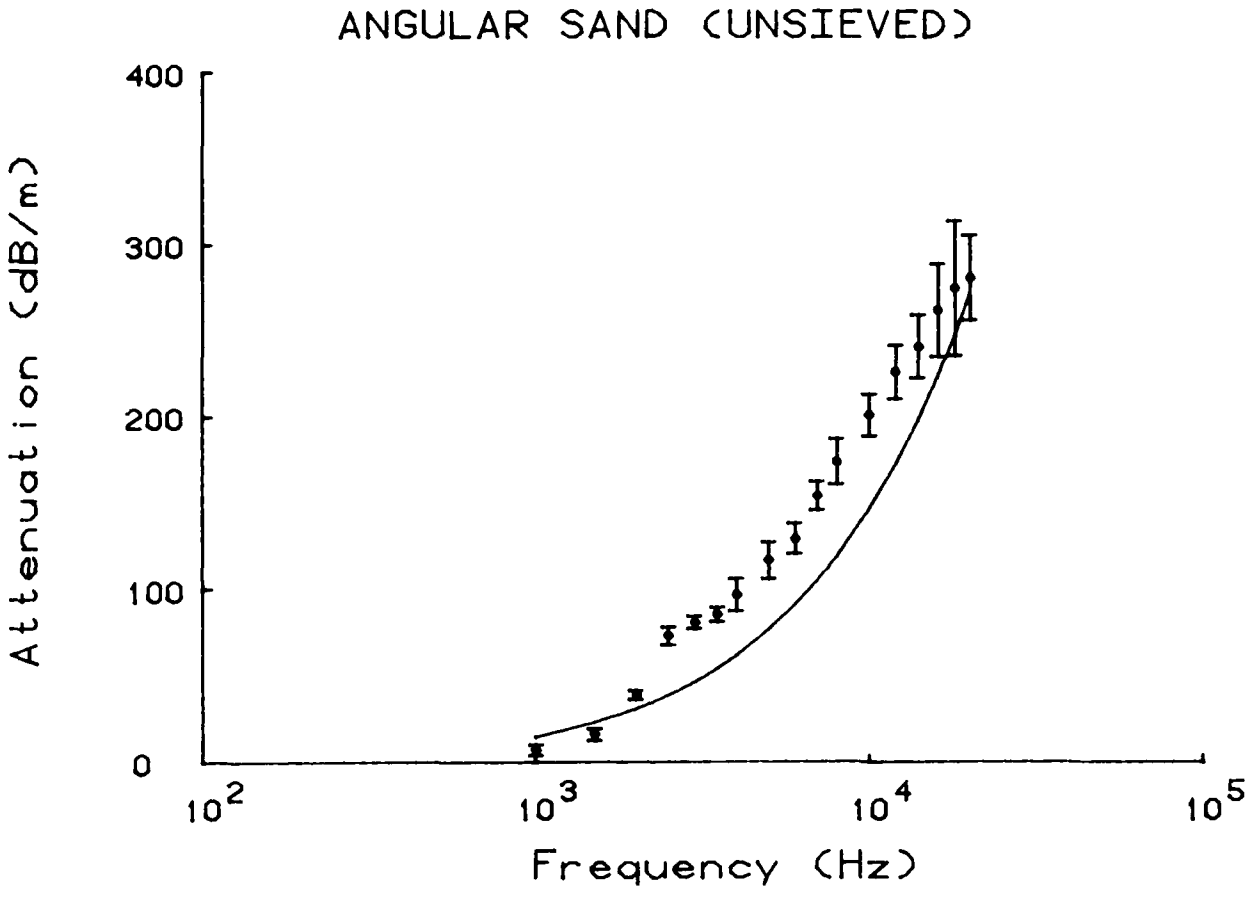

FIGURE VIII-13. COMPARISON OF BIOT-STOLL MODEL ATTENUATION PREDICTIONS TO ANGULAR SAND (UNSIEVED) DATA FOR OPTIMUM VALUE OF PORE SIZE PARAMETER AND STRUCTURE FACTOR

model passes through the upper and lower extremities of the data, but offers poor estimates of the middle frequency attenuation observations. As was true of the well-sorted angular band, the model is unable to reproduce the sudden increase in loss observed between 2 kHz and 3 kHz. The data appear to exhibit a greater frequency dependence overall. Examination of the model predictions reveal a frequency power curve with an exponent of 0.96 to be a good estimator of the model predictions at the seventeen observation frequencies. This may be contrasted with the frequency exponent of 1.05 reported in Chapter VII for the attenuation data. Varying the structure factor from 1.0 to 3.0 and the pore size parameter from 0.0001 cm to 0.1 cm did not improve the fit. We reported that allowing the structure factor to assume physically unrealistic values improved the model fit in the well-sorted angular sand. The same is true of the unsieved angular sand. However, a similar improvement could be attained by simply increasing the frame log decrement. Raising the log decrement by the amount needed to significantly improve the model-to-data fit is not justified in light of the confidence interval placed on the measured value of log decrement (see Table VI-1). In addition, the use of a frequency dependent dry frame log decrement is not justified since measurements reported in Chapter VI at frequencies of 5 kHz, 10 kHz, and 20 kHz yielded the same values for log decrement. There exists the possibility that, if we accept the validity of the data given the confidence intervals provided, there are other loss mechanisms at work in the saturated frame which are not included in the model. Stoll[5,113] has discussed this possibility concluding that in a general model, it may be necessary to allow for both frictional

38. R.W. Cunny and Z.B. Fry, "Vibratory In Situ and Laboratory Soil Moduli Compared," J. Soil Mech. Found. Div. ASCE 99 SM 12, 1055-1076 (1973).

39. D. Davies, "Dispersed Stoneley Waves on the Ocean Bottom," Bull. Seismol. Soc. Am. 55, 903-918 (1965).

40. K.H. Stokoe, II, and R.D. Woods, "In Situ Shear Wave Velocity by Cross Hole Method," J. Soil Mech. Found. Div. ASCE 98 SM5, 443-460 (1972).

41. B.B. Barnes, R.F. Corwin, T.G. Hildebrand, L. Jackson, R. Kessler, W. Takeyama, M. Hornick, and R. Jenkins, Geophysics Applied to Geotechnical Problems in a Marine Environment, a Case Study: Monterey Bay, California, Annual Report 1972-1973 (Environmental Res. Labs., NOAA, Washington, D.C., 1973).

42. J.E. White and R.L. Sengebush, "Velocity Measurements in Near-Surface Formations," Geophysics 18, 54-69 (1953).

43. K. Iida, "The Velocity of Elastic Waves in Sand," Bull. Earthquake Res. Inst., Tokyo Imperial Univ. 16, 131-144 (1938).

44. H. Schmidt, "Die Schallausbreitung in Kornigen Substanzen," Acustica (in German, English summary) 4, 639-652 (1954).

45. S.D. Wilson and R.P. Miller, discussion of "Foundation Vibrations" by F.E. Richart, Jr., in Transactions ASCE 127, part 1, p. 913 (1962).

46. B.O. Hardin and W.L. Black, "Vibration Modulus of Normally Consolidated Clay," J. Soil Mech. Found. Div., ASCE 94 SM2, 353-369 (1968).

47. F.E. Richart, Jr., J.R. Hall, Jr., and R.D. Woods, Vibrations of Soils and Foundations (Prentice-Hall, Englewood Cliffs, 1970).

48. R.W. Morse, "Acoustic Propagation in Granular Media," J. Acoust. Soc. Am. 24, 696-700 (1952).

49. M.A. Ferrero and G.G. Sacerdote, "Parameters of Sound Propagation in Granular Absorbent Materials," Acustica 1, 137-142 (1951).

50. W.L. Nyborg, I. Rudnick, and H.K. Schilling, "Experiments on Acoustic Absorption in Sand and Soil," J. Acoust. Soc. Am. 22, 422-425 (1950).

26. D.J. Shirley and L.D. Hampton, "Shear Wave Measurements in Laboratory Sediments," J. Acoust. Soc. Am. 63, 607-613 (1978).

27. D.W. Bell, Shear Wave Propagation in Unconsolidated Fluid Saturated Porous Media, ARL-TR-79-31 (Applied Research Laboratories, University of Texas, Austin, 1979).

28. D.J. Shirley, Laboratory and In Situ Sediment Acoustics, ARL-TR-77-46 (Applied Research Laboratories, University of Texas, Austin, 1977).

29. K. Kudo and E. Shima, "Attenuation of Shear Waves in Soil," Bull. Earthquake Res. Inst., University of Tokyo 48, 145-158 (1970).

30. R.E. Warrick, "Seismic Investigation of a San Francisco Bay Mud Site," Bull. Seismol. Soc. Am. 64, 375-385 (1974).

31. R.N. Jolly, "Investigation of Shear Waves," Geophysics 21, 905-938 (1956).

32. E. Shima and Y. Ohta, "Experimental Study on Generation and Propagation of S Waves I. Designing of SH Wave Generator and Its Field Tests," Bull. Earthquake Res. Inst., University of Tokyo 45, 19-32 (1967).

33. J.T. Cherry and K.H. Waters, "Shear Wave Recording Using Continuous Signal Methods I. Early Development," Geophysics 33, 229-239 (1968).

34. Y. Ohta and E. Shima, "Experimental Study on Generation and Propagation of S Waves II. Preliminary Experiments on Generation of SV Waves," Bull, Earthquake Res. Inst., University of Tokyo 45, 32-42 (1967).

35. R.S. Jacobson, Linear Inversion of Body Wave Data, Ph. D. dissertation, University of California, San Diego (1980).

36. E.L. Hamilton, "Shear Wave Velocity Versus Depth in Marine Sediments: A Review," Geophysics 41, 985-996 (1976).

37. L.V. Molotova and Yu. I. Vassil'ev, "Velocity Ratio of Longitudinal and Transverse Waves in Rock, II," Bull. Acad. Sci. USSR Geophys. Ser (English translation) 8, 731-743 (1960).

14. M.A. Biot, "Generalized Theory of Acoustic Propagation in Porous Dissipative Media," J. Acoust. Soc. Am. 34, 1254-1264 (1962).

15. T.J. Plona, "Observation of a Second Bulk Compressional Wave in a Porous Medium at Ultrasonic Frequencies," Appl. Phys. Lett. 36, 259-261 (1980).

16. D.L. Johnson and T.J. Plona, "Acoustic Slow Waves and the Consolidation Transition," J. Acoust. Soc. Am. 72, 556-565 (1982).

17. J.M. Hovem and G.D. Ingram, "Viscous Attenuation of Sound in Saturated Sand," J. Acoust. Soc. Am. 66, 1807-1812 (1979).

18. A.W. Nolle, W.A. Hoyer, J.F. Mifsud, W.R. Runyan, and M.A. Ward, "Acoustical Properties of Water Filled Sands," J. Acoust. Soc. Am. 35, 1394-1408 (1963).

19. L.D. Hampton, "Acoustic Properties of Sediments," J. Acoust. Soc. Am. 42, 882-890 (1967).

20. E.L. Hamilton, "Compressional Wave Attenuation in Marine Sediments," *Geophysics* 37, 620-646 (1972).

21. B.A. Brunson and R.K. Johnson, "Laboratory Measurements of Shear Wave Attenuation in Saturated Sand," J. Acoust. Soc. Am. 68, 1371-1375 (1980).

22. E.L. Hamilton, H.P. Bucker, D.L. Keir, and J.A. Whitney, "Velocity of Compressional and Shear Waves in Marine Sediments Determined In Situ from a Research Submersible," J. Geophys. Res. 75, 4039-4049 (1970).

23. B.O. Hardin and F.E. Richart, Jr., "Elastic Wave Velocities in Granular Soils," J. Soil Mech. Found. Div., ASCE 89 SM1, 33-65 (1963).

24. C.C. Pilbeam and J.R. Vaisnys, "Acoustic Velocities and Energy Losses in Granular Aggregates," J. Geophys. Res 78, 810-824 (1973).

25. S.N. Domenico, "Elastic Properties of Unconsolidated Porous Sand Reservoirs," Geophysics 42, 1339-1368 (1977).

X. BIBLIOGRAPHY

1. E.L. Hamilton, "Geoacoustic Modeling of the Sea Floor," J. Acoust. Soc. Am. 68, 1313-1340 (1980).

2. E.L. Hamilton, "Prediction of In Situ Acoustic and Elastic Properties of Marine Sediments," Geophysics 36, 266-284 (1971).

3. H.W. Menard, Marine Geology of the Pacific (McGraw-Hill, New York, 1964).

4. F.P. Shepard, Submarine Geology (Harper and Row, New York, 1973), 3rd ed.

5. R.D. Stoll, "Theoretical Aspects of Sound Transmission in Sediments," J. Acoust. Soc. Am. 68, 1341-1350 (1980).

6. R.D. Stoll and G.M. Bryan, "Wave Attenuation in Saturated Sediments," J. Acoust. Soc. Am. 47, 1440-1447 (1970).

7. R.D. Stoll, "Acoustic Waves in Saturated Sediments," in Physics of Sound in Marine Sediments, edited by L. Hampton (Plenum, New York, 1974), pp. 19-39.

8. R.D. Stoll, "Acoustic Waves in Ocean Sediments," Geophysics 42, 715-725 (1977).

9. R.D. Stoll, "Damping in Saturated Soil," in Proceedings of the Specialty Conference on Earthquake Engineering and Soil Dynamics (ASCE, New York, 1978), pp. 960-975.

10. R.D. Stoll, "Experimental Studies of Attenuation in Sediments," J. Acoust. Soc. Am. 66, 1152-1160 (1979).

11. M.A. Biot, "Theory of Propagation of Elastic Waves in a Fluid-Saturated Porous Solid. I. Low Frequency Range," J. Acoust. Soc. Am. 28, 168-178 (1956).

12. M.A. Biot, "Theory of Propagation of Elastic Waves in a Fluid-Saturated Porous Solid. II. Higher Frequency Range," J. Acoust. Soc. Am. 28, 179-191 (1956).

13. M.A. Biot, "Mechanics of Deformation and Acoustic Propagation in Porous Media," J. Appl. Phys. 33, 1482-1498 (1962).

8. The Biot/Stoll model as presently formulated does not appear to be capable of reproducing detailed observations of shear wave attenuation in angular sands. The cause of the model's inability is not known, but the possibility exists that additional mechanisms which take into account grain shape and size sorting should be included. These may be related to viscoelastic effects in the sediment frame which are not considered in the present form of the model.[5,113]

frame or grains. This is borne out by the apparent frequency dependence in the measured shear wave logarithmic decrements.

4. The effect of angularity on attenuation is to increase the magnitude of fluid-to-grain viscous losses at lower frequencies.

5. The effect of a broad distribution of grain sizes in an angular sand is to increase both the grain-to-grain friction and fluid-to-grain viscous contributions to attenuation. This results in a uniformly higher total attenuation in sands composed of angular grains of diverse sizes. Such assemblages present a broad range of nonlinear frequency dependence due to the distribution of interstitial pore sizes. Sorting effects appear to become unimportant at high frequency.

6. Sediment permeability may be accurately estimated for unconsolidated sands if grain angularity and grain size distribution are taken into account.

7. The Biot/Stoll model empirical parameters known as the structure factor and the pore size parameter cannot be predicted from sediment physical properties in the absence of acoustic data. However, the structure constant appears to assume values near 1.0 for angular sands and 3.0 for spherical grains under low overburden pressure. This is consistent with previously reported findings.[25]

IX. CONCLUSIONS

The stated objectives of this study are to determine the effect of grain shape and sorting on the frequency dependence of attenuation in unconsolidated water-saturated sediments; and to test the ability of the Biot/Stoll model to predict the shear wave attenuation observed in simple and complex sediment assemblages. Those objectives have been met.

As a result of the research described in this report, we are able to conclude that:

1. High quality shear wave attenuation and speed measurements can be made in unconsolidated sediments, under laboratory conditions, at frequencies spanning at least the range from 1.0 kHz to 20.0 kHz.

2. Careful measurement of sediment physical properties must be made under the same conditions of stress, saturation, and packing as those prevailing during acoustic measurements if the results are to be useful in comparisons with other experimental data or model predictions.

3. Shear wave attenuation in unconsolidated permeable sediments may be described by a linear frequency relationship, but there are significant nonlinear effects apparent over certain frequency ranges. These effects appear to be related to the permeability of the sediments and are probably attributable to viscous losses due to fluid moving relative to the sediment

consistent with the low attenuation estimate. Comparison of the shear logarithmic decrement yields a predicted value of 0.33 and a measured value of 0.42. The model estimates of speed and attenuation do not offset one another to yield a log decrement consistent with observations. In a related vein, the model predicts a 6 percent dispersion in shear speed relative to the speed at 10 kHz, most of which occurs below 3 kHz.

We have demonstrated that adding the additional complication of grain size distribution to grain shape worsens the fit between the Biot/Stoll model and observed shear wave attenuation data. The changes in physical properties observed between the unsieved angular sand and the well-sorted angular sand are insufficient to allow the model to obtain a good fit to the measured shear wave attenuation. There are apparently other factors at play in the sediment which the model does not account for. One possibility is that additional loss mechanisms due to viscoelastic effects in the frame may be required for the model to apply in the more general sense approximated by this sediment. One such mechanism is the localized movement of fluid in and out of the annular space between particles near points of contact leading to a frequency-dependent frame viscous loss.[5,113] Such a loss would depend not only upon frequency, but also upon the number and nature of grain contacts. It would probably be apparent only in fluid-saturated, unconsolidated sediments, under low to moderate overburden pressure; the conditions of the present experiments.

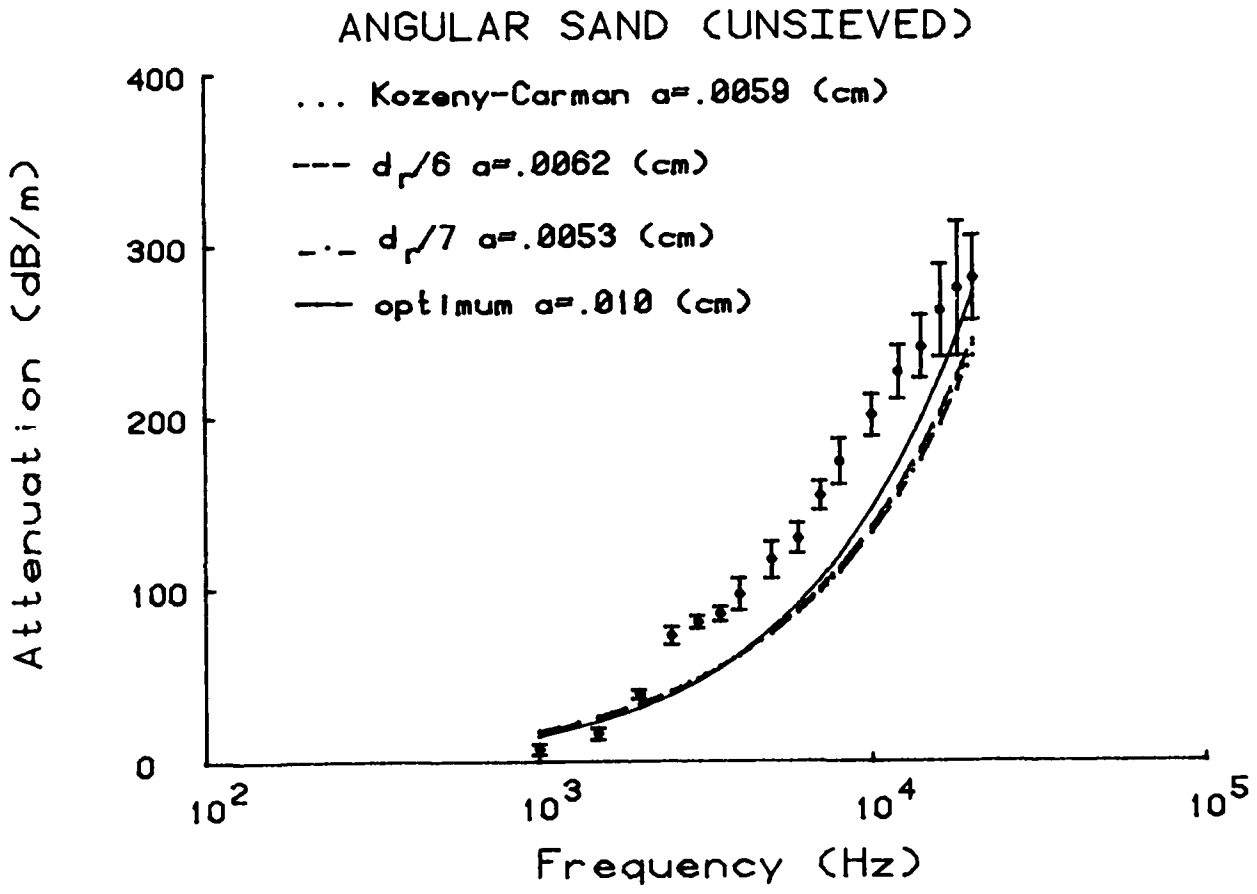

FIGURE VIII-16. COMPARISON OF PORE SIZE PARAMETER EFFECTS ON ATTENUATION PREDICTIONS FOR SATURATED ANGULAR SAND (UNSIEVED)

ships reported by Hovem and Ingram,[17] Carman,[98] and Stoll.[7] Figure VIII-16 displays the result of using the estimates tabulated in Table VI-5 as inputs to the Biot/Stoll model. All estimates are smaller than the optimum value of .01 cm, and all lead to estimates of attenuation which are too low at high frequency. Using these smaller values of pore size tends to shift the transition frequency higher. In this case the viscous losses are important at low frequency (1 kHz to 5 kHz), but are dominated by friction losses beyond. Thus we see that although the smaller pore size parameters result in greater attenuation below 5 kHz, the frequency exponent is lower; thus the optimum case attenuation is greater beyond that frequency as the relative contribution from viscous losses diminish in the small pore size cases. If we were to apply the Biot sinuosity factor, ξ, to the predicted pore size parameters to bring them into line with the optimum, values between 2.6 and 3.6 would be required. This is in line with values used by Biot, but still unrelatable to sediment physical properties. Given the lack of agreement between the model fits, we are left without a reliable estimator of the pore size parameter in the absence of acoustic data.

As with the other two sediments, shear wave speed measurements and observations were obtained for the unsieved angular sand. The measured dry frame speed is 204.2 $\pm$15.7 m/sec. The predicted dry frame speed is 204.7 m/sec. A comparison of the shear speeds in the saturated sediment at 10 kHz yields an 8 percent difference with the model overestimating the speed. The measured value is 179.8 $\pm$5.6 m/sec, while the model predicts 194.9 m/sec. This overestimation of speed is

for grain angularity and sorting. They both yield attenuation estimates indistinguishable from the measured permeability case. The Kozeny-Carman permeability estimate based on spherical grains was shown to be an overestimate of permeability for the unsieved angular sand. This is manifested as an underestimation of viscous losses from the model. Thus the consideration of grain size and shape is shown to be important in establishing permeability estimates for angular sands.

The two other factors which affect the magnitude and shape of the predicted attenuation curve are the structure factor and pore size parameter. The structure factor obtained using the approach proposed by Brown[103] is the same as that discussed in the well-sorted sand case (1.92-2.52). The use of such values for the structure factor results in significantly poorer fits, generally underestimating the attenuation by not allowing for sufficient viscous loss in the model. Hovem and Ingram[11] have proposed a frequency-dependent structure constant which reduces to a value of 1.0 for the Biot/Stoll model application. As before, the equality of this structure factor with the value used in the present study is probably fortuitous given that their structure constant is indeed constant for all sediments. The best estimate appears to come from the Domenico[25] findings which relate the structure factor to grain shape and overburden pressure. His data indicates that the structure factor should fall between 1.0 and 1.2 for sands at low pressure.

The estimation of the pore size parameter has been discussed in Chapter VI. Values were derived from grain size, permeability, and porosity using relation-

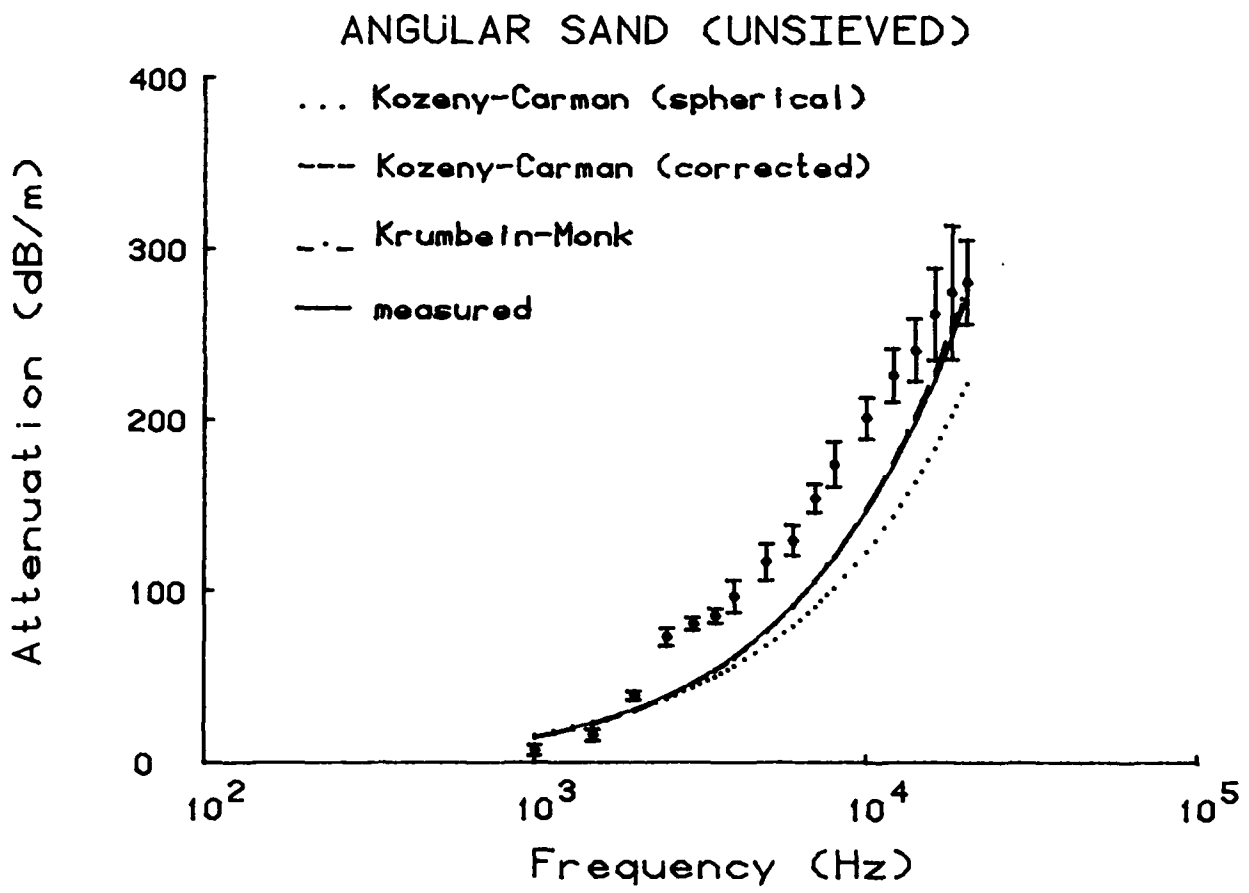

FIGURE VIII-15. COMPARISON OF PERMEABILITY ESTIMATE EFFECTS ON ATTENUATION PREDICTIONS FOR SATURATED ANGULAR SAND (UNSIEVED)

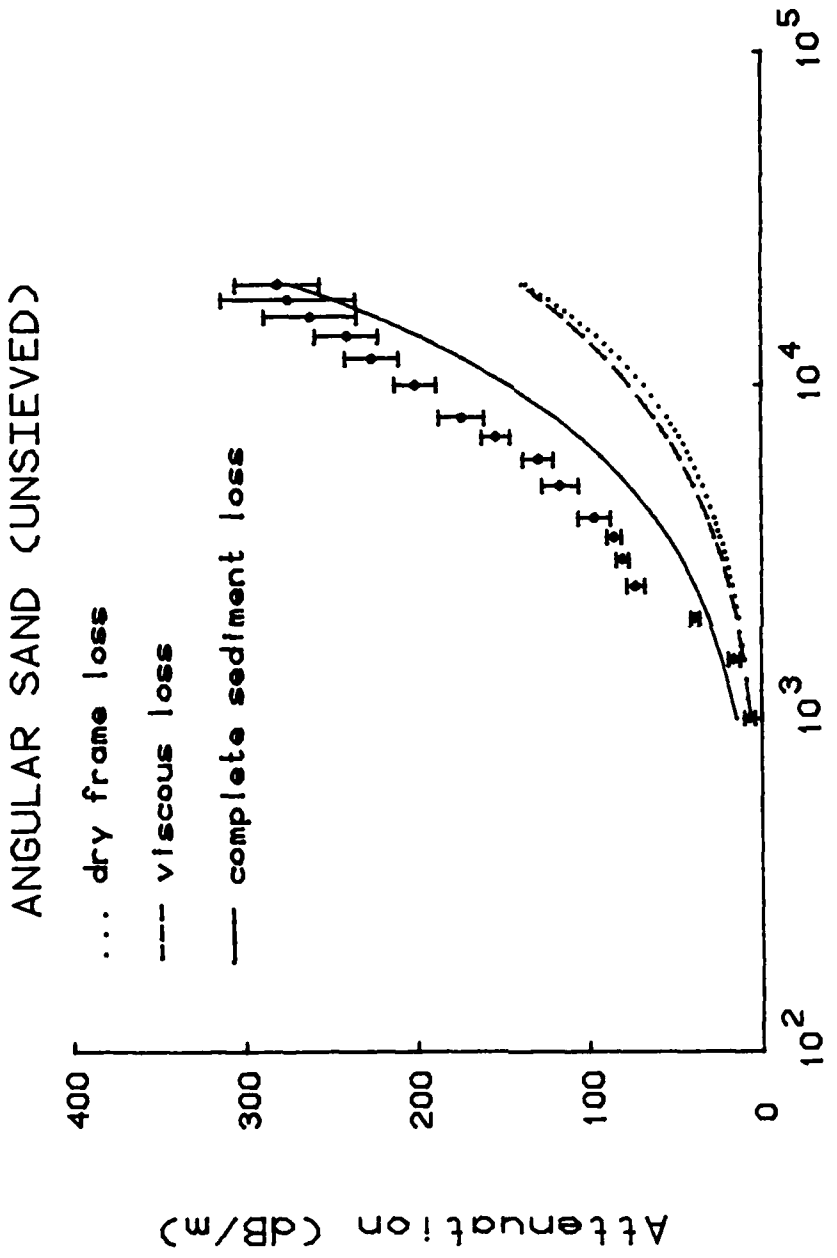

FIGURE VIII-14. COMPARISON OF FRAME, VISCOUS, AND TOTAL ATTENUATION PREDICTIONS TO ANGULAR SAND (UNSIEVED) DATA

and viscous losses in the parameters that describe the response of the skeletal frame. Such parameters may result in a viscoelastic response that may depend on the spectrum of particle sizes and shapes as well as the packing of the sediment leading to a significant nonlinearity of attenuation with frequency. Such viscous losses due to local motion are separate from losses owing to the overall relative motion between the fluid and frame in coarse sediments.

Figure VIII-14 shows graphically how the predicted total loss is apportioned between viscous and frame friction losses. We see the two mechanisms are nearly equal with the viscous loss being slightly greater above 1 kHz. This near equality contrasts with the larger difference between the two contributions observed in the well-sorted sand. The decreased permeability has allowed the model to achieve a significant increase in predicted viscous loss, but the larger frame log decrement in the unsieved angular sand has had an even greater effect on the total loss predicted by the model.

Since permeability appears to play a very important role in our ability to predict attenuation for angular sands, we have investigated the relative merits of the various theoretical and empirical relationships which can be used to estimate permeability from physical properties such as porosity, grain size distribution, and grain shape. Figure VIII-15 is a display of the results of model runs using the various permeability estimates from Table VI-3. The Krumbein-Monk permeability derived from both mean and standard deviation of the grain size is nearly equal to the measured permeability. The same is true once the Kozeny-Carman relationship is corrected

51. G. Shumway, "A Resonant Chamber Method for Sound Velocity and Attenuation Measurements in Sediments," Geophysics 21, 305-319 (1956).

52. G. Shumway, "Sound Speed and Absorption Studies of Marine Sediments by a Resonance Method-Part I," Geophysics 25, 451-467 (1960).

53. G. Shumway, "Sound Speed and Absorption Studies of Marine Sediments by a Resonance Method-Part II," Geophysics 25, 659-682 (1960).

54. E.L. Hamilton, Sound Attenuation in Marine Sediments, NUC TP281 (Naval Undersea Center, San Diego, 1972).

55. F.J. McDonal, F.A. Angona, R.L. Mills, R.L. Sengbush, R.G. Van Nostrand, and J.E. White, "Attenuation of Shear and Compressional Waves in Pierre Shale," Geophysics 23, 421-439 (1958).

56. J. Busby and E.G. Richardson, "The Absorption of Sound in Sediments," Geophysics 22, 821-828 (1957).

57. M.R.J. Wyllie, G.H.F. Gardner, and A.R. Gregory, "Studies of Elastic Wave Attenuation in Porous Media," Geophysics 21, 41-70 (1956).

58. J.R. Hall and F.E. Richart, "Dissipation of Elastic Wave Energy in Granular Soils," J. Soil Mech. Found Div., ASCE 89, SM6, 27-58 (1963).

59. G.H.F. Gardner, M.R.J. Wyllie, and D.M. Droschak, "Effects of Pressure and Fluid Saturation on the Attenuation of Elastic Waves in Sands," J. Petroleum Tech., AIME 16, 189-198 (1964).

60. B.O. Hardin, "The Nature of Damping in Sand," J. Soil Mech. Found. Div., ASCE 91 SM1, 63-97 (1965).

61. L.D. Hampton, "Acoustic Properties of Sediments," J. Acoust. Soc. Am. 42, 882-890 (1967).

62. E.G. McLeroy and A. DeLoach, "Sound Speed and Attenuation From 15 to 1,500 kHz, Measured in Natural Sea Floor Sediments," J. Acoust. Soc. Am. 44, 1148-1150 (1968).

63. C. McCann and D.M. McCann, "The Attenuation of Compressional Waves in Marine Sediments," Geophysics 34, 882-892 (1969).

64. B.O. Hardin and V.P. Drnevich, "Shear Modulus and Damping in Soils: Measurement and Parameter Effects," J. Soil Mech. Found. Div., ASCE 98 SM6, 603-624 (1972).

65. M.N. Toksoz, D.H. Johnston, and A. Timur, "Attenuation of Seismic Waves in Dry and Saturated Rocks: I. Laboratory Measurements," Geophysics 44, 681-690 (1979).

66. K.E. Winkler and A. Nur, "Seismic Attenuation: Effects of Pore Fluids and Frictional Sliding," Geophysics 47, 1-15 (1982).

67. J.E. White, Seismic Waves: Radiation, Transmission, and Attenuation (McGraw-Hill Book Co., New York, 1965).

68. H. Kolsky, Stress Waves in Solids, (Dover Publications, Inc., New York, 1963).

69. E.L. Hamilton, "Geoacoustic Models of the Sea Floor," in Physics of Sound in Marine Sediments, edited by L. Hampton (Plenum Press, New York, 1974), pp. 181-221.

70. J.D. Ferry, Viscoelastic Properties of Polymers (Wiley, New York, 1961).

71. N. Yamakawa, "Scattering and Attenuation of Elastic Waves," Geoph. Magazine 31 (Tokyo), 63-103 (1962).

72. T.J. Plona and L. Tsang, "Characteristics of the Average Microscopic Dimension in Granular Media Using Ultrasonic Pulses: Theory and Experiments (abstract)," Geophysics 44, 344 (1974).

73. D.H. Johnston, M.N. Toksoz, and A. Timur, "Attenuation of Seismic Waves in Dry and Saturated Rocks: II. Mechanisms," Geophysics 44, 691-711 (1979).

74. A.B. Wood, A Textbook of Sound, (G. Bell and Sons Ltd., London, 1941).

75. J.E. Nafe and C.L. Drake, "Variation with Depth in Shallow and Deep Water Marine Sediments of Porosity, Density, and the Velocities of Compressional and Shear Waves," Geophysics 22, 523-552 (1957).

76. G.H. Sutton, H. Berckhemer, and J.E. Nafe, "Physical Analysis of Deep Sea Sediments," Geophysics 22, 779-812 (1957).

77. G. Shumway, "Sound Velocity vs. Temperature in Water Saturated Sediments," Geophysics 23, 494-505 (1958).

78. D.J. Shirley and D.W. Bell, Acoustics of In Situ and Laboratory Sediments, ARL-TR-78-36 (Applied Research Laboratories, University of Texas, Austin, 1978).

79. J.M. Hovem, "Viscous Attenuation of Sound in Suspensions and High Porosity Marine Sediments," J. Acoust. Soc. Am. 67, 1559-1563 (1980).

80. R.J. Urick, "The Absorption of Sound in Suspensions of Irregular Particles," J. Acoust. Soc. Am. 20, 283-289 (1948).

81. R.J. Urick and W.S. Ament, "The Propagation of Sound in Composite Media," J. Acoust. Soc. Am. 21, 115-119 (1949).

82. J.M. Hovem, "Attenuation of Sound in Marine Sediments," in Bottom Interacting Ocean Acoustics, edited by W.A.Kuperman and F.B. Jensen (Plenum Press, New York, 1980), pp. 1-14.

83. F. Gassman, "Elastic Waves Through a Packing of Spheres," Geophysics 16, 673 (1951).

84. E.L. Hamilton, "Elastic Properties of Marine Sediments," J. Geophys. Res. 76, 579-604 (1971).

85. C. Zwikker and C.W. Kosten, Sound Absorbing Materials, (Elsevier, New York, 1949).

86. J. Geertsma and D.C. Smit, "Some Aspects of Elastic Wave Propagation in Fluid Saturated Porous Solids," Geophysics 26, 169-181 (1961).

87. J.H. Beebe, An Experimental Investigation of Ocean Sediment Effects Upon Long-Range Transmission Loss in Shallow Water, Ph. D. Dissertation, The Pennsylvania State University (1981).

88. D.J. Shirley, "An Improved Shear Wave Transducer," J. Acoust. Soc. Am. 63, 1644-1645 (1978).

89. J.E. Matthews, B.A. Brunson, and D.C. Young, Construction of the S-1 Shear Wave Transducer (unpublished Laboratory Item 3-81, Sea Floor Division, Naval Ocean Research and Development Activity, Bay St. Louis, Mississippi, 1981).

90. J. Thiede, T. Chriss, M. Clauson, and S.A. Swift, Settling Tubes for Size Analysis of Fine and Coarse Fractions of Oceanic Sediments, Reference 76-8 (School of Oceanography, Oregon State University, Corvallis, 1976).

91. R.J. Gibbs, M.D. Matthews, and D.A. Link, "The Relationship Between Sphere Size and Settling Velocity," J. Sed. Petrol. 41, 7-18 (1971).

92. D.L. Inman, "Measures for Describing the Size Distribution of Sediments," J. Sed. Petrol. 22, 125-145 (1952).

93. J.E. Bowles, Engineering Properties of Soils and Their Measurement (McGraw-Hill Book Co., New York, 1970), pp. 33-40.

94. J.E. Matthews and D.C. Young, Construction and Operation of a Permeameter (unpublished Laboratory Item 2-80, Sea Floor Division, Naval Ocean Research and Development Activity, Bay St. Louis, Mississippi, 1980).

95. Cataphote Division-Ferro Corporation, World's Largest Catalog of Small Glass Beads (Ferro Corporation, Jackson Mississippi, 1977).

96. H.J. Fraser, "Experimental Study of the Porosity and Permeability of Clastic Sediments," J. Geology 43, 910-1010 (1935).

97. N.D. Stearns, "Laboratory Tests on Physical Properties of Water-Bearing Materials," U.S. Geol. Surv. Water Supply Paper 596-F, pp. 163-169 (1927).

98. P.C. Carman, Flow of Gases Through Porous Media, (Academic Press, New York, 1956).

99. W.C. Krumbein and G.D. Monk, "Permeability as a Function of the Size Parameters of Unconsolidated Sand," Petroleum Technology, Am. Inst. Mining and Metallurgical Engineers, Tech. Pub. 1942, 1-9 (1942).

100. W.F. Murphy, III, Effects of Microstructure and Pore Fluids on the Acoustic Properties of Granular Sedimentary Materials, Ph. D. dissertation, Stanford University (1982).

101. V.P. Drnevich, J.R. Hall, Jr., and F.E. Richart, Jr., "Effects of Amplitude of Vibration on the Shear Modulus of Sand," in Proceedings of the

International Symposium on Wave Propagation and Dynamic Properties of Earth Materials (Albuquerque, N.M., 1967), pp. 189-199.

102. M.A. Ferrero and G.G. Sacerdote, "Parameters of Sound Propagation in Granular Absorbent Materials," Acustica 1, 137-142 (1951).

103. R.J.S. Brown, "Connection Between Formation Factor for Electrical Resistivity and Fluid-Solid Coupling Factor in Biot's Equations for Acoustic Waves in Fluid-Filled Porous Media," Geophysics 45, 1269-1275 (1980).

104. P.D. Jackson, D. Taylor Smith, and P.N. Stanford, "Resistivity-Porosity-Particle Shape Relationships for Marine Sands," Geophysics 43, 1250-1268 (1978).

105. G.E. Archie, "The Electrical Resistivity Log as an Aid in Determining Some Reservoir Characteristics," Transactions AIME 146, 54-62 (1942).

106. W.O. Sinsauer, H.M. Shearin, P.H. Masson, and M. Williams, "Resistivity of Brine-Saturated Sands in Relation to Pore-Geometry," Bull, AAPG 36, pp. 253-277 (1952).

107. J.G. Berryman, "Confirmation of Biot's Theory," Appl. Phys. Lett. 37, 382-384 (1980).

108. J.G. Berryman, "Elastic Wave Propagation in Fluid-Saturated Porous Media," J. Acoust. Soc. Am. 69, 416-424 (1981).

109. H. Lamb, Hydrodynamics (Dover, New York, 1945), pp. 152-156.

110. N.R. Draper and H. Smith, Applied Regression Analysis (John Wiley and Sons, Inc., New York, 1966), pp. 1-43.

111. J.M. Hovem and J-A Langeland, "Propagation of Sound in Marine Sediments," in Underwater Acoustics and Signal Processing, edited by L. Bjorno (D. Reidel Publishing Co., New York, 1981), pp. 179-186.

112. L.C. Graton and H.J. Fraser, "Systematic Packing of Spheres with Particular Relation to Porosity and Permeability," J. Geology. 43, 785-909 (1935).

113. R.D. Stoll and R.E. Houtz, "Attenuation Measurement with Sonobuoys," J. Acoust. Soc. Am. 73, 163-172, (1983).

UNCLASSIFIED

SECURITY CLASSIFICATION OF THIS PAGE (When Data Entered)

REPORT DOCUMENTATION PAGE		READ INSTRUCTIONS BEFORE COMPLETING FORM
1. REPORT NUMBER NORDA Technical Note 159	2. GOVT ACCESSION NO. AD-A152 612	3. RECIPIENT'S CATALOG NUMBER
4. TITLE (and Subtitle) Shear Wave Attenuation in Unconsolidated Laboratory Sediments		5. TYPE OF REPORT & PERIOD COVERED FINAL 6. PERFORMING ORG. REPORT NUMBER
7. AUTHOR(s) Burlie A. Brunson		8. CONTRACT OR GRANT NUMBER(s) N0014-81-C-0275 P0003
9. PERFORMING ORGANIZATION NAME AND ADDRESS Planning Systems Incorporated 7900 Westpark Drive, Suite 600 McLean, Virginia 22102		10. PROGRAM ELEMENT, PROJECT, TASK AREA & WORK UNIT NUMBERS
11. CONTROLLING OFFICE NAME AND ADDRESS Naval Ocean Research and Development Activity NSTL Station, Mississippi 39529		12. REPORT DATE June 1983 13. NUMBER OF PAGES 251
14. MONITORING AGENCY NAME & ADDRESS(if different from Controlling Office)		15. SECURITY CLASS. (of this report) UNCLASSIFIED 15a. DECLASSIFICATION/DOWNGRADING SCHEDULE

16. DISTRIBUTION STATEMENT (of this Report)

Distribution Unlimited

17. DISTRIBUTION STATEMENT (of the abstract entered in Block 20, if different from Report)

18. SUPPLEMENTARY NOTES

Presented to Oregon State University in partial fulfillment of the requirements for the degree of Doctor of Philosophy in Physical Oceanography.

19. KEY WORDS (Continue on reverse side if necessary and identify by block number)

Shear waves
Sediment properties
Seafloor acoustics
Attenuation
Acoustic modeling

20. ABSTRACT (Continue on reverse side if necessary and identify by block number)

Shear wave attenuation measurements were made using ceramic bimorph transducers to excite transverse vibrations in a cylindrical column of unconsolidated sediment. Three different water-saturated sediments were used in an attempt to determine the effects of grain

DD FORM 1 JAN 73 1473 EDITION OF 1 NOV 65 IS OBSOLETE
S/N 0102-LF-014-6601

UNCLASSIFIED

SECURITY CLASSIFICATION OF THIS PAGE (When Data Entered)

shape and sorting on the frequency dependence of attenuation. The mean grain size of the sediments was held constant while the grain shape and size distributions were varied. The sediment assemblages used in the attenuation measurements included a moderately-sorted angular quartz sand, a well-sorted angular quartz sand, and well-sorted spherical glass beads. The moderately-sorted sand showed the greatest attenuation over the measurement frequency range of 1 to 20 kHz. The well-sorted sand and the glass beads showed generally lower attenuation with the beads being the least lossy propagation medium. All three sediments showed evidence of viscous attenuation due to fluid-to-grain relative motion. This mechanism leads to a non-linear relationship between attenuation and frequency.

Sediment physical properties were measured for use as inputs to a theoretical attenuation model based on the Biot theory of propagation of waves in porous media. The model allowed attenuation versus frequency predictions to be made for each of the three sediment assemblages. The resultant comparisons between the measured and predicted attenuations demonstrated the importance of using measured model inputs obtained under controlled laboratory conditions when theoretical model capabilities are being evaluated. The model comparison shed significant light on the ability of this particular model to predict shear wave attenuation in non-ideal sediments.

END

FILMED

5-85

DTIC